NASA
Technical
Paper
2642

January 1987

Subsonic Maneuver Capability of a Supersonic Cruise Fighter Wing Concept

Gregory D. Riebe and
Charles H. Fox, Jr.

NASA

NASA Technical Paper 2642

1987

Subsonic Maneuver Capability of a Supersonic Cruise Fighter Wing Concept

Gregory D. Riebe and
Charles H. Fox, Jr.

Langley Research Center
Hampton, Virginia

National Aeronautics
and Space Administration

**Scientific and Technical
Information Branch**

CONTENTS

SUMMARY

A theoretical and experimental investigation was conducted of the subsonic maneuver capability of a fighter wing concept designed for supersonic cruise. To improve the subsonic maneuver capability, the wing utilized full-span leading- and trailing-edge flaps that were designed with the aid of a subsonic-analysis computer program.

The wing, mounted on a generic fuselage, was tested in the Langley 7- by 10-Foot High-Speed Tunnel at Mach numbers of 0.3, 0.5, and 0.7. Force and moment data obtained were compared with theoretical predictions at Mach 0.5 from two subsonic-analysis computer programs. The two theoretical programs gave a good prediction of the lift and drag characteristics but only a fair prediction of the pitching moment. The experimental results of this study show that with the proper combination of leading- and trailing-edge flap deflections, a suction parameter of nearly 90 percent can be attained at a Mach number of 0.5 and a lift coefficient of 0.73; this is a three-fold improvement from 30 percent for the basic wing. Trailing-edge deflection alone gives a greater improvement in suction parameter than leading-edge deflection alone; however, the best performance is obtained with a combination of the two.

INTRODUCTION

A wing designed for efficient supersonic cruise would generally be highly swept and would utilize a mildly cambered thin wing. In contrast, the design of a highly maneuverable wing would favor a higher aspect ratio and a more highly cambered wing. These conflicting requirements must be dealt with when designing a supersonic cruise fighter that needs to possess good maneuver capability at high subsonic speeds. One solution to this problem is to camber the wing for efficient supersonic cruise and then use leading- and trailing-edge flaps to approximate the increased camber requirement at maneuver conditions. This solution is the approach used here.

The wing discussed in this report is designed for cruise at Mach 1.8. In an attempt to meet a design maneuver requirement of 5g (where $1g = 32.17\ ft/sec^2$) at subsonic speeds, full-span leading- and trailing-edge flaps are used. The planform shape and the deflection combination of these flaps were determined with the aid of the subsonic-analysis computer program of reference 1 (referred to hereinafter as the "Carlson code") that enables the user to analyze quickly many flap concepts at multiple combinations of leading- and trailing-edge deflection angles. The wing, mounted on a generic fuselage, was tested in the Langley 7- by 10-Foot High-Speed Tunnel at Mach numbers of 0.3, 0.5, and 0.7. In addition to the present test results, this report presents theoretical predictions from the Carlson code and from another aerodynamic analysis computer code referred to as the "vortex lattice method-suction analogy" (VLM-SA). (See ref. 2.)

SYMBOLS

A	aspect ratio, b^2/S
b	wing span, 18.40 in.

C_A axial-force coefficient, Axial force/qS

C_D drag coefficient, Drag/qS

$C_{D,o}$ zero-lift drag coefficient for case with no flaps deflected, 0.013 at M = 0.5

C_L lift coefficient, Lift/qS

$C_{L,M}$ lift coefficient at maneuver point

C_{L_α} lift-curve slope, $\partial C_L/\partial\alpha$ at $C_L = 0$, for case with no flaps deflected, deg^{-1}

C_m pitching-moment coefficient, Pitching moment/$qS\bar{c}$

C_N normal-force coefficient, Normal force/qS

$\bar{c}$ mean aerodynamic chord, 9.78 in.

L/D lift-drag ratio

M free-stream Mach number

N_{Re} Reynolds number, per foot

q dynamic pressure, psf

S reference area of wing projected to body centerline, 149.72 in^2

S_s suction parameter, $\dfrac{C_L \tan(C_L/C_{L_\alpha}) + C_{D,o} - C_D}{C_L \tan(C_L/C_{L_\alpha}) - C_L^2/\pi A}$

t/c maximum thickness-to-chord ratio

y spanwise distance measured from body centerline

α angle of attack, deg

Λ angle of sweep, deg

Subscripts:

I inboard

O outboard

Abbreviations:

IVOROP vortex location option

LE leading edge

TE trailing edge

THEORETICAL METHODS

Two different methods are used in the theoretical analysis of the wing with various flap deflections. One of these methods, the Carlson code described in reference 1, was used in the design of the flaps for the wing. This subsonic-analysis computer program provides for the analysis of up to 25 pairs of leading- and trailing-edge flap deflection combinations. The program uses an empirical method to estimate attainable leading-edge thrust. This method of estimating the theoretical leading-edge thrust includes effects of Mach number, Reynolds number, wing planform, camber surface, and airfoil geometry, as described in reference 3. That portion of the full theoretical leading-edge thrust that is not considered attainable is treated as a separated leading-edge vortex force by use of the Polhamus suction analogy.

The user of the Carlson code has three vortex location options (IVOROP's) concerning where and how that vortex force acts on the wing. The first vortex option (IVOROP = 0) places all the vortex force at the wing leading edge perpendicular to the wing reference plane, thus offering no contribution to C_A. The second and third options distribute the vortex force chordwise about a point called the vortex action point. For the second option (IVOROP = 1), the vortex action point is determined by an empirical relationship derived from experimental delta wing data, as described in reference 1. The third option (IVOROP = 2) uses a concept derived by Lan and Chang (ref. 4) to locate the vortex action point. For both the second and third options, the vortex force is distributed over the wing using a sinusoidal distribution.

The other theoretical aerodynamic analysis program used is the vortex lattice method of reference 2 by Lamar and Herbert. This program, referred to as the "vortex lattice method-suction analogy" (VLM-SA), is an extension of the program of reference 5 by Lamar and Gloss. The VLM-SA program utilizes the concept derived by Lan for locating the vortex action point. The vortex force is not distributed over the wing as in the Carlson code; rather the entire force acts at the vortex action point, except in the C_m calculations where vortex force is placed at the leading edge normal to the local camber surface. The VLM-SA program also has a method of differentiating between leading-edge suction and vortex forces. Unlike Carlson's method, which estimates an attainable leading-edge suction, the VLM-SA program uses a procedure developed by Kulfan (ref. 6) to determine the vortex force and then uses the suction analogy to determine what portion of the full theoretical suction remains as a residual suction force.

For both theoretical methods, the geometry was modeled using the wing-body camber surface. The wing leading-edge radius was also an input in both programs.

The Carlson code was used in the flap design process; therefore most of the theoretical results presented will be from this code. Theoretical predictions from the VLM-SA code are included for reference and comparison.

WING DESIGN

The primary requirements for this wing include efficient cruise at Mach 1.8 and the ability to sustain a 5g turn at Mach 0.9 at an altitude of 30 000 ft. Because of the Mach 1.8 cruise condition, the leading-edge sweep angle Λ_{LE} of the wing is set at 60°, which is high enough to produce a subsonic leading edge at cruise but not unnecessarily reduce the aspect ratio and thus penalize performance. An NACA 64A004 airfoil section is used which has a leading-edge radius of 0.10 percent chord. The wing is twisted and cambered according to the method of reference 7 for cruise at Mach 1.8.

Using a wing loading typical of a lightweight fighter results in a $C_{L,M}$ of 0.73 for the 5g turn at Mach 0.9. According to the theory of reference 4, this $C_{L,M}$ can be attained at an angle of attack of 14° with $C_D = 0.16$ for the wing with no flaps. The use of flaps would lower this drag, thus requiring less engine thrust for maneuver. The goal of this study was to design a set of leading- and trailing-edge flaps that would lower the drag at maneuver as much as possible.

The thin (t/c = 4 percent), mildly cambered wing gives low drag at supersonic cruise. At subsonic maneuver conditions, however, the thin wing does not attain much leading-edge thrust and therefore has high drag due to lift. Leading-edge flaps attempt to recover the theoretical leading-edge thrust that is not attained by the flat wing. This recovery is accomplished by the flap producing a force distributed over its surface rather than by a concentrated thrust force at the leading edge. The loading over the leading-edge flap can be produced either by attached flow or by a leading-edge vortex that is confined over the flap. One design goal was to maintain attached flow over the whole wing. The leading-edge radius of the NACA 64A004 airfoil contributes to this goal by delaying the formation of the leading-edge vortex.

The Carlson code was used in the design of the leading- and trailing-edge flaps for this wing. The way in which the program was used in the design by iteration of the flaps is described in reference 1. This program does not optimize but is used only to analyze input flap geometry and deflection angles. A number of flap planform sizes and shapes were analyzed over a wide range of combinations of deflection angles, with the goal of minimizing drag at the maneuver point. In varying the flap geometry, only the hinge line location and sweep were changed so that the resulting wing with undeflected flaps would be unchanged from the original wing. The best flap geometry from those analyzed was selected for wind-tunnel testing, along with deflection angle combinations that would bracket the best theoretical flap deflections. As will be discussed later, two different inboard leading-edge flap shapes were chosen to test the predictions made by the program, which indicated that they would have nearly identical results at the maneuver C_L.

MODEL DESCRIPTION

A drawing of the model is shown in figure 1, and a photograph of the model mounted in the Langley 7- by 10-Foot High-Speed Tunnel is shown in figure 2. Geometric characteristics of the wing, vertical tail, and fuselage are presented in table I. A numerical description of the model in the format described in reference 8 is found in table II.

The model consists of a wing mounted on a flat-sided generic fuselage with a vertical tail. The wing has a leading-edge sweep angle of 60°, a cranked trailing edge with an inboard sweep angle of 7.45°, and an outboard sweep angle of 28°. A drawing of the wing cross section at the root, the midchord, and the tip chord is shown in figure 3. The vertical tail has a 4-percent-thick biconvex airfoil section.

The leading- and trailing-edge flaps are in two segments, as shown in figure 1. Leading-edge deflection angles include 0°, 15°, 20°, and 25° measured streamwise, positive downward. Trailing-edge streamwise deflection angles (positive downward) include 0° and 15° inboard and 0° and 12° outboard. For each deflection angle, a separate flap was constructed. Two different inboard leading-edge flaps were constructed, differing in root chord length and hinge line location as shown in figure 1. The larger flap is designated "flap A" and the smaller, inverse tapered flap is designated "flap B."

It should be noted that the deflected inboard and outboard leading-edge flap segments did not make a completely perfect fit where they came together at the wing midspan, even when at the same deflection angle. Effects from this misfit can often be seen in the oil-flow photographs presented later in this report.

EXPERIMENTAL PROCEDURE AND CORRECTIONS

Tests were conducted in the Langley 7- by 10-Foot High-Speed Tunnel. Forces and moments were measured by a six-component strain-gauge balance. Tests were made at Mach numbers of 0.3, 0.5, and 0.7 under the following conditions:

M	N_{Re}, ft^{-1}	q, psf
0.3	1.9×10^6	125
.5	2.9	315
.7	3.3	525

The model was tested at zero sideslip over a range of angle of attack from -5° to 16°. Some configurations were limited in angle of attack because of model fouling, as indicated by a fouling strip at the base of the model. As outlined in reference 9, a 1/16-in-wide strip of No. 120 grit was applied to the wing and vertical tail 0.6 in. back chordwise from the leading edge and also to the body 1.0 in. back from the nose.

The data were corrected for jet boundary and blockage effects as computed from references 10 and 11, respectively. Corrections to angle of attack for sting and balance deflection have been applied to the data. Axial force is corrected to a condition of free-stream static pressure acting over the fuselage base area and balance cavity.

Oil-flow visualization photographs of the flow over the wing surface were made by first coating the model with a mixture of oil and fluorescent powder and then taking photographs of the model at test conditions using ultraviolet strobe lights. For these oil-flow test runs, the model was held at an angle of attack of 0° while the tunnel speed was brought up to Mach 0.5. The model was then set at the desired angle of attack; and as soon as the flow pattern developed, a series of three photographs were taken over a 10- to 15-sec interval.

DISCUSSION

Flap Deflection Notation

A shorthand notation is used in this report when referring to a particular combination of flap deflections. This method will list four deflection angles, all separated by a slash. The angles are in the order of inboard to outboard, front to rear. For example, the configuration 0/20/15/12 would mean inboard leading-edge flap down 0°, outboard leading-edge flap down 20°, inboard trailing-edge flap down 15°, and outboard trailing-edge flap down 12°. If only two angles are shown, they are in the order of inboard to outboard, with the text indicating leading edge or trailing edge. Note that all angles are measured in the streamwise direction.

Experimental Results

Wind-tunnel data were taken at Mach numbers of 0.3, 0.5, and 0.7. However, since only minor differences are seen between the Mach numbers, only the data and theory at $M = 0.5$ will be discussed here. The data for all three Mach numbers can be found in appendix A. (See figs. A1 to A4.)

Several drag polars for the model at $M = 0.5$ with inboard flap A on the wing are shown in figure 4. Also shown in the figure are the theoretical upper and lower limits on the drag given, respectively, by the expressions $C_L \tan\left(C_L/C_{L_\alpha}\right) + C_{D,o}$, representing zero suction, and $\left(C_L^2/\pi A\right) + C_{D,o}$, representing full suction. These limits are used in the calculation of the suction parameter S_s, which is a measure of the percent of suction recovered by the wing. For the configuration with no flaps deflected, the suction parameter equals 30 percent at $C_{L,M}$. This amount of suction was attained by virtue of the camber and leading-edge radius of the wing and by the augmentation of the full potential lift with a vortex force. Of all the cases tested, this case with no flaps deflected had the highest drag at $C_{L,M}$. Deflecting the leading edges alone 15° resulted in an S_s of 62 percent at $C_{L,M}$. Deflecting the trailing edges alone 15° inboard and 12° outboard resulted in a greater improvement in the suction parameter than with the leading edges alone; S_s is 73 percent when the trailing edges are deflected. Combining leading- and trailing-edge deflections (15/15/15/12) results in an S_s of 87 percent.

Oil-flow photographs for these four configurations are presented in figure 5. This sequence of photographs demonstrates the effects of various combinations of flap deflections on the flow over the wing at a lift coefficient near the maneuver C_L of 0.73. The wing with no flaps deflected (0/0/0/0) achieves a C_L of 0.73 at an angle of attack of 15°. The oil-flow photograph of the wing near this condition shows a system of multiple vortices over the wing with flow reattachment behind the main vortex. Deflecting the leading edge down 15° results in a smaller main vortex that is farther forward on the wing and that acts mainly on the flap. Therefore, the effective force from this vortex points more forward, resulting in the drag reduction seen in figure 4, even though the wing must go above $\alpha = 16°$ to reach $C_L = 0.73$.

Figure 5(c) shows the wing with only the trailing-edge flaps deflected (0/0/15/12). When comparing this configuration with the 0/0/0/0 configuration it is seen that the two flows are similar, although the main vortex is farther forward and smaller with trailing-edge deflection. The trailing-edge deflection, however, yields a large increment in C_L resulting in a much lower angle of attack for $C_{L,M}$, a decrease which results in a much lower drag level. Further improvement on the 0/0/15/12 case can be obtained by deflecting the leading edge, a deflection resulting in the flow shown in figure 5(d). This photograph shows the flow over the inboard leading edge to be attached while a small vortex occurs along the outboard deflected leading edge. The maneuver point for the 15/15/15/12 configuration is reached at $\alpha = 10.8°$.

A bar graph comparing the suction parameters at $C_L = 0.73$ for all configurations tested using inboard leading-edge flap A can be seen in figure 6. As can be seen in the figure, the best leading-edge deflection combination is 15° inboard and 20° outboard, both with and without a trailing-edge deflection. Also note that the worst case with trailing-edge deflection, the 0/0/15/12 configuration, has a suction parameter that is higher than that of the best case with leading-edge deflection

alone. This result illustrates the importance of trailing-edge flaps in reducing drag due to lift.

As mentioned previously, two different inboard flaps were tested. The drag polars for the wing with these flaps at three different leading-edge deflections (15°, 20°, and 25°), both with and without trailing-edge deflections, are presented in figure 7. As seen in the figure, there is very little difference between the drag polars of the two flaps except at conditions that depart greatly from design. For example, when the leading-edge flaps are substantially overdeflected, as in figure 7(f) at low values of C_L, the larger flap (flap A) causes a larger drag penalty. Conversely, when the flaps are underdeflected, the wing with the smaller flap (flap B) shows an increase in drag at maneuver C_L.

Oil-flow photographs showing the flow over the wing with these flaps are presented in figure 8. Photographs of the wing at three angles of attack are presented; those for flap A are on the left, and those for flap B are on the right. In all cases, the flap deflection combination is 15/15/15/12. For a particular angle of attack, the flow patterns for both wings in the vicinity of the leading-edge flaps are very similar and appear to show attached flow. The main difference between the two configurations is the presence of a vortex over the wing with flap B. This vortex appears to originate at the wing apex, being easily seen on the wing at $\alpha = 10.52°$ but barely visible at $\alpha = 8.35°$.

A comparison of the pitching-moment-coefficient variation with leading-edge deflection for both flaps A and B, and with and without trailing-edge deflection, can be seen in figure 9. Deflecting either the leading edge or the trailing edge causes a nose-down increment in pitching movement, with the trailing edge being considerably more influential than the leading edge. The change in C_m with leading-edge deflection tends to level off at the higher deflection angles. The smaller sized, inboard leading-edge flap (flap B) has less effect on C_m than flap A.

Plots of L/D, C_D, C_m, and α as a function of C_L for all configurations at all Mach numbers can be found in appendix A (figs. A1 to A4). At the beginning of appendix B there is a sample photograph on which the main features of the wing geometry are noted (fig. B1). Oil-flow photographs of the right wing of all configurations in which oil-flow tests were made can be found in appendix B (figs. B2 to B7).

Comparison of Experimental Data and Theory

Figure 10 presents a comparison between the Carlson theory (ref. 1) and experimental data for six combinations of leading- and trailing-edge flaps. Each figure shows C_N and C_A plotted as functions of α, and C_m and C_D plotted as functions of C_L. Note that in figures 10 to 12, the second vortex location option (IVOROP = 1) described earlier is used in the Carlson code. Figure 10(a) shows that for the wing with no flaps deflected, the agreement between the data and theory is excellent, except for the failure of the theory to predict the break in C_m at $C_L = 0.5$. This break may be associated with a change from predominantly attached flow to vortex flow. (See fig. B2 in appendix B.) The theoretical predictions of the data for the 15/15/0/0 and the 25/25/0/0 configurations are shown in figures 10(b) and 10(c), respectively. The inability of the theory to predict adequately the axial force and therefore the drag at the lower values of C_L is probably due to flow separation on the underside of the leading-edge flaps.

The theory does not perform as well for a trailing edge alone at 15° as for the leading edge at 15° as shown in figure 10(d). Here again, the prediction of C_N is very good, but not of C_A. This overprediction of C_A continues when leading-edge deflection is added as seen in figures 10(e) and 10(f).

Figure 11 presents both the data and theoretical results from the Carlson code for leading-edge flaps A and B and the flap deflection combination 15/15/15/12. The data and theory for flap A seen in figure 10(e) are repeated in this figure. In figure 11 it is seen that the data and theory are in very good agreement for both C_N and C_m. Note that the increment in C_m between the two flap configurations is well-predicted by the theory. As seen before, the theory does not predict the axial-force coefficient as well as the normal-force coefficient. Note, however, that the relative difference in C_A between flaps A and B is predicted by the theory. This trend is also seen in the drag polars.

Figure 12 presents a comparison of the drag polars computed by the Carlson code (ref. 1) and the VLM-SA code (ref. 2). Four configurations are presented in the figure: (1) no flaps deflected, (2) leading-edge deflection only, (3) trailing-edge deflection only, and (4) the combination of these leading- and trailing-edge deflections. For each combination of flap deflections, the drag polars from the two computer codes are presented, along with the data and the theoretical upper and lower bounds on drag.

When no flaps are deflected (fig. 12(a)), the Carlson code follows the data very well, whereas the VLM-SA code underpredicts the drag at higher values of C_L. Both codes perform very well for leading-edge deflection only as seen in figure 12(b). When trailing-edge deflection is added, the Carlson code tends to overpredict the drag. The VLM-SA code, however, continues to do well in following the data as seen in figures 12(c) and 12(d). Neither code, of course, is able to predict correctly the larger increase in drag at higher values of C_L where undoubtedly large areas of separated flow develop.

Figure 13 shows C_m plotted as a function of C_L for these same four combinations of flap deflections. Each figure shows the data as well as the theoretical predictions from the VLM-SA and Carlson codes. In all cases shown, the Carlson code is more accurate than the VLM-SA code in predicting C_m. Both codes do well in predicting C_m near $C_L = 0$, but neither is able to predict the sudden decrease in stability at higher values of C_L. When the trailing edge is deflected, as in figures 13(c) and 13(d), the Carlson code follows the data very well at low-to-moderate C_L values. As would be expected, holding the vortex force at the leading edge (IVOROP = 0) results in the least amount of nose-down pitching moment. This vortex location option follows the trend of the data better than the other two options, which show an increase in stability at higher values of C_L as does the prediction from the VLM-SA code.

CONCLUDING REMARKS

A theoretical and experimental investigation has been conducted of the subsonic maneuver capability of a fighter wing concept designed for supersonic cruise. To improve the subsonic maneuver capability, the wing utilized full-span leading- and trailing-edge flaps. These flaps were designed with the aid of a Carlson subsonic-analysis computer program (NASA CR-3675) that enables the user to analyze quickly many flap concepts at multiple combinations of deflection angles.

The wing, mounted on a generic fuselage, was tested at Mach numbers of 0.3, 0.5, and 0.7. The data obtained were compared with theoretical predictions at Mach 0.5 from the Carlson subsonic-analysis program and from the vortex lattice method-suction analogy (VLM-SA) of NASA TM-83303. The results of this study show that with the proper combination of leading- and trailing-edge flap deflections, a suction parameter of nearly 90 percent can be attained at a Mach number of 0.5 and a lift coefficient of 0.73; this is a three-fold improvement from 30 percent for the basic wing. Trailing-edge deflection alone gives a greater improvement in suction parameter than leading-edge deflection alone; however, the best performance is obtained with a combination of the two.

Two different inboard leading-edge flaps were tested. Results indicate that the smaller flap, when properly deflected, has the same drag level at maneuver conditions as the larger flap, but it yields a smaller increment in nose-down pitching moment.

Both the Carlson code and the VLM-SA code gave a good prediction of the shape of the drag polar of the wing with leading-edge flap deflection angles of 0° and 15°. The VLM-SA code also performed very well when trailing-edge deflection was added. The Carlson code, however, did not predict the trailing-edge performance as well.

In predicting the pitching-moment coefficient C_m, the Carlson code performed better than the VLM-SA code for all configurations presented. The Carlson code predicted C_m very well when the trailing edge was deflected and was only fair at other conditions. Both codes performed well in predicting C_m near a lift coefficient of 0.

NASA Langley Research Center
Hampton, VA 23665-5225
November 21, 1986

REFERENCES

1. Carlson, Harry W.; and Walkley, Kenneth B.: An Aerodynamic Analysis Computer Program and Design Notes for Low Speed Wing Flap Systems. NASA CR-3675, 1983.

2. Lamar, John E.; and Herbert, Henry E.: Production Version of the Extended NASA-Langley Vortex Lattice FORTRAN Computer Program. Volume I - User's Guide. NASA TM-83303, 1982.

3. Carlson, Harry W.; Mack, Robert J.; and Barger, Raymond L.: Estimation of Attainable Leading-Edge Thrust for Wings at Subsonic and Supersonic Speeds. NASA TP-1500, 1979.

4. Lan, C. Edward; and Chang, Jen-Fu: Calculation of Vortex Lift Effect for Cambered Wings by the Suction Analogy. NASA CR-3449, 1981.

5. Lamar, John E.; and Gloss, Blair B.: Subsonic Aerodynamic Characteristics of Interacting Lifting Surfaces With Separated Flow Around Sharp Edges Predicted by a Vortex-Lattice Method. NASA TN D-7921, 1975.

6. Kulfan, R. M.: Wing Geometry Effects on Leading-Edge Vortices. AIAA Paper 79-1872, Aug. 1979.

7. Middleton, W. D.; and Lundry, J. L.: A System for Aerodynamic Design and Analysis of Supersonic Aircraft. Part 1 - General Description and Theoretical Development. NASA CR-3351, 1980.

8. Craidon, Charlotte B.: Description of a Digital Computer Program for Airplane Configuration Plots. NASA TM X-2074, 1970.

9. Braslow, Albert L.; Hicks, Raymond M.; and Harris, Roy V., Jr.: Use of Grit-Type Boundary-Layer-Transition Trips on Wind-Tunnel Models. NASA TN D-3579, 1966.

10. Gillis, Clarence L.; Polhamus, Edward C.; and Gray, Joseph L., Jr.: Charts for Determining Jet-Boundary Corrections for Complete Models in 7- by 10-Foot Closed Rectangular Wind Tunnels. NACA WR L-123, 1945. (Formerly NACA ARR L5G31.)

11. Herriot, John G.: Blockage Corrections for Three-Dimensional-Flow Closed-Throat Wind Tunnels, With Consideration of the Effect of Compressibility. NACA Rep. 995, 1950. (Supersedes NACA RM A7B28.)

TABLE I.- GEOMETRIC CHARACTERISTICS OF MODEL

Wing:	
Area (reference), in^2	149.72
Aspect ratio	2.26
Span, in.	18.40
Λ_{LE}, deg	60
Λ_{TE} (inboard), deg	7.45
Λ_{TE} (outboard), deg	28
Mean aerodynamic chord, in.	9.78
Airfoil section	NACA 64A004
Local LE radius, percent of chord	0.10
Vertical tail:	
Area, in^2	18.41
Aspect ratio	1.24
Span, in.	4.78
Λ_{LE}, deg	45
Airfoil section (t/c = 4 percent)	Circular arc
Thickness ratio, percent	4
Fuselage:	
Length, in.	33.55
Height (maximum), in.	4.25
Width, in.	2.40
Base area, in.	4.97
Chamber area, in.	2.55
Moment center, in.	20.64

TABLE II.- GEOMETRY OF WAVE-DRAG INPUT

```
        BODY AND FIN WITH 60 DEG MODIFIED DELTA WING   DIMENSIONS IN INCHES
 1  1   1  0  1  0  0  9 18  1 26 20  0  0  0  0  0  0  0  0  1 10  0  0
148.63
  0.000    .491    .739   1.236   2.481   4.975   7.469   9.965 14.959 19.954  XAF   18
29.950 39.948 49.953 59.960 69.968 79.979 89.990100.000                       XAF   18
13.391  1.200    .085 13.211                                                   WAFORG 1
15.123  2.200    .110 11.608                                                   WAFORG 2
16.854  3.200    .160 10.004                                                   WAFORG 3
18.585  4.200    .238  8.401                                                   WAFORG 4
20.315  5.200    .321  6.799                                                   WAFORG 5
22.047  6.200    .355  5.599                                                   WAFORG 6
23.778  7.200    .397  4.399                                                   WAFORG 7
25.510  8.200    .442  3.199                                                   WAFORG 8
27.241  9.200    .487  1.998                                                   WAFORG 9
  0.000  -.002  -.003  -.007  -.012  -.023  -.031  -.039  -.050  -.061  TZORD  1
  -.081  -.100  -.114  -.116  -.103  -.080  -.051  -.019                 TZORD  1
  0.000   .001   .001   .002   .003   .002   .003   .001  -.000  -.003  TZORD  2
  -.007  -.007  -.004   .002   .013   .023   .036   .046                 TZORD  2
  0.000   .001   .003   .005   .009   .015   .021   .026   .033   .041  TZORD  3
   .043   .046   .054   .063   .073   .085   .097   .109                 TZORD  3
  0.000   .002   .003   .006   .009   .016   .022   .029   .039   .049  TZORD  4
   .056   .061   .072   .083   .094   .106   .118   .131                 TZORD  4
  0.000   .001   .002   .003   .006   .012   .017   .023   .031   .039  TZORD  5
   .052   .065   .077   .089   .101   .112   .125   .137                 TZORD  5
  0.000   .001   .002   .003   .006   .010   .015   .020   .028   .035  TZORD  6
   .049   .061   .073   .085   .097   .107   .120   .132                 TZORD  6
  0.000   .001   .002   .002   .005   .009   .013   .017   .023   .030  TZORD  7
   .042   .053   .064   .074   .085   .095   .105   .115                 TZORD  7
  0.000   .001   .001   .002   .003   .006   .009   .012   .019   .024  TZORD  8
   .033   .043   .052   .060   .069   .077   .086   .095                 TZORD  8
  0.000   .000   .000   .001   .001   .003   .004   .006   .010   .014  TZORD  9
   .024   .033   .042   .052   .062   .072   .081   .091                 TZORD  9
  0.000   .325   .393   .492   .673   .930  1.120  1.278  1.520  1.702  WAFORD 1
 1.929  1.998  1.884  1.627  1.272   .856   .431   .008                 WAFORD 1
  0.000   .322   .387   .491   .680   .930  1.120  1.274  1.524  1.705  WAFORD 2
 1.929  1.998  1.886  1.628  1.275   .853   .431   .009                 WAFORD 2
  0.000   .319   .390   .490   .675   .935  1.119  1.279  1.519  1.709  WAFORD 3
 1.929  1.999  1.879  1.629  1.269   .859   .430   .010                 WAFORD 3
  0.000   .321   .387   .488   .678   .928  1.119  1.273  1.523  1.702  WAFORD 4
 1.928  1.999  1.880  1.630  1.273   .857   .428   .012                 WAFORD 4
  0.000   .316   .390   .500   .676   .926  1.118  1.279  1.515  1.706  WAFORD 5
 1.926  2.000  1.882  1.632  1.264   .853   .426   .015                 WAFORD 5
  0.000   .330   .393   .500   .679   .929  1.125  1.286  1.518  1.696  WAFORD 6
 1.928  2.000  1.875  1.625  1.268   .857   .428  0.000                 WAFORD 6
  0.000   .330   .386   .500   .682   .932  1.114  1.273  1.523  1.705  WAFORD 7
 1.932  2.000  1.886  1.636  1.273   .863   .432  0.000                 WAFORD 7
  0.000   .328   .391   .484   .687   .938  1.125  1.281  1.531  1.719  WAFORD 8
 1.938  2.000  1.875  1.625  1.281   .844   .437  0.000                 WAFORD 8
  0.000   .300   .400   .500   .700   .950  1.125  1.300  1.500  1.701  WAFORD 9
 1.951  2.001  1.901  1.651  1.251   .850   .450  0.000                 WAFORD 9
  0.000  1.010  2.000  2.990  4.000  5.000  5.990  6.700  7.500  8.500  XFUS  20
 9.500 10.500 12.000 14.000 16.000 19.500 23.000 26.500 30.000 33.500  XFUS  20
  0.000  0.000  0.000  0.000  0.000  0.000  0.000  0.000  0.000  0.000  Y     1
  0.000  0.000  0.000  0.000  0.000  0.000  0.000  0.000  0.000  0.000  Y     1
  0.000  0.000  0.000  0.000  0.000  0.000                              Y     1
  0.000  0.000  0.000  0.000  0.000  0.000  0.000  0.000  0.000  0.000  Z     1
  0.000  0.000  0.000  0.000  0.000  0.000  0.000  0.000  0.000  0.000  Z     1
  0.000  0.000  0.000  0.000  0.000  0.000                              Z     1
```

TABLE II.- Continued

0.000	.001	.002	.003	.119	.220	.289	.314	.314	.314	Y	2
.314	.314	.314	.314	.289	.221	.120	.003	.002	.001	Y	2
.001	.001	.001	.001	.000	0.000					Y	2
-.301	-.301	-.301	-.301	-.277	-.215	-.119	-.003	-.003	-.003	Z	2
-.003	-.003	-.003	-.003	.114	.211	.276	.300	.300	.300	Z	2
.300	.300	.300	.300	.300	.300					Z	2
0.000	.002	.004	.006	.226	.413	.540	.585	.585	.585	Y	3
.585	.585	.585	.585	.540	.414	.227	.006	.005	.003	Y	3
.003	.003	.002	.001	.001	0.000					Y	3
-.580	-.580	-.580	-.580	-.534	-.411	-.226	-.006	-.006	-.006	Z	3
-.006	-.006	-.006	-.006	.215	.401	.526	.572	.572	.572	Z	3
.572	.572	.572	.572	.572	.572					Z	3
0.000	.003	.006	.009	.322	.583	.754	.818	.818	.818	Y	4
.818	.818	.818	.818	.754	.582	.321	.009	.007	.004	Y	4
.004	.004	.003	.002	.001	0.000					Y	4
-.842	-.842	-.842	-.842	-.775	-.591	-.322	-.009	-.009	-.009	Z	4
-.009	-.009	-.009	-.009	.304	.572	.755	.821	.821	.821	Z	4
.821	.821	.821	.821	.821	.821					Z	4
0.000	.005	.010	.016	.406	.729	.934	1.010	1.010	1.010	Y	5
1.010	1.010	1.010	1.010	.933	.725	.404	.016	.011	.006	Y	5
.006	.006	.004	.003	.001	0.000					Y	5
-1.083	-1.083	-1.083	-1.083	-.994	-.755	-.412	-.017	-.016	-.014	Z	5
-.013	-.011	-.010	-.008	.383	.721	.954	1.041	1.041	1.041	Z	5
1.041	1.041	1.041	1.041	1.041	1.041					Z	5
0.000	.085	.169	.254	.605	.892	1.076	1.145	1.145	1.145	Y	6
1.145	1.145	1.145	1.145	1.076	.891	.604	.254	.131	.007	Y	6
.007	.007	.006	.004	.002	0.000					Y	6
-1.257	-1.254	-1.249	-1.240	-1.154	-.936	-.625	-.269	-.184	-.099	Z	6
-.014	.071	.156	.241	.595	.905	1.121	1.205	1.219	1.225	Z	6
1.225	1.225	1.225	1.225	1.225	1.225					Z	6
0.000	.172	.343	.513	.791	1.011	1.147	1.198	1.198	1.198	Y	7
1.198	1.198	1.198	1.198	1.147	1.011	.791	.513	.262	.009	Y	7
.009	.009	.007	.005	.002	0.000					Y	7
-1.388	-1.382	-1.367	-1.344	-1.264	-1.078	-.822	-.537	-.362	-.188	Z	7
-.014	.160	.335	.509	.795	1.050	1.236	1.315	1.349	1.362	Z	7
1.362	1.362	1.364	1.365	1.365	1.366					Z	7
0.000	.241	.481	.721	.926	1.078	1.166	1.198	1.198	1.198	Y	8
1.198	1.198	1.198	1.198	1.166	1.078	.926	.721	.612	.503	Y	8
.503	.503	.417	.294	.151	0.000					Y	8
-1.461	-1.452	-1.430	-1.398	-1.323	-1.165	-.963	-.745	-.501	-.257	Z	8
-.013	.231	.476	.720	.938	1.140	1.299	1.374	1.405	1.433	Z	8
1.433	1.433	1.558	1.647	1.698	1.717					Z	8
0.000	.317	.633	.947	1.063	1.141	1.183	1.198	1.198	1.198	Y	9
1.198	1.198	1.198	1.198	1.182	1.141	1.063	.947	.802	.656	Y	9
.656	.656	.565	.419	.224	0.000					Y	9
-1.524	-1.512	-1.483	-1.444	-1.383	-1.277	-1.151	-1.019	-.682	-.345	Z	9
-.008	.329	.666	1.003	1.133	1.258	1.364	1.424	1.462	1.500	Z	9
1.500	1.500	1.710	1.887	2.006	2.051					Z	9
0.000	.349	.697	1.043	1.100	1.148	1.184	1.198	1.198	1.198	Y	10
1.198	1.198	1.198	1.198	1.185	1.151	1.102	1.043	.869	.695	Y	10
.676	.657	.575	.421	.221	0.000					Y	10
-1.577	-1.564	-1.531	-1.480	-1.456	-1.420	-1.370	-1.311	-.880	-.448	Z	10
-.017	.414	.845	1.277	1.340	1.395	1.437	1.465	1.509	1.553	Z	10
1.709	1.866	2.073	2.235	2.334	2.371					Z	10
0.000	.350	.698	1.043	1.102	1.152	1.185	1.198	1.198	1.198	Y	11
1.198	1.198	1.198	1.198	1.186	1.154	1.105	1.043	.842	.539	Y	11
.615	.592	.527	.398	.214	0.000					Y	11
-1.604	-1.590	-1.554	-1.496	-1.470	-1.429	-1.374	-1.311	-.879	-.448	Z	11

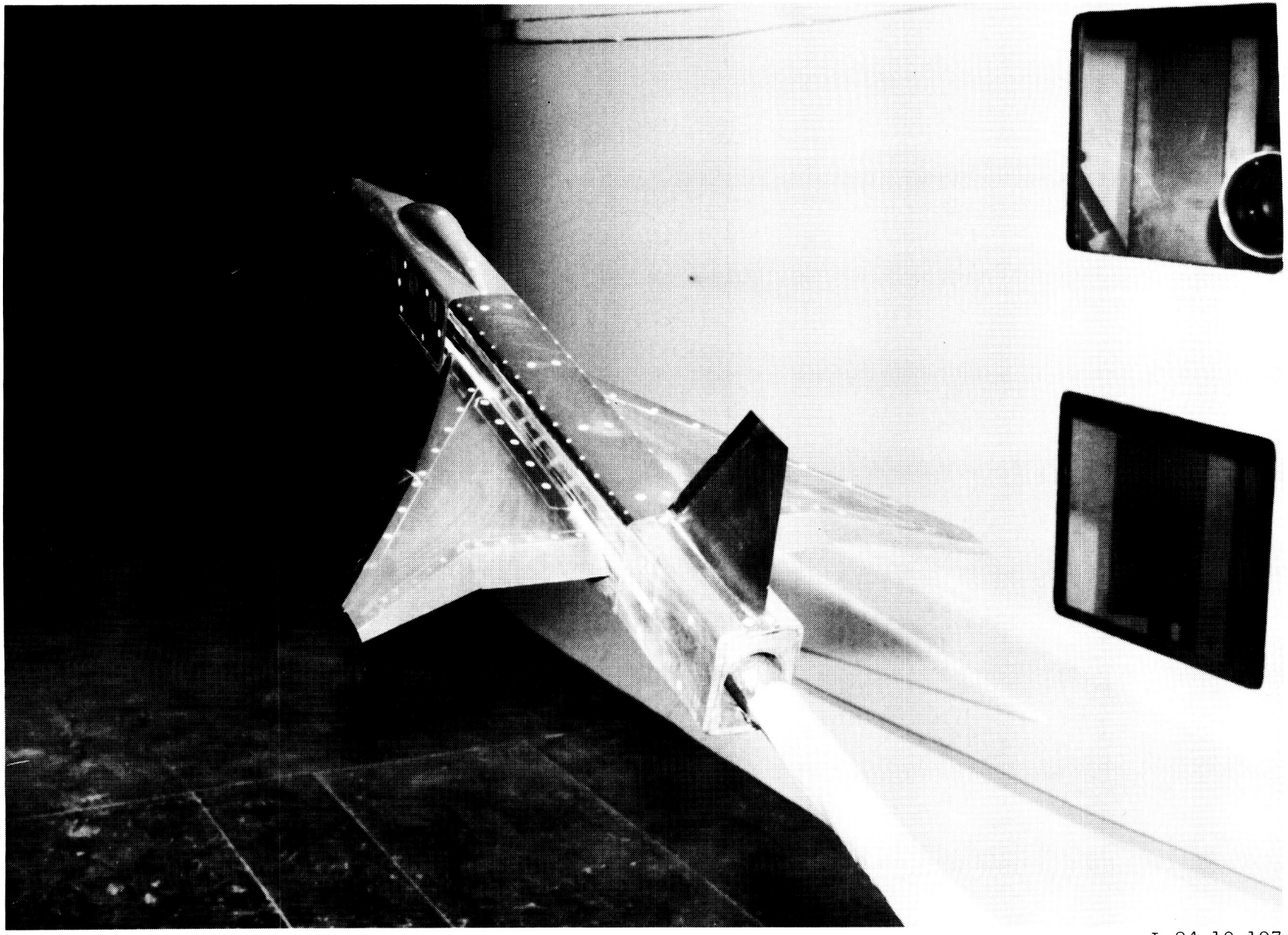

L-84-10,197

Figure 2.- Photograph of model in the Langley 7- by 10-Foot High-Speed Tunnel.

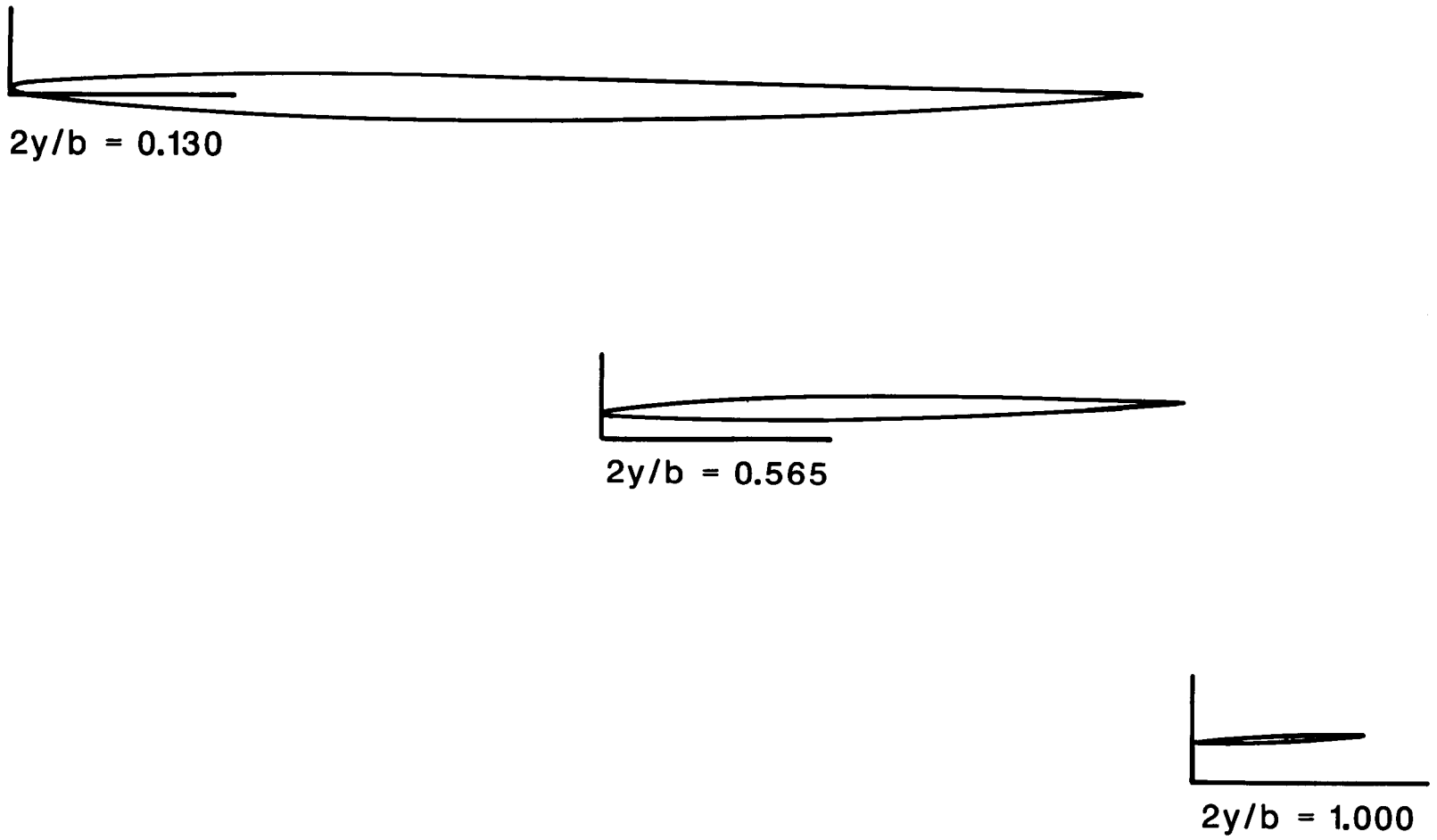

Figure 3.- Drawing of wing cross section at three spanwise locations.

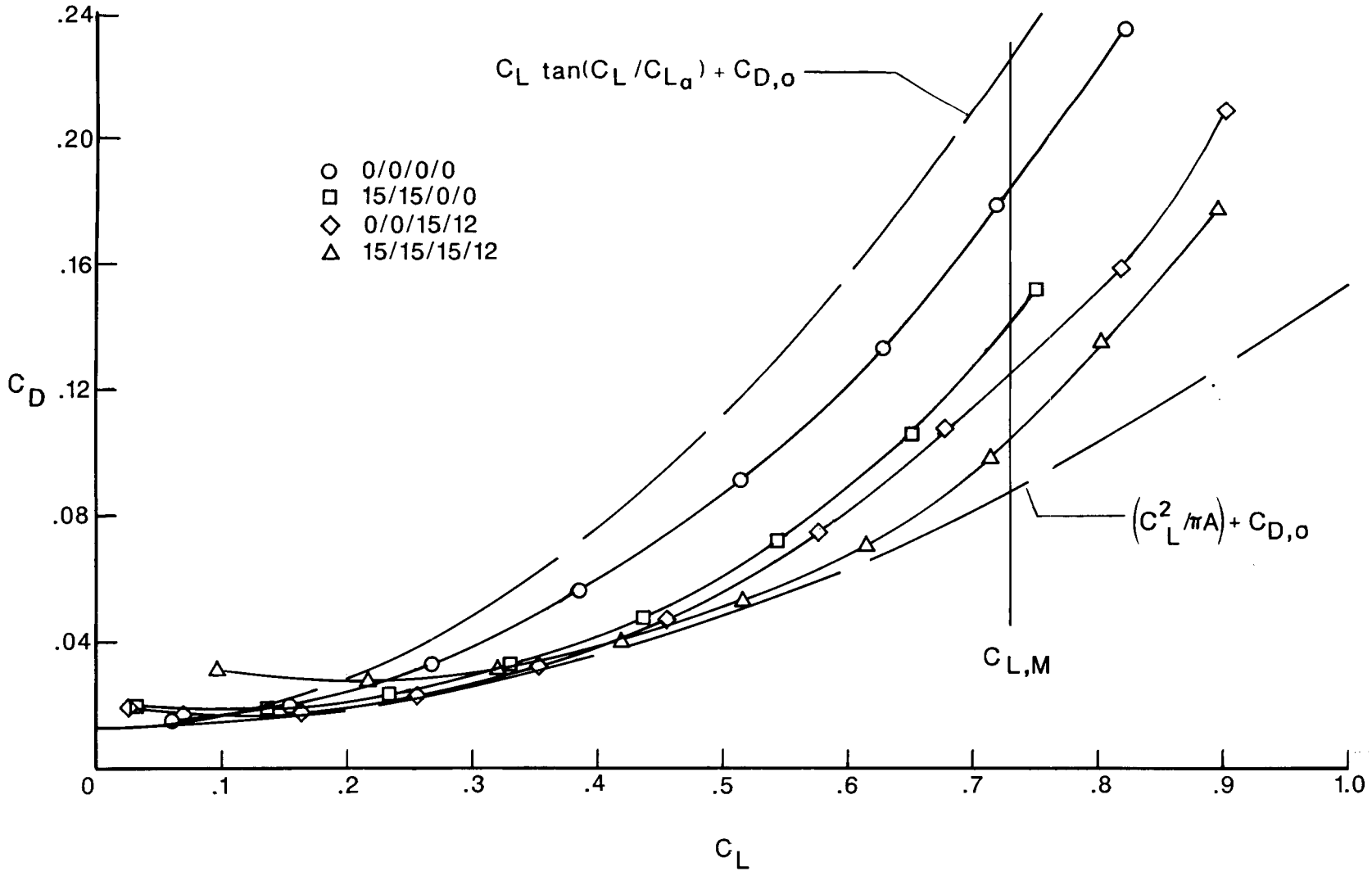

Figure 4.- Experimental drag polars of several flap deflection combinations. M = 0.5; flap A.

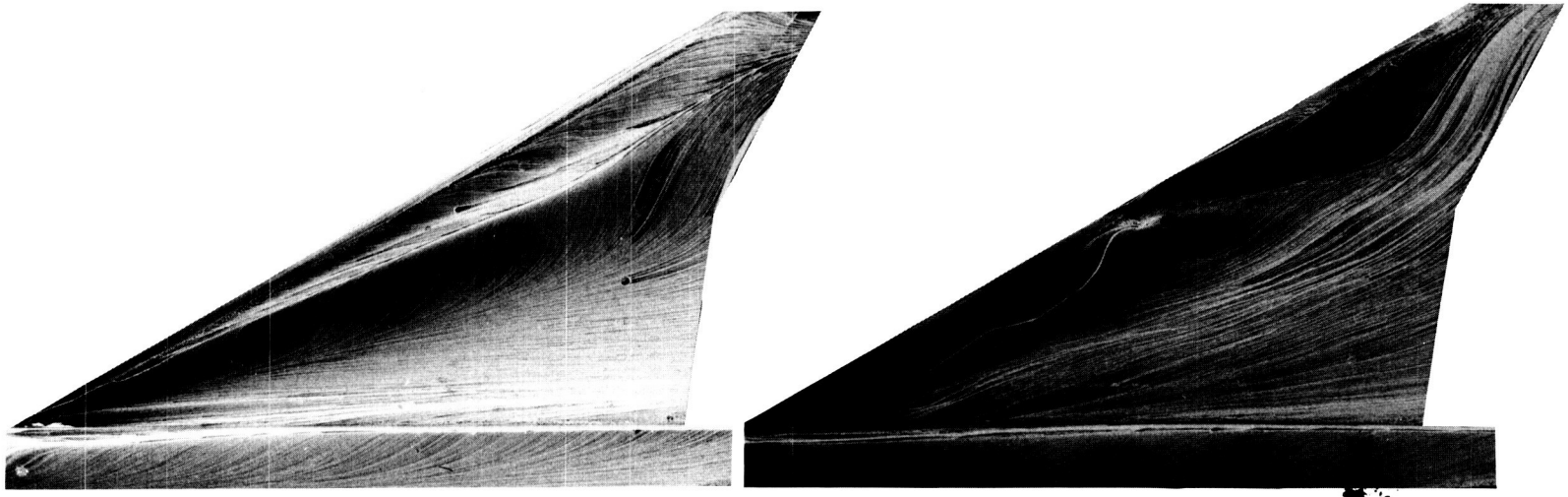

(a) 0/0/0/0. C_L = 0.72; α = 14.8°.

(b) 15/15/0/0. C_L = 0.75; α = 16.5°.

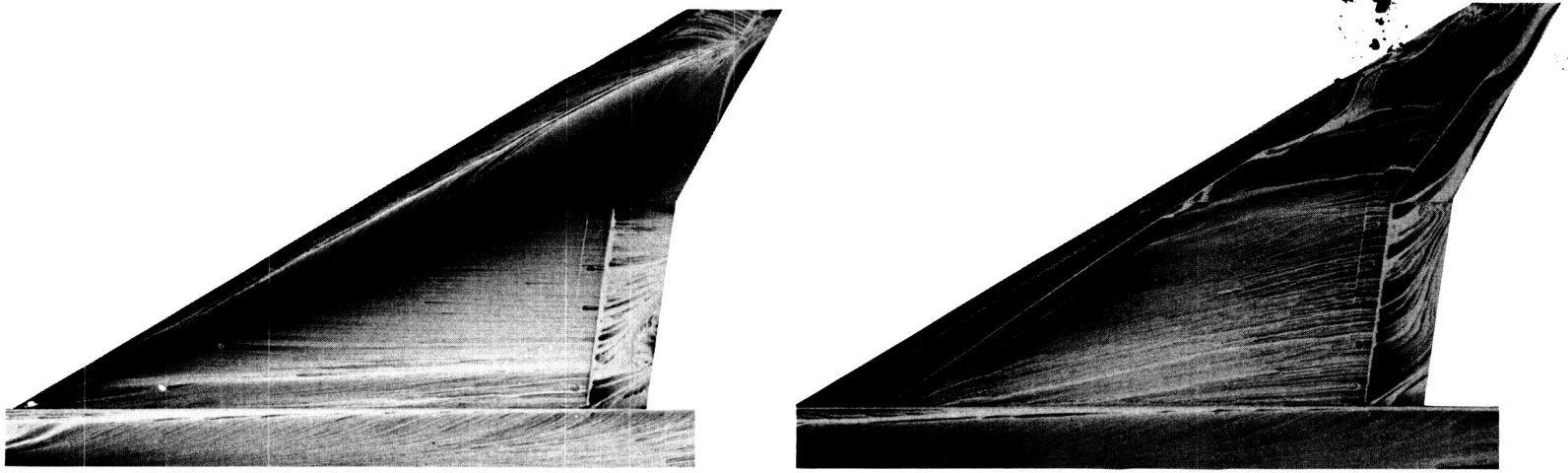

(c) 0/0/15/12. C_L = 0.68; α = 8.5°.

(d) 15/15/15/12. C_L = 0.71; α = 10.4°.

L-86-389

Figure 5.- Oil-flow photographs of wing showing four combinations of flap deflections. M = 0.5; flap A.

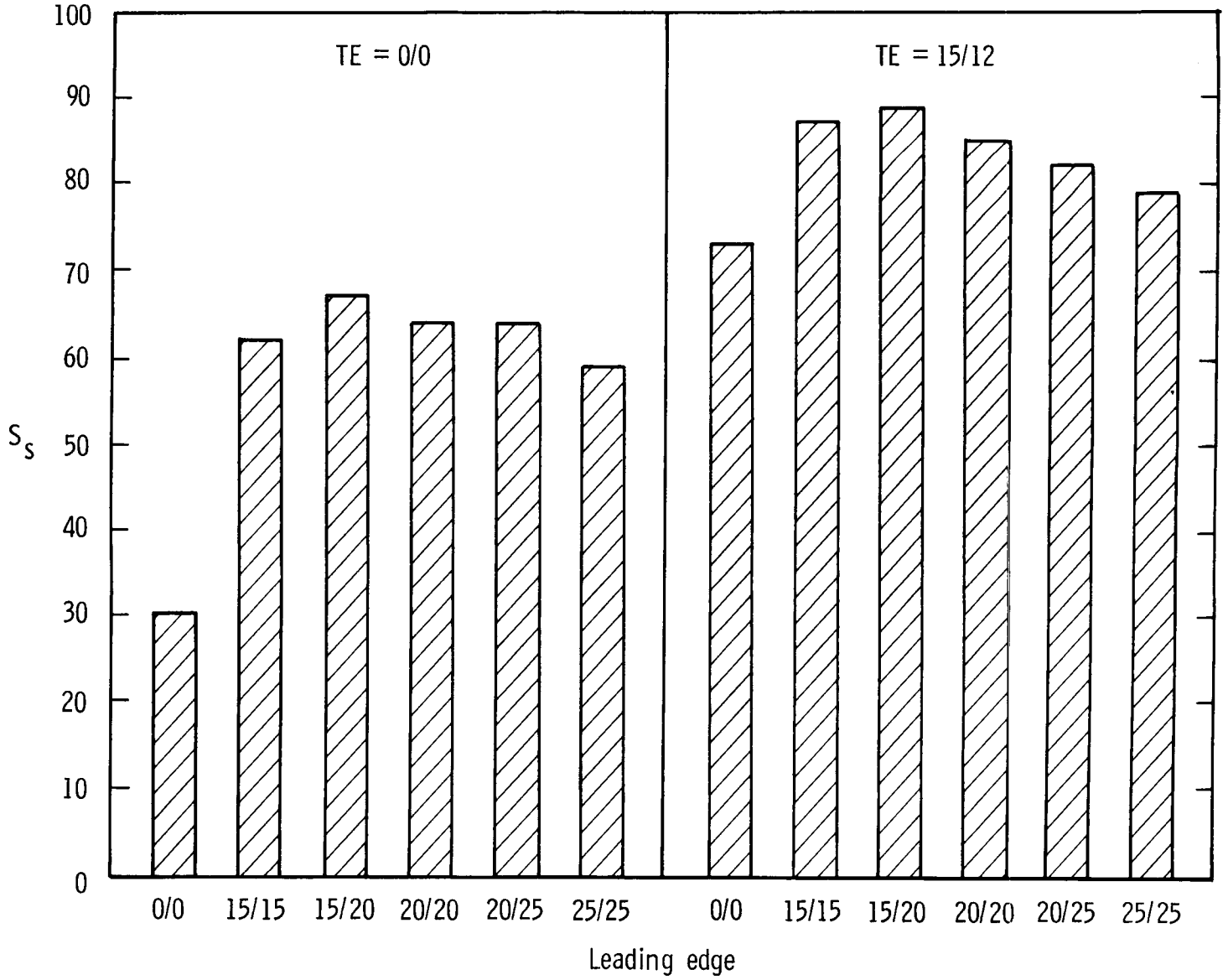

Figure 6.- Comparison of suction parameters for model with different flap deflections. C_L = 0.73; M = 0.5; flap A.

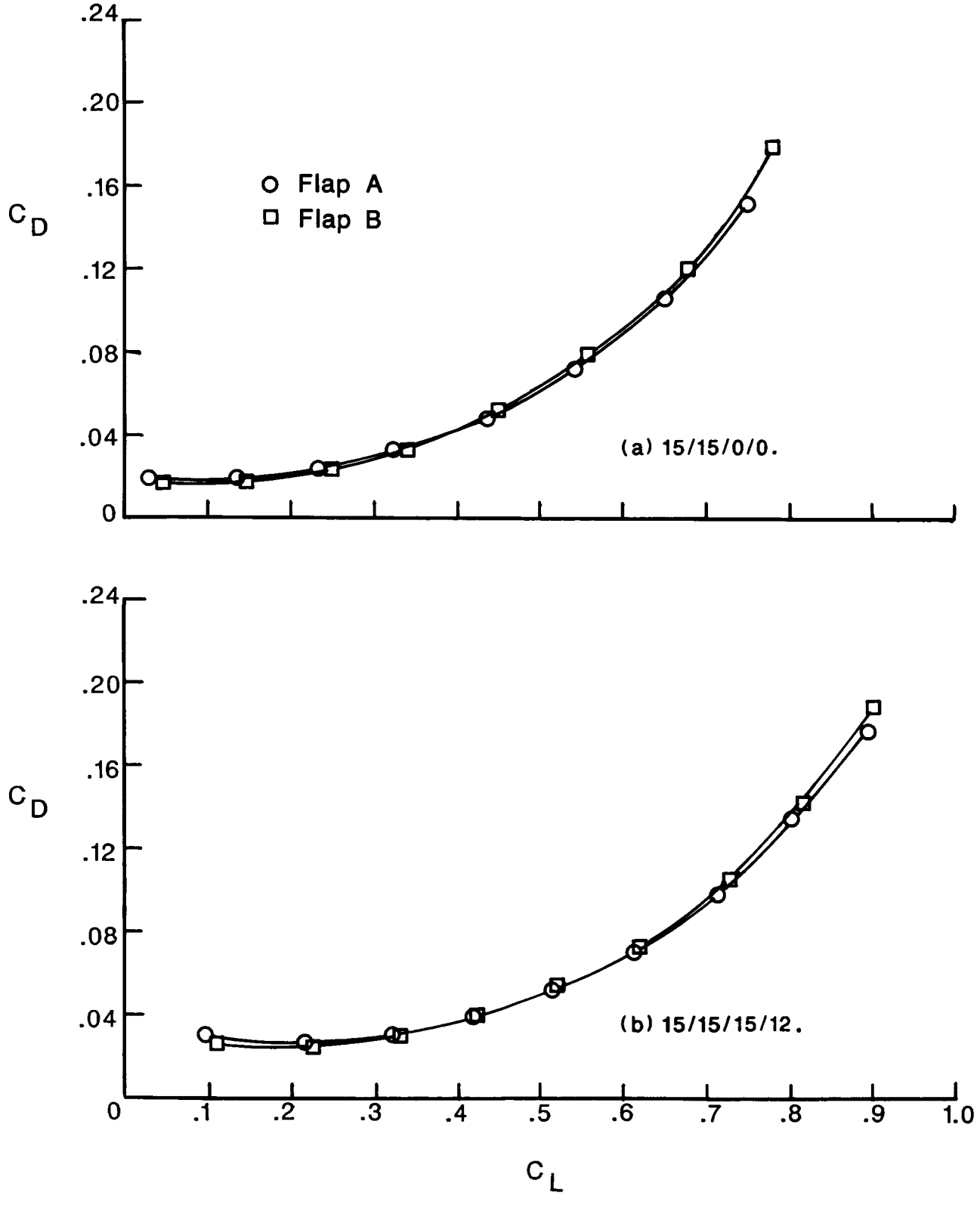

Figure 7.- Comparison of experimental drag polars for flaps A and B. M = 0.5.

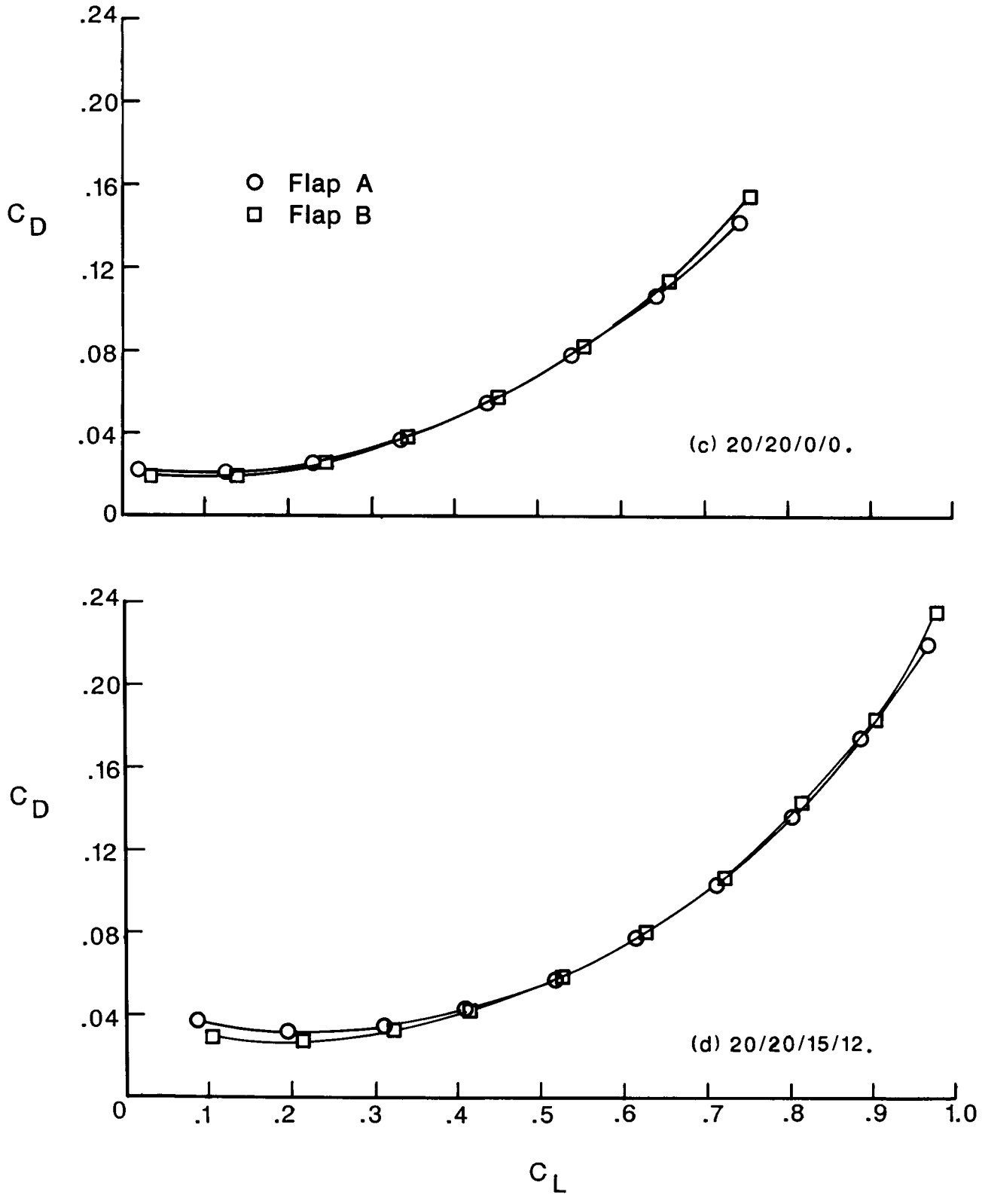

Figure 7.- Continued.

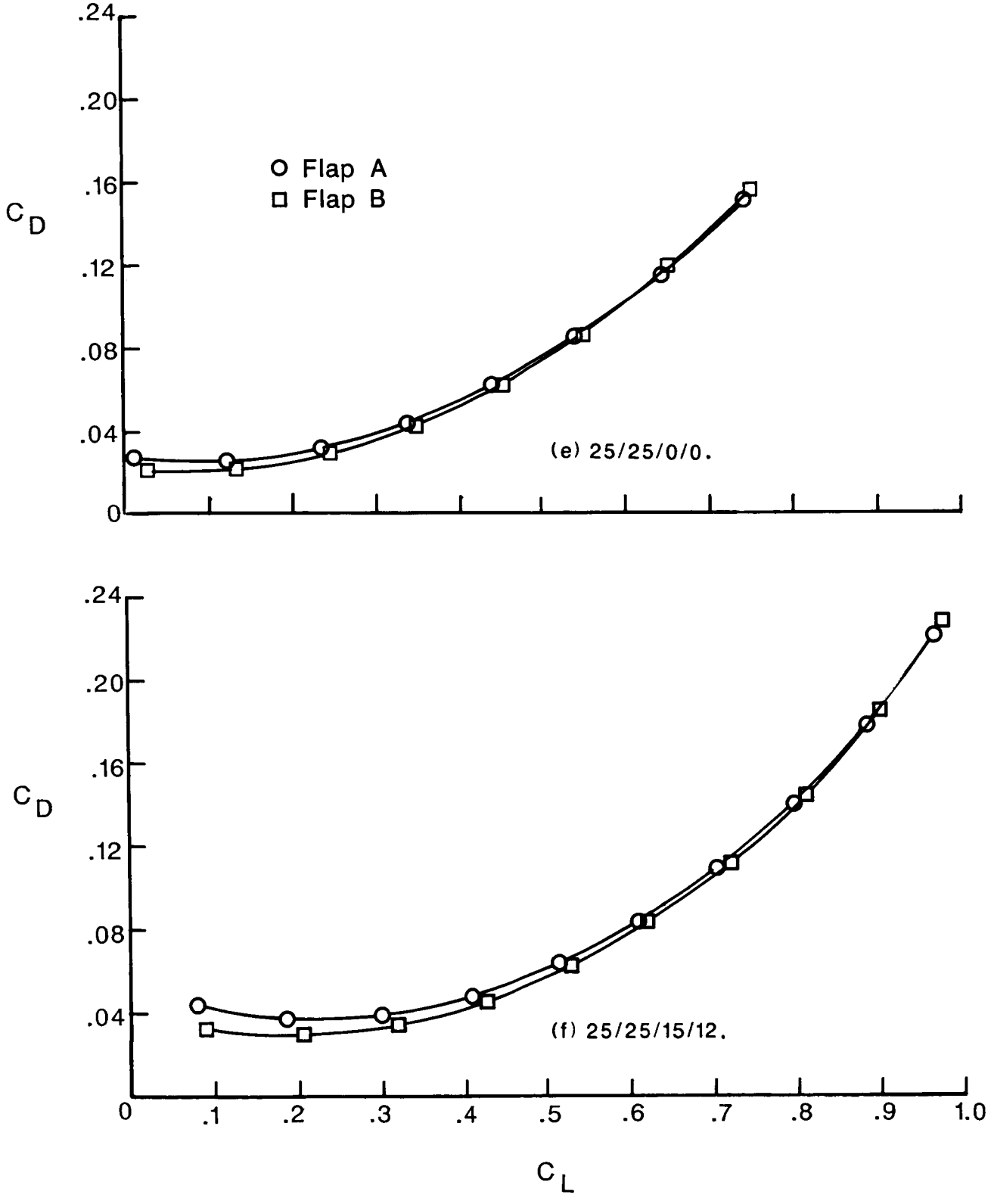

Figure 7.- Concluded.

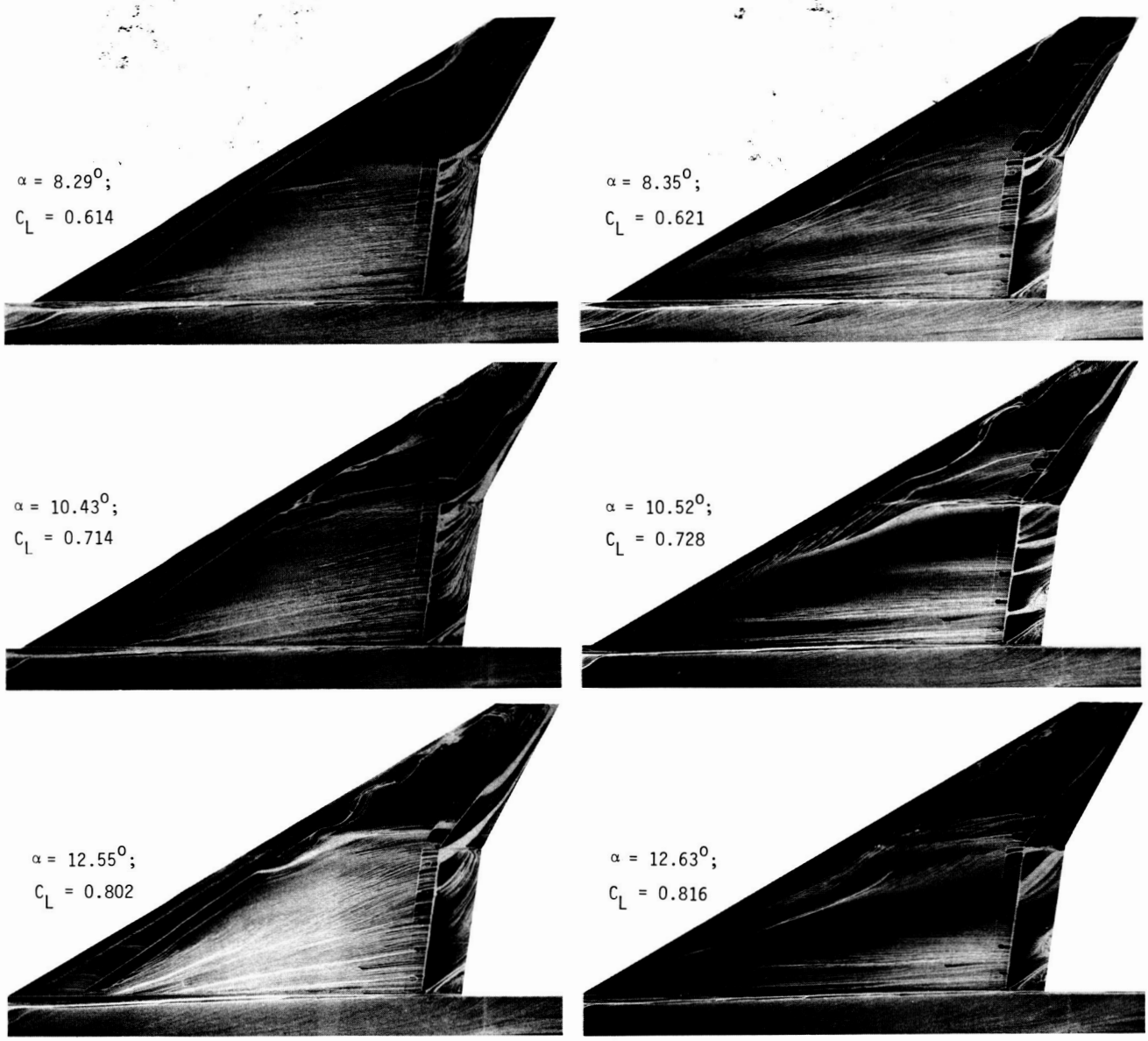

(a) Wing with flap A.

(b) Wing with flap B.

L-86-390

(a) Wing with flap A. (b) Wing with flap B.

Figure 8.- Oil-flow photographs of 15/15/15/12 configuration comparing flaps A and B. M = 0.5.

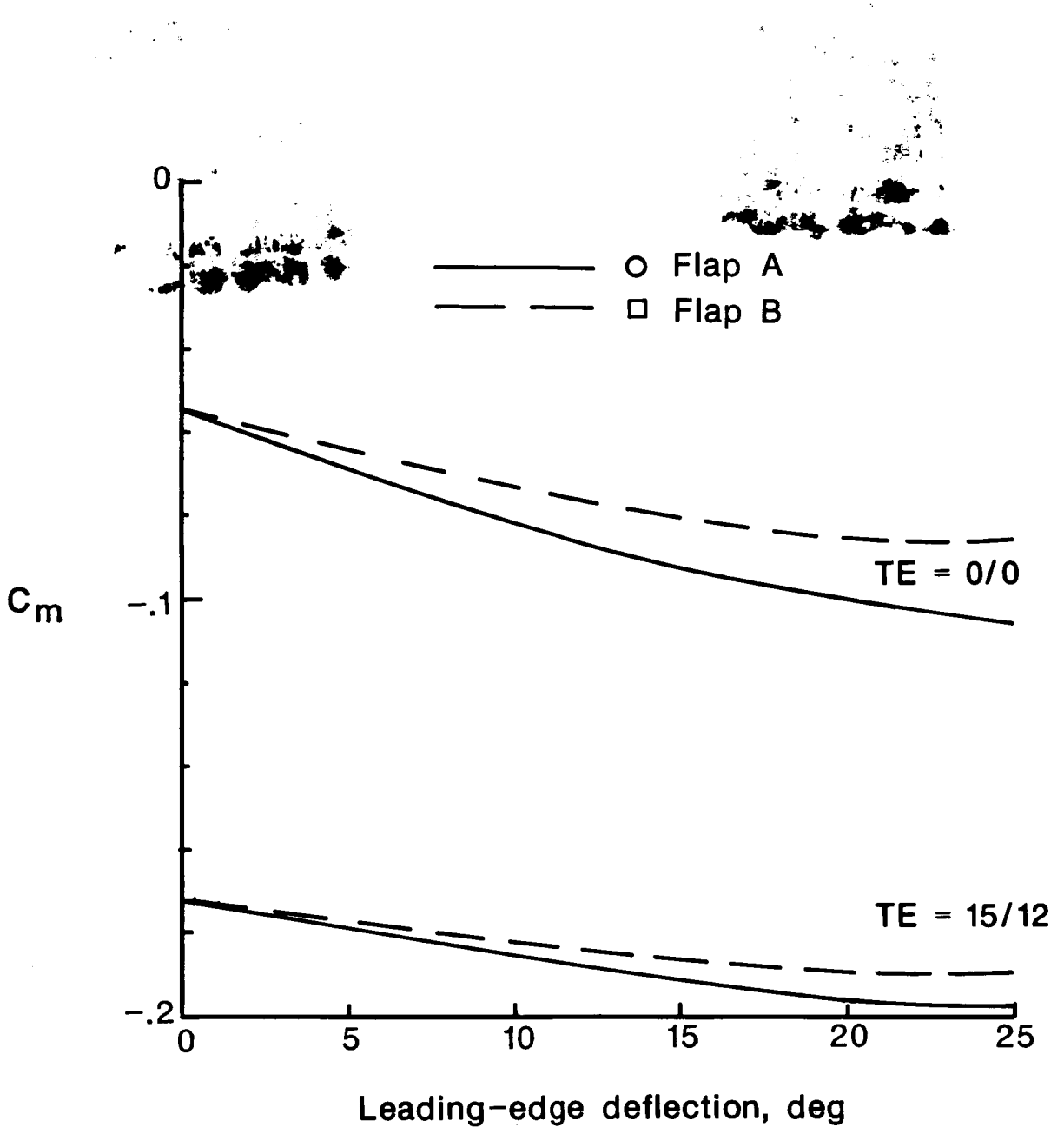

Figure 9.- Effect of flap deflections on experimental pitching-moment coefficient. $C_L = C_{L,M}$; M = 0.5.

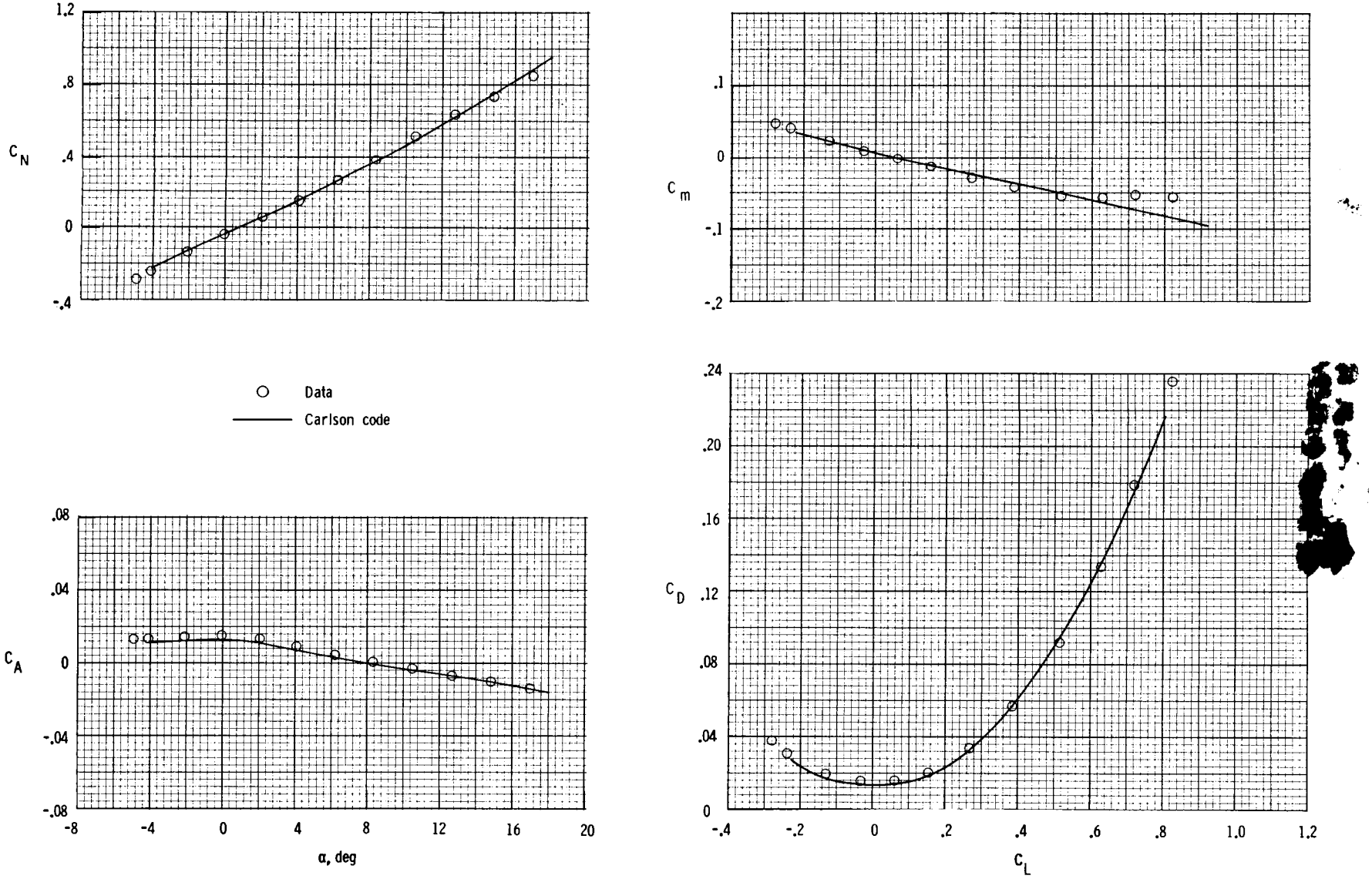

(a) 0/0/0/0.

Figure 10.- Comparison of experimental data with predictions from Carlson computer code.
M = 0.5; flap A; IVOROP = 1.

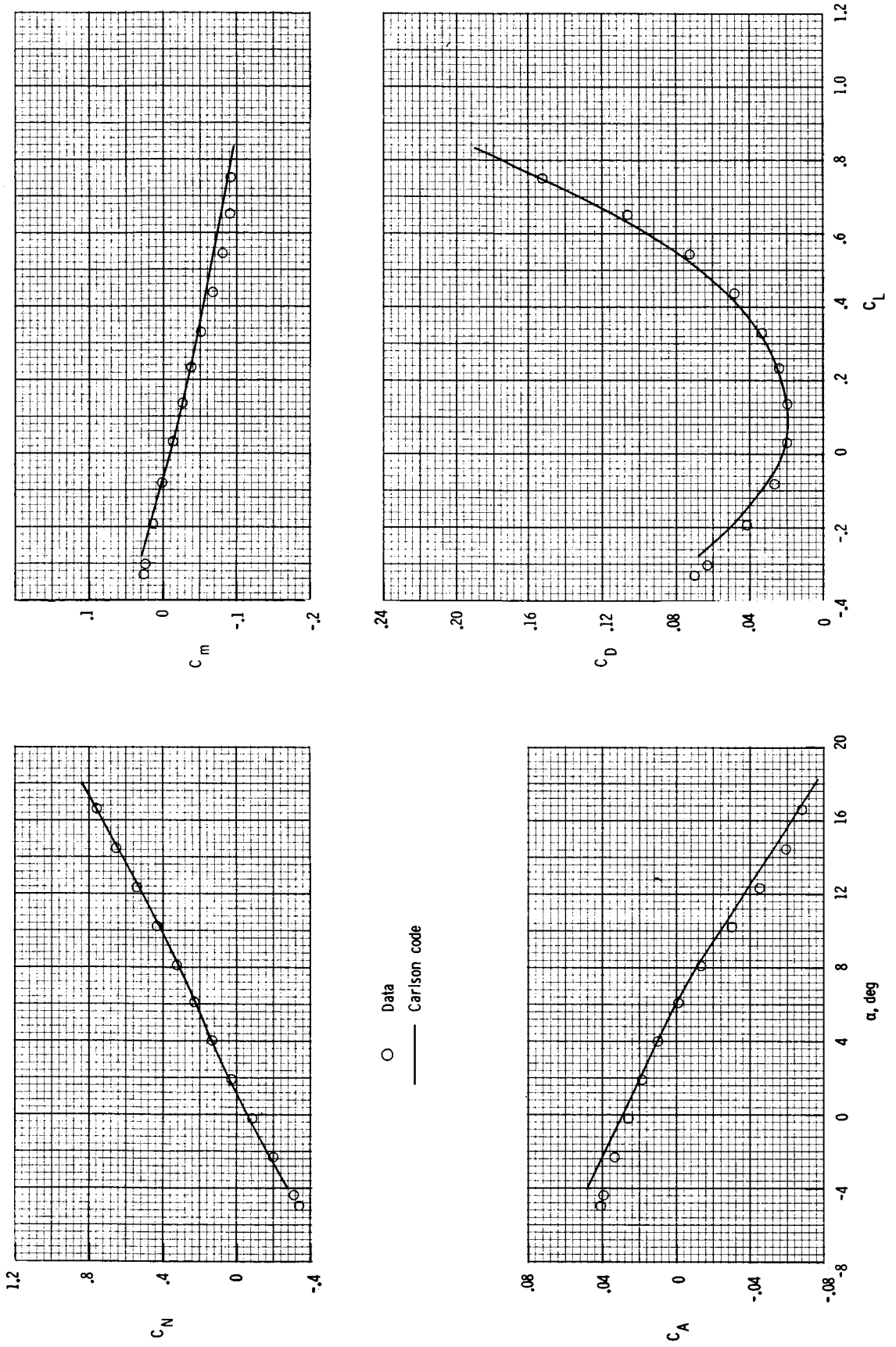

(b) 15/15/0/0.

Figure 10.- Continued.

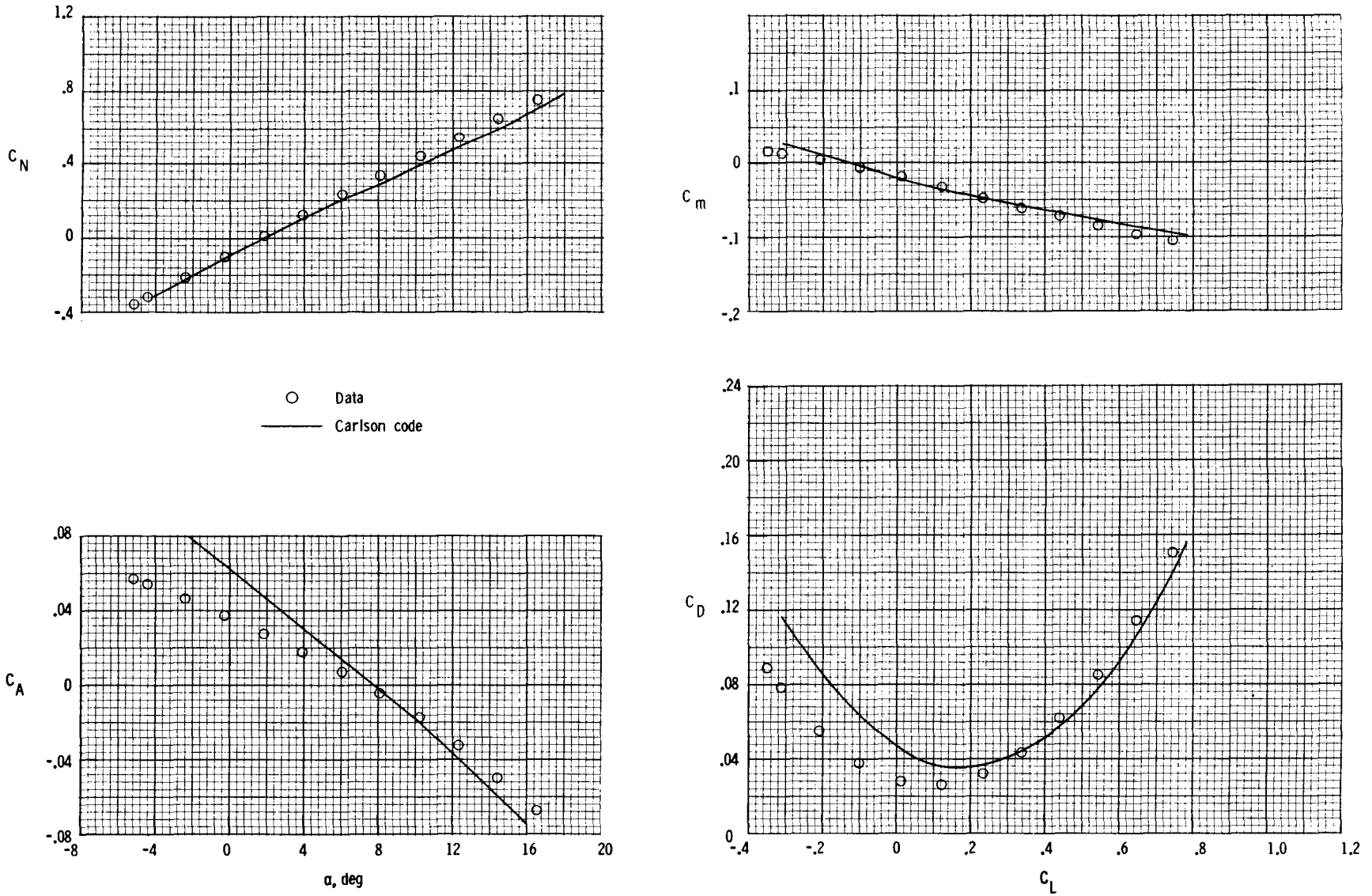

(c) 25/25/0/0.

Figure 10.- Continued.

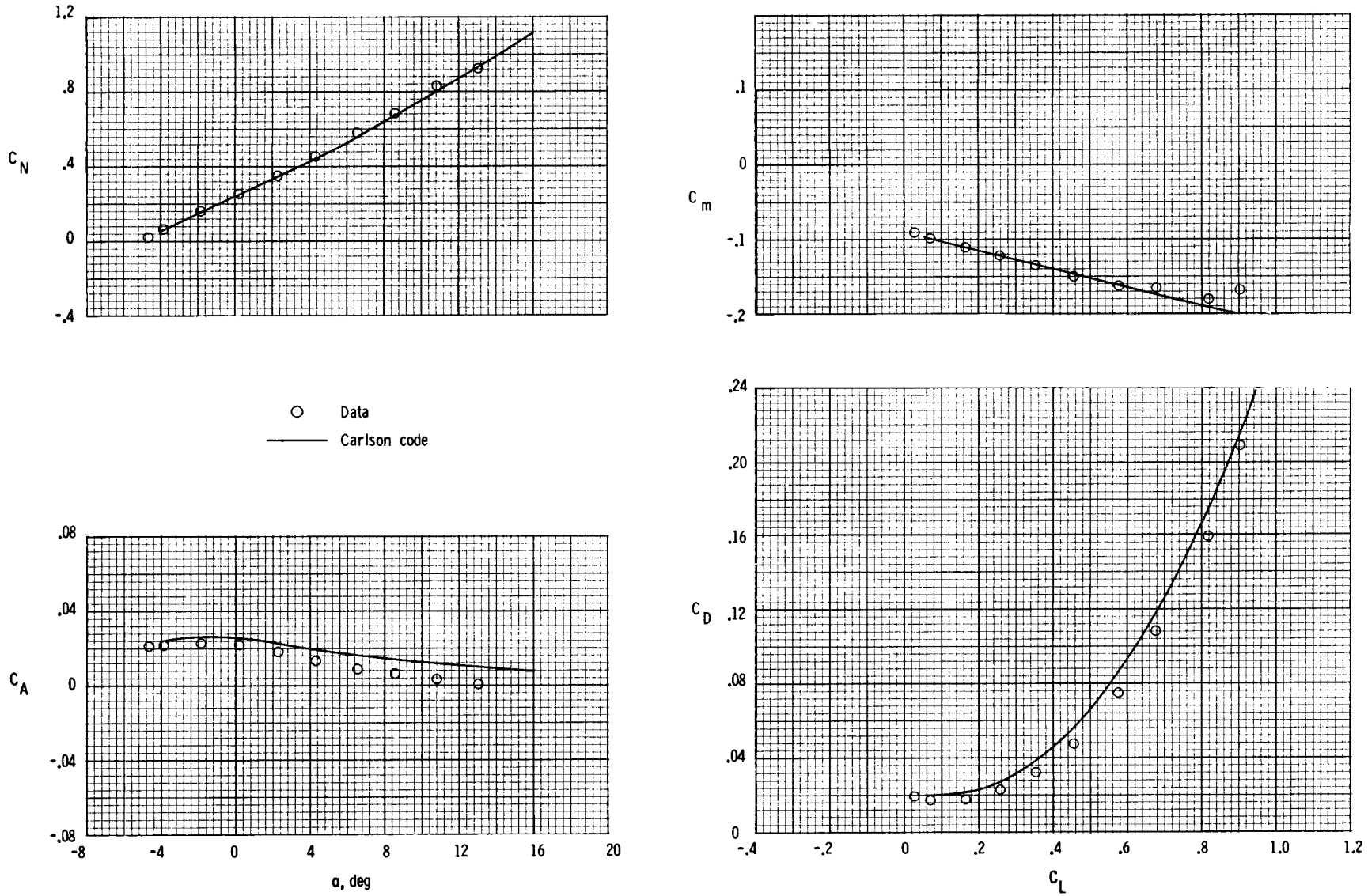

(d) 0/0/15/12.

Figure 10.- Continued.

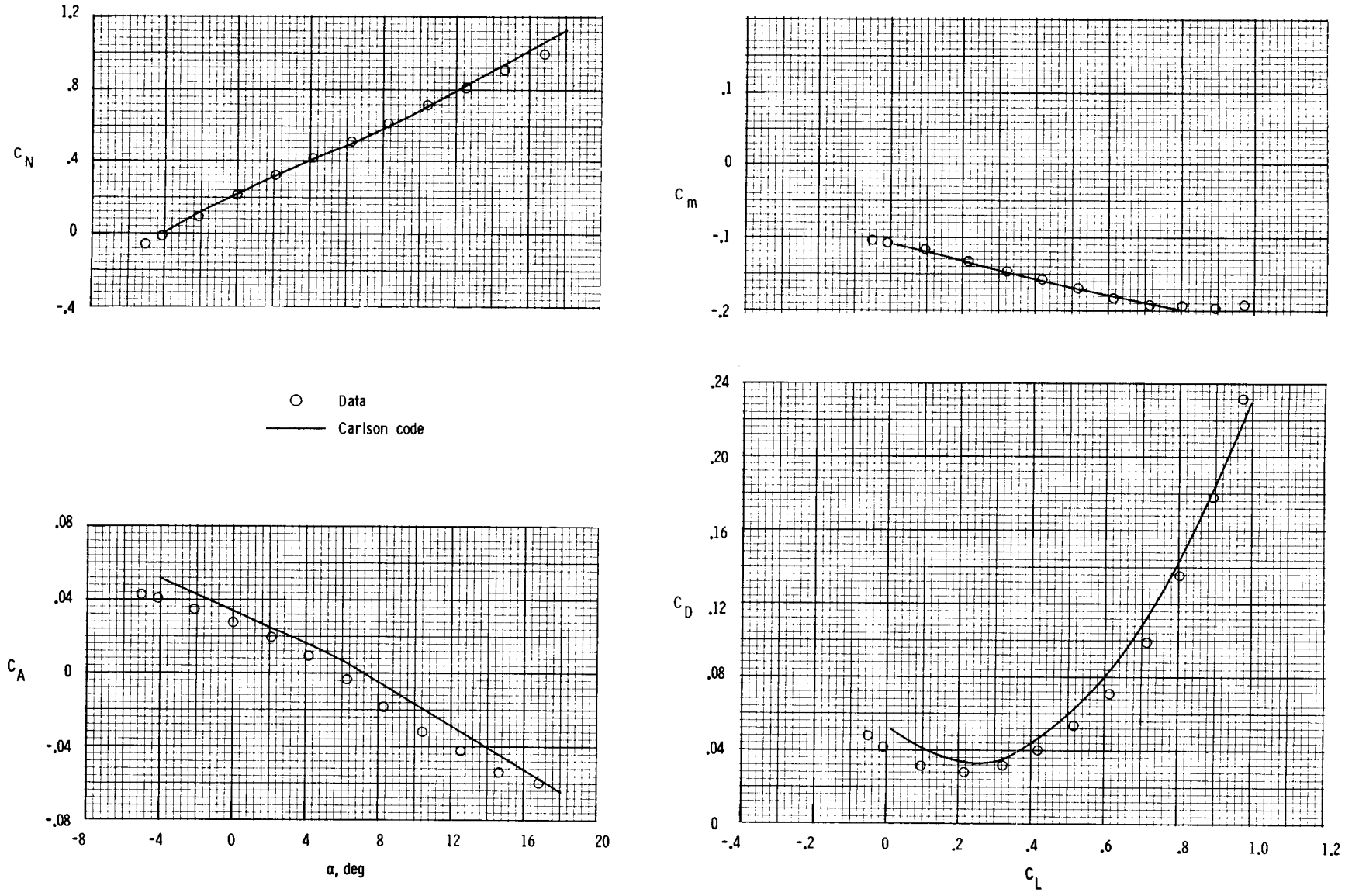

(e) 15/15/15/12.

Figure 10.- Continued.

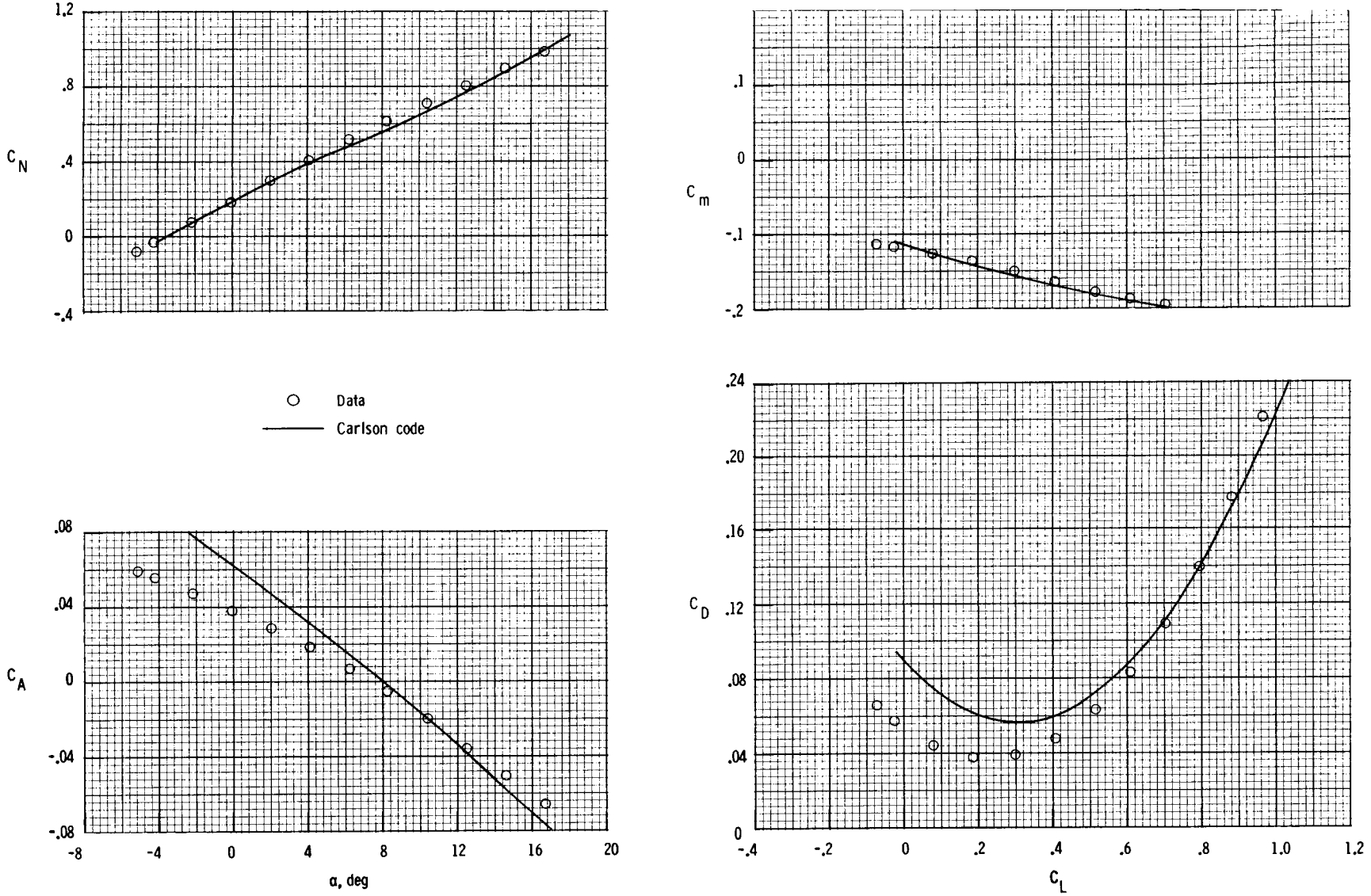

(f) 25/25/15/12.

Figure 10.- Concluded.

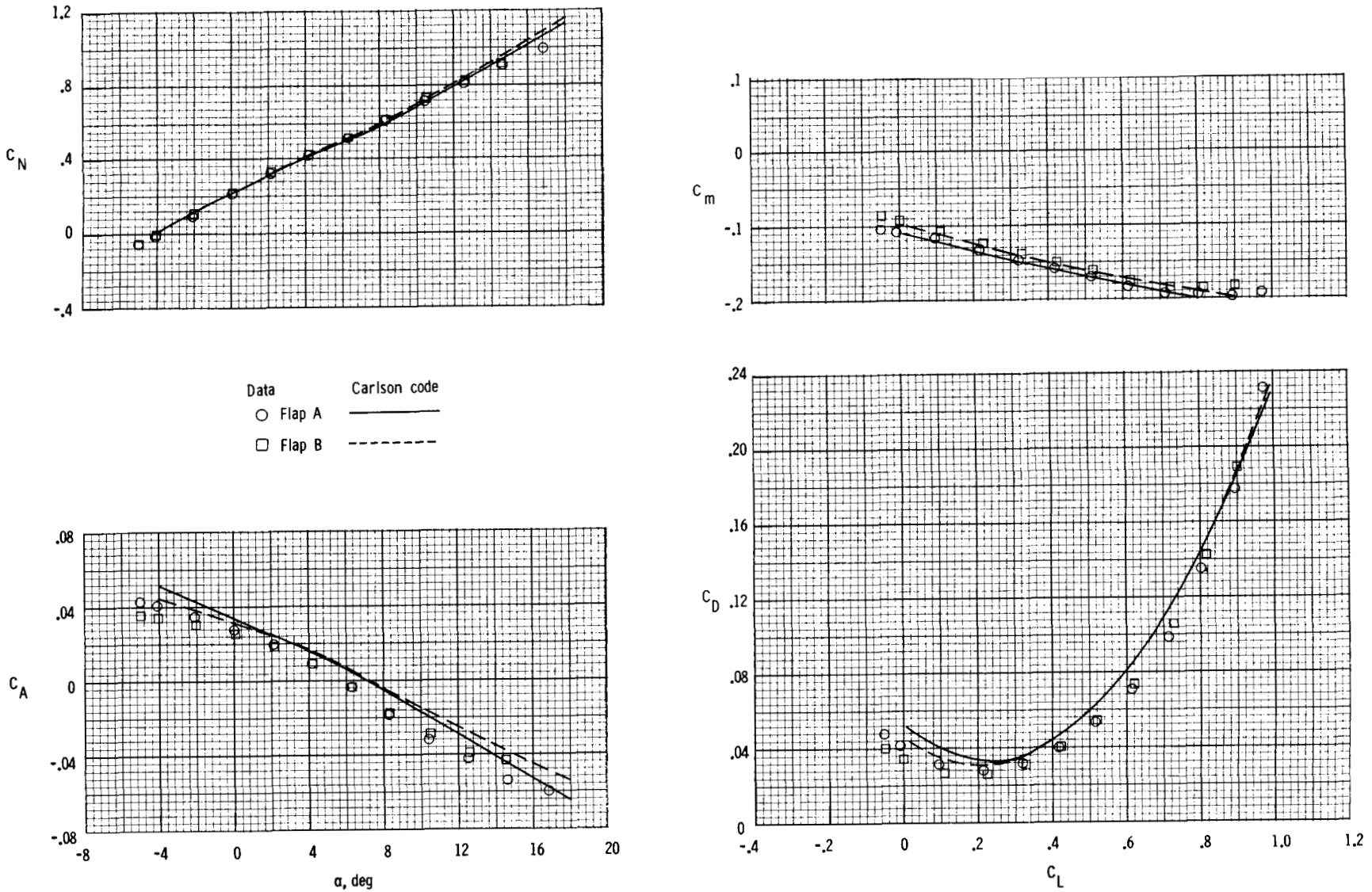

Figure 11.- Comparison of data and theory for 15/15/15/12 configuration for flaps A and B. M = 0.5; IVOROP = 1.

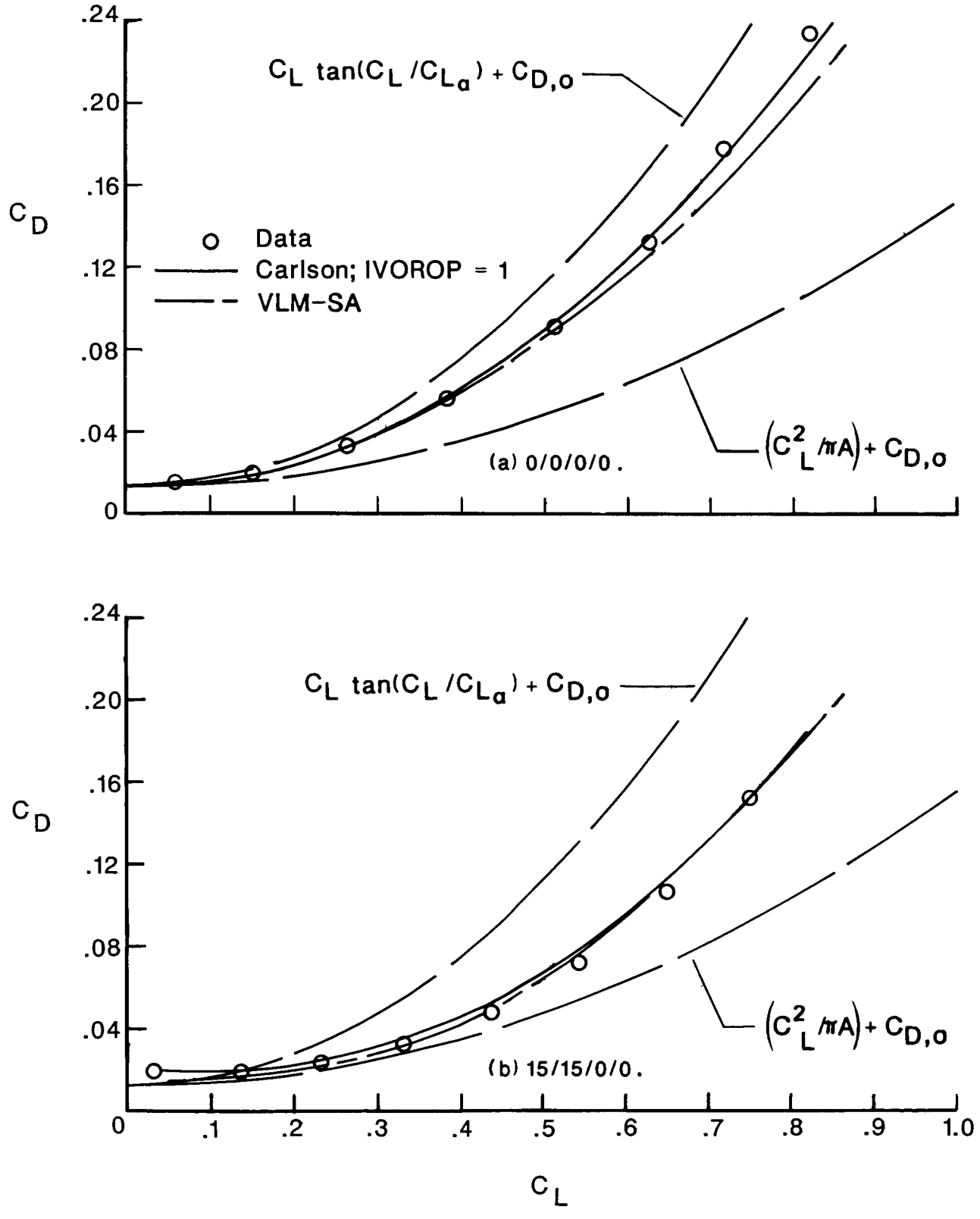

Figure 12.- Comparison of experimental and theoretical drag polars. M = 0.5; flap A.

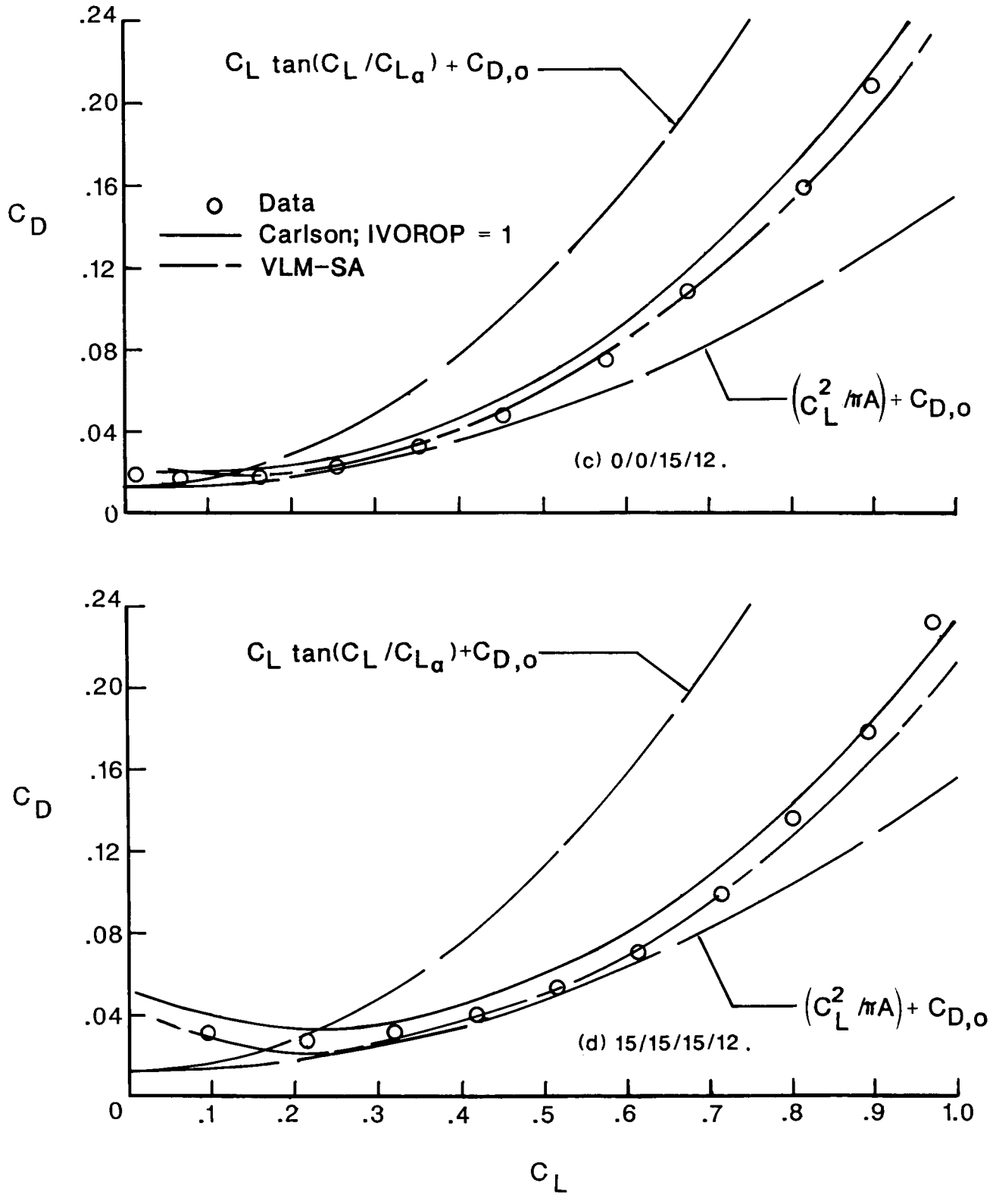

Figure 12.- Concluded.

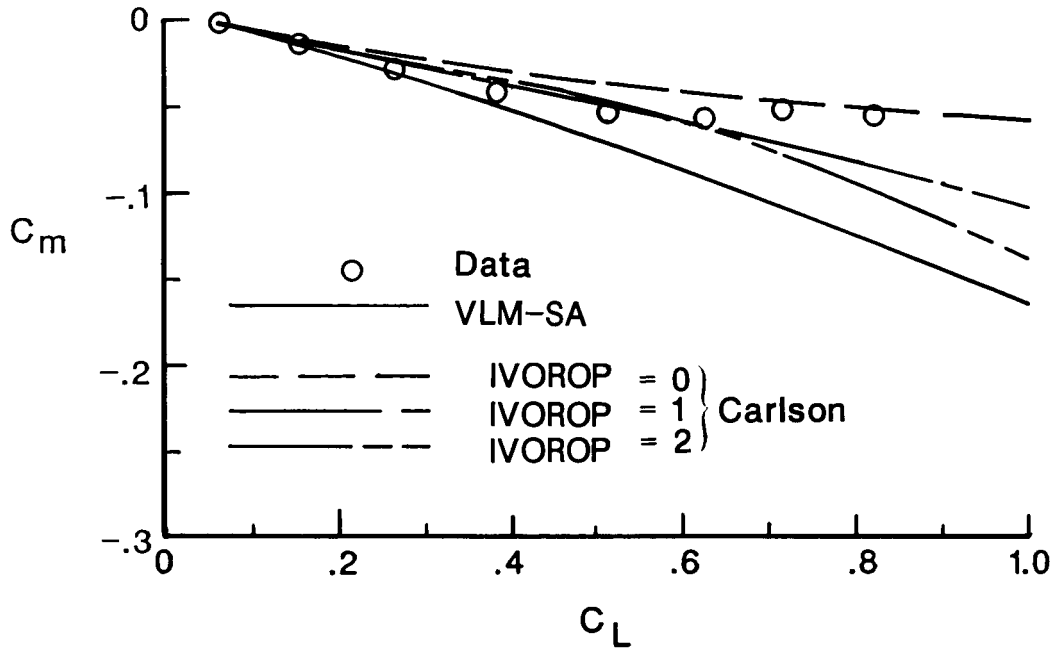

(a) 0/0/0/0.

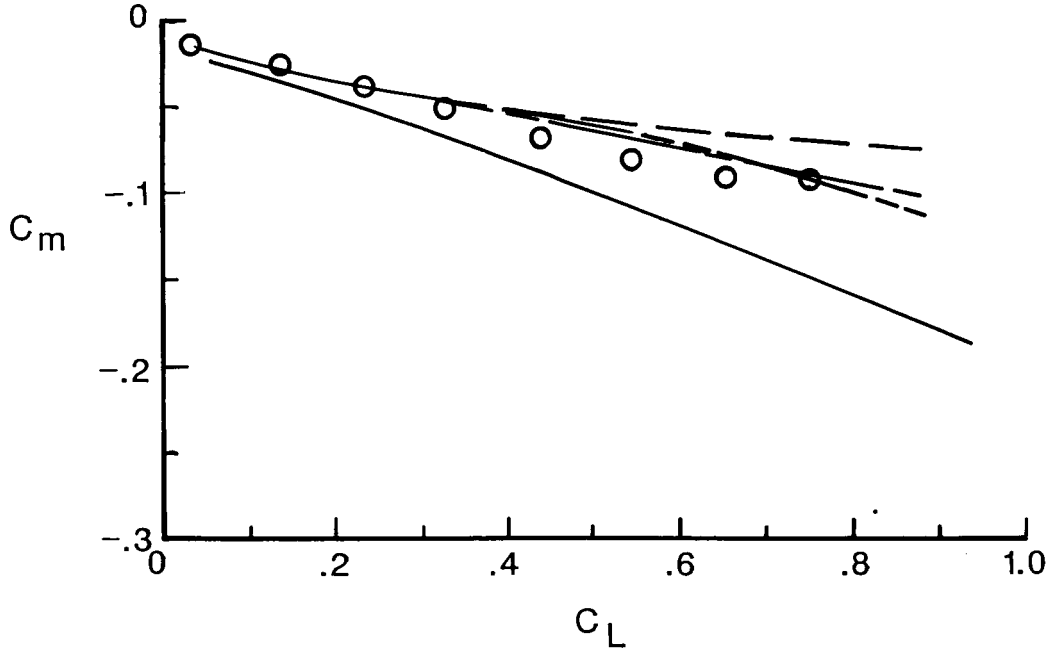

(b) 15/15/0/0.

Figure 13.- Comparison of experimental and theoretical pitching-moment coefficients. M = 0.5; flap A.

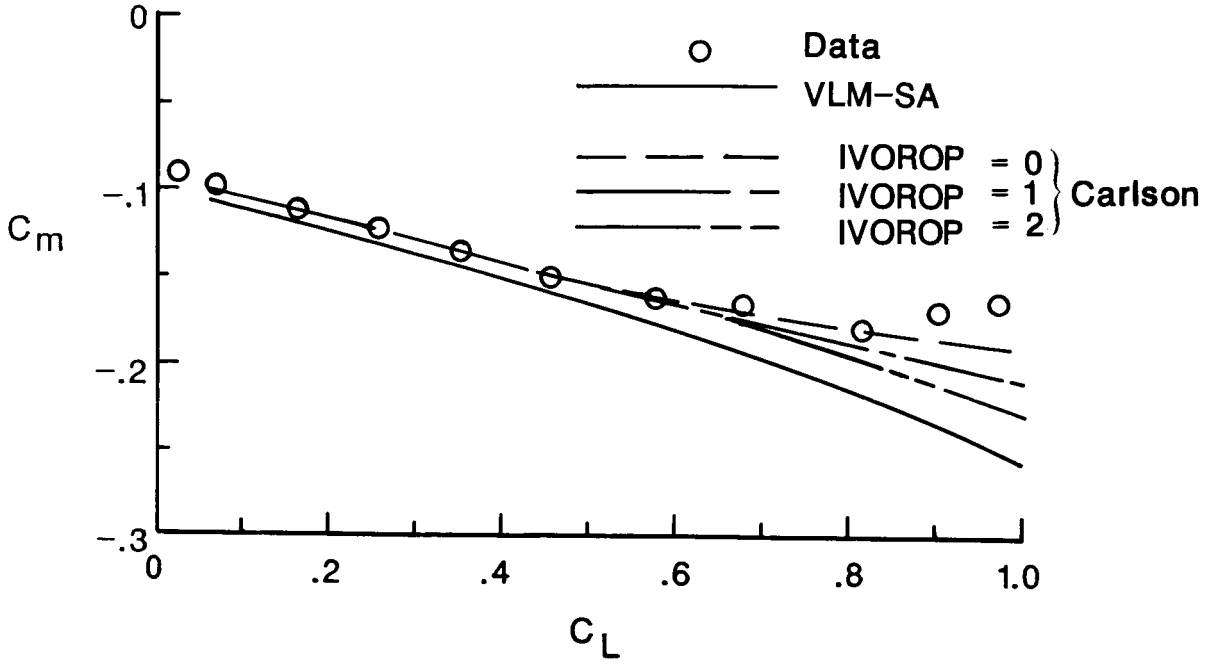

(c) 0/0/15/12.

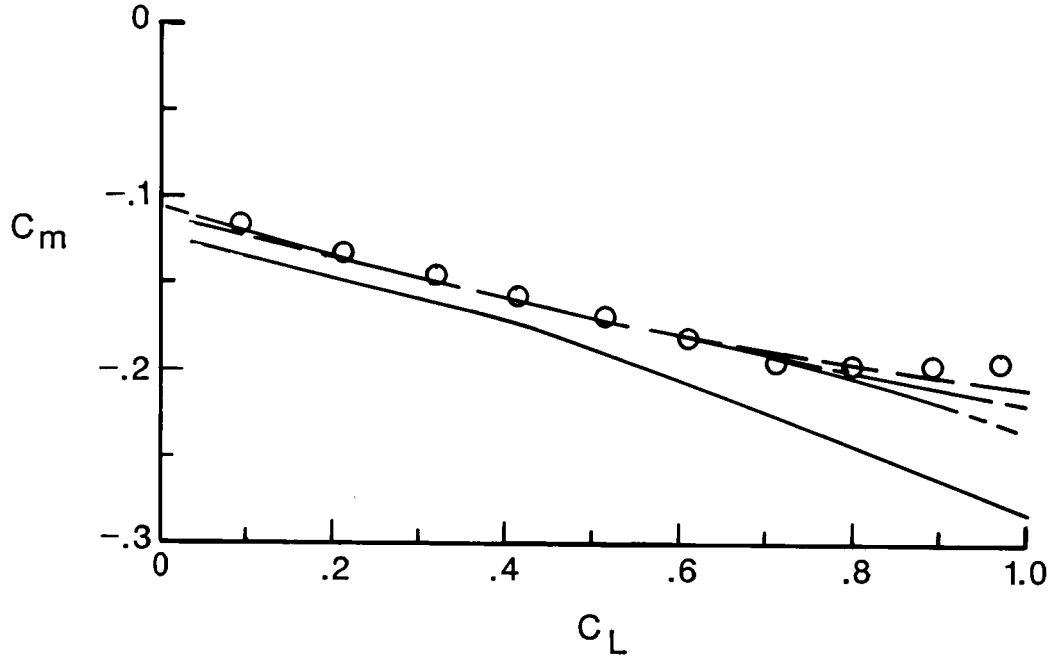

(d) 15/15/15/12.

Figure 13.- Concluded.

APPENDIX A

PLOTS OF ALL EXPERIMENTAL DATA

Plots of the longitudinal aerodynamic characteristics for all configurations tested at all three Mach numbers (0.3, 0.5, and 0.7) are presented in this appendix as figures A1 to A4.

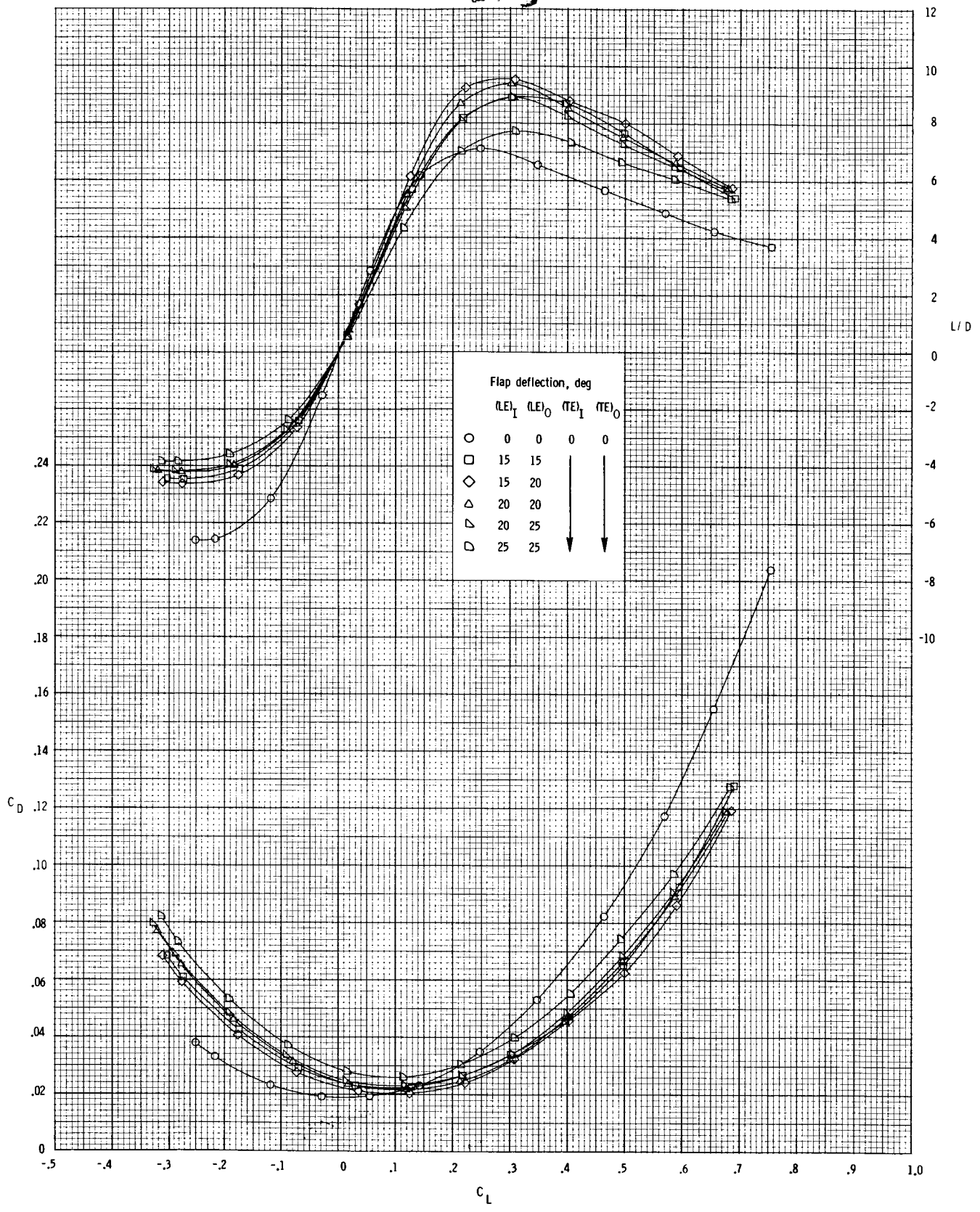

(a) M = 0.3.

Figure A1.- Effect of leading-edge deflection with no trailing-edge deflection for flap A.

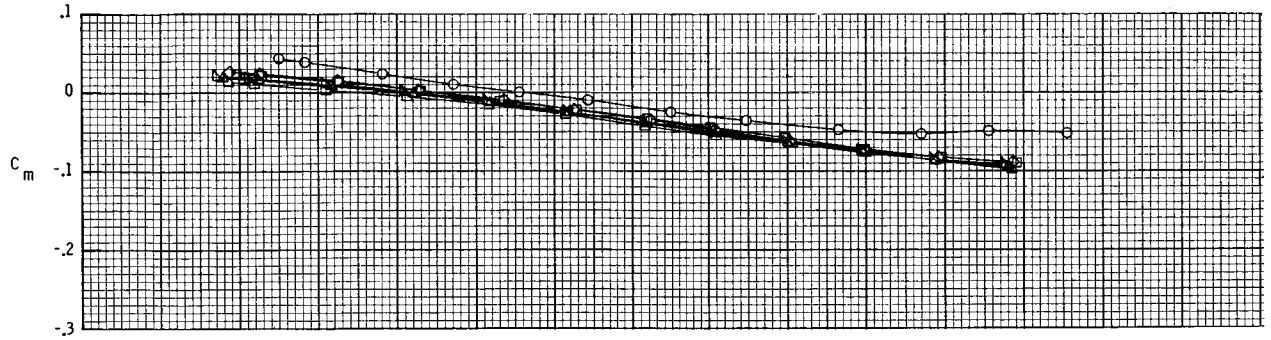

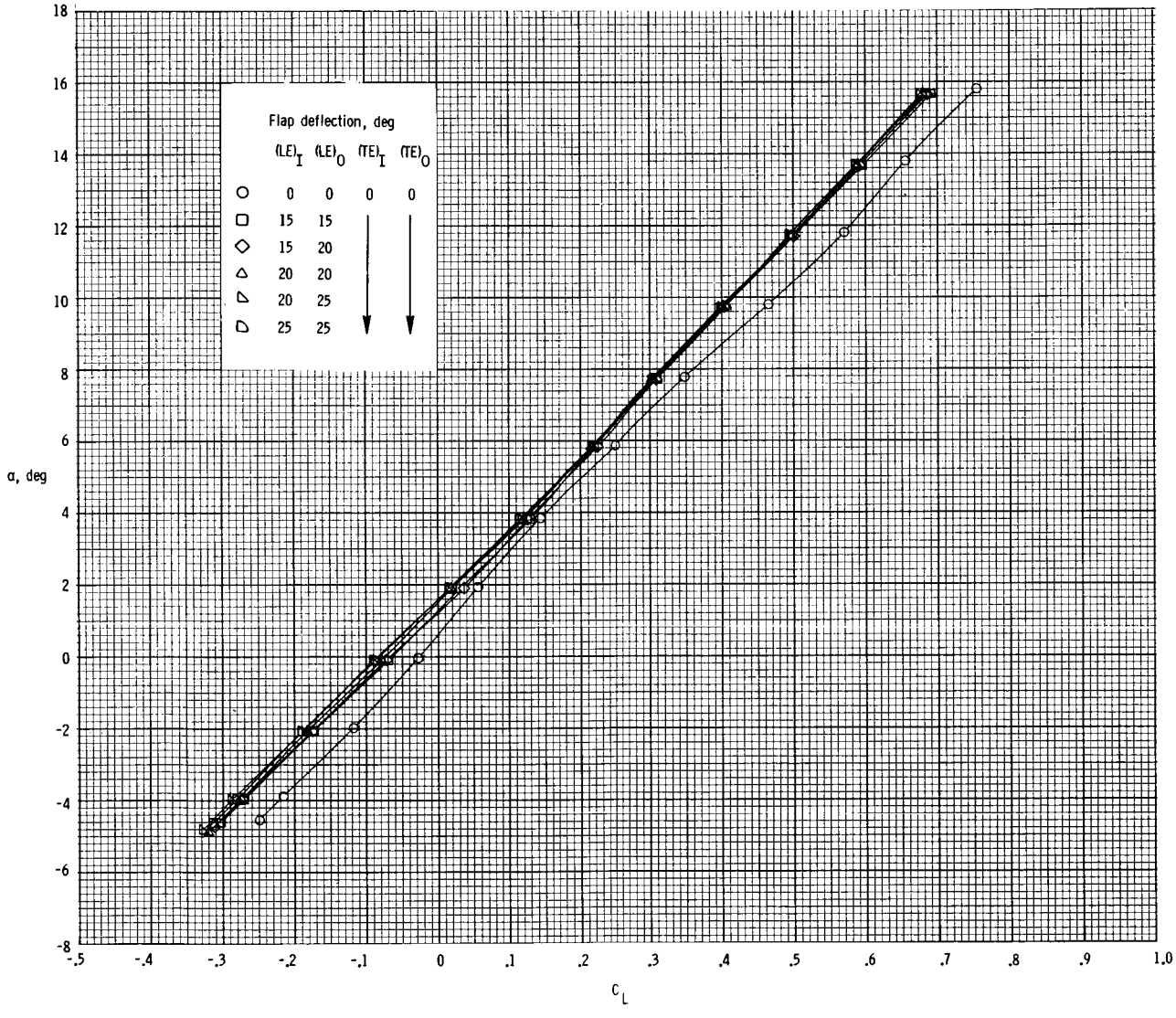

(a) Concluded.

Figure A1.- Continued.

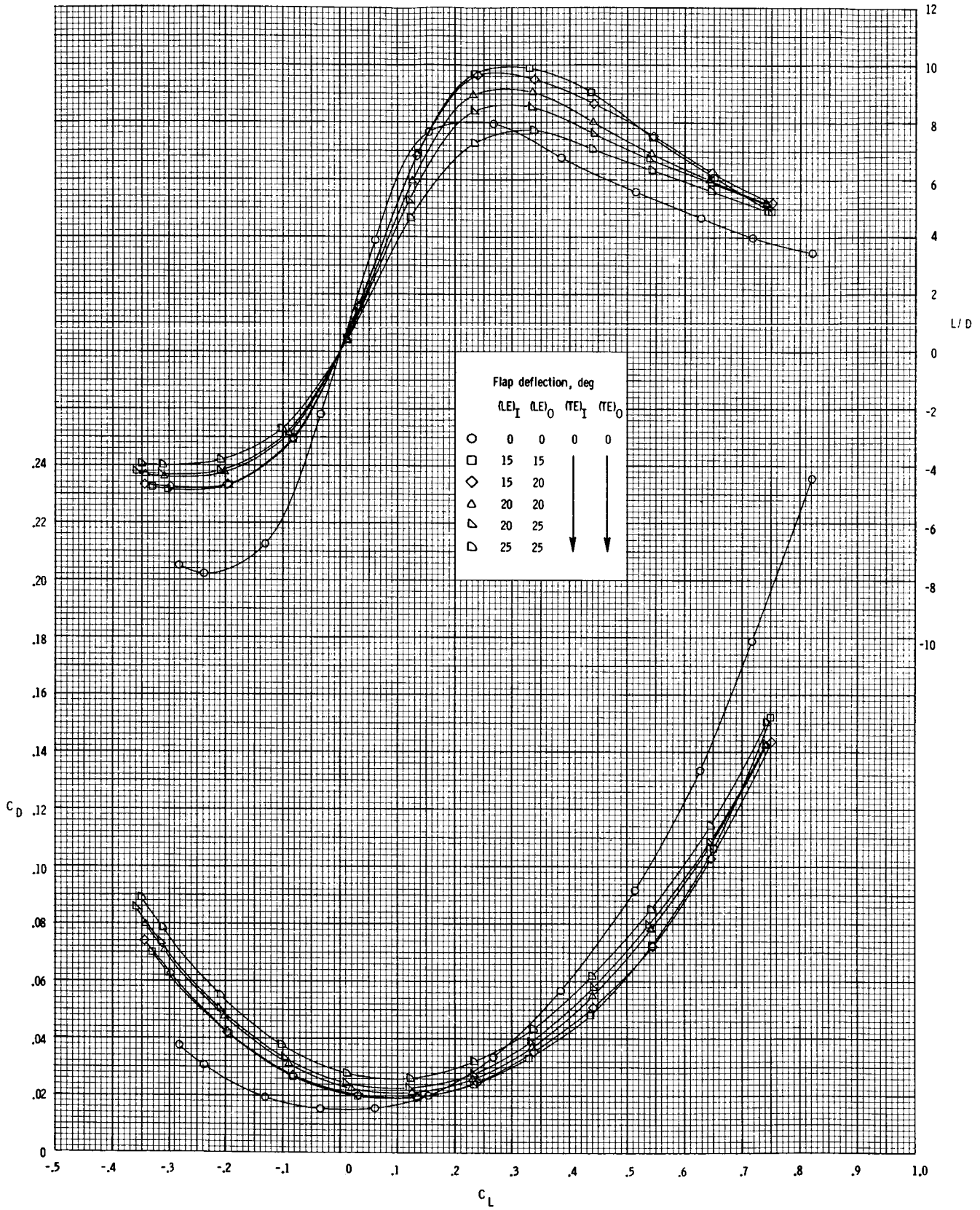

(b) M = 0.5.

Figure A1.- Continued.

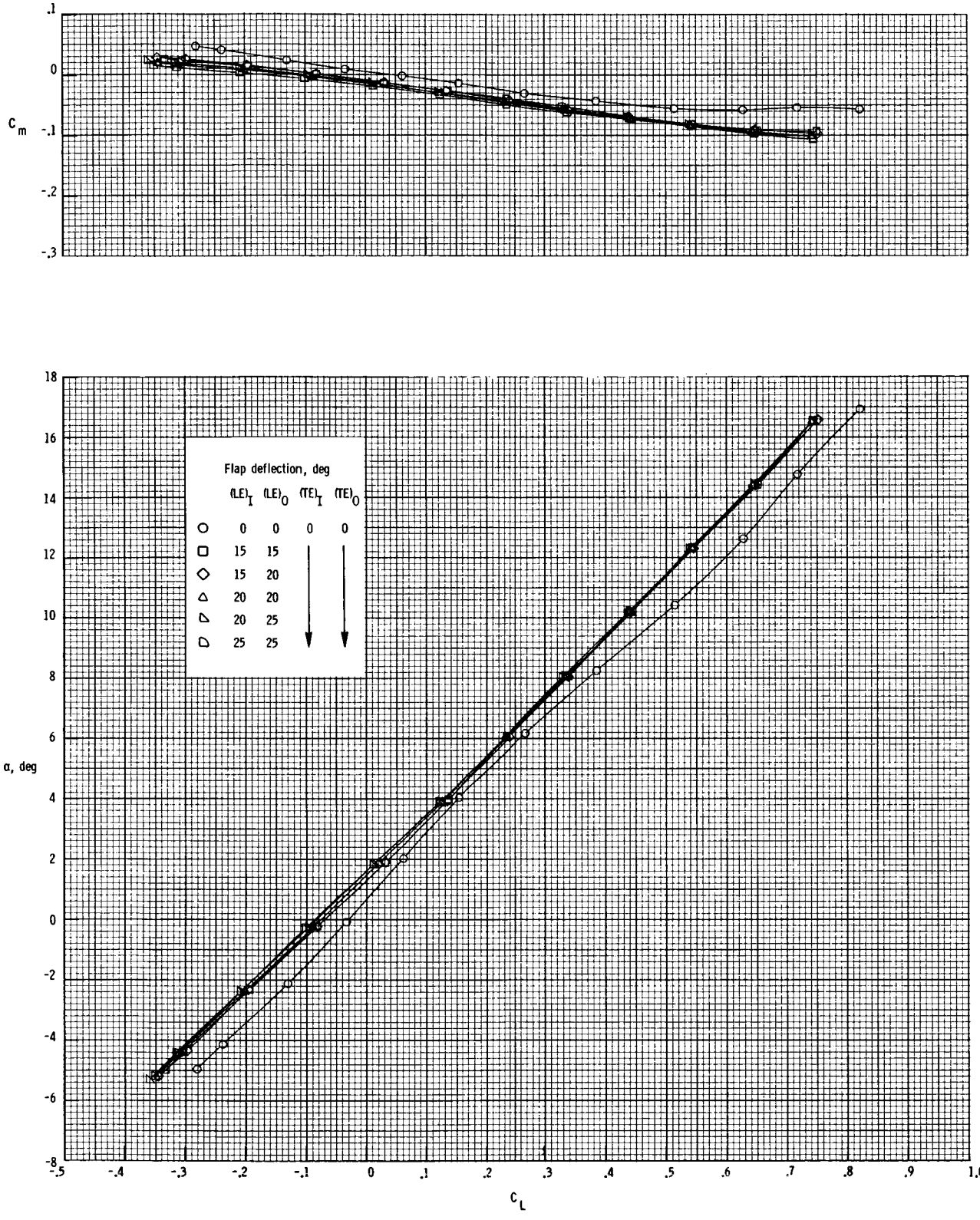

(b) Concluded.

Figure A1.- Continued.

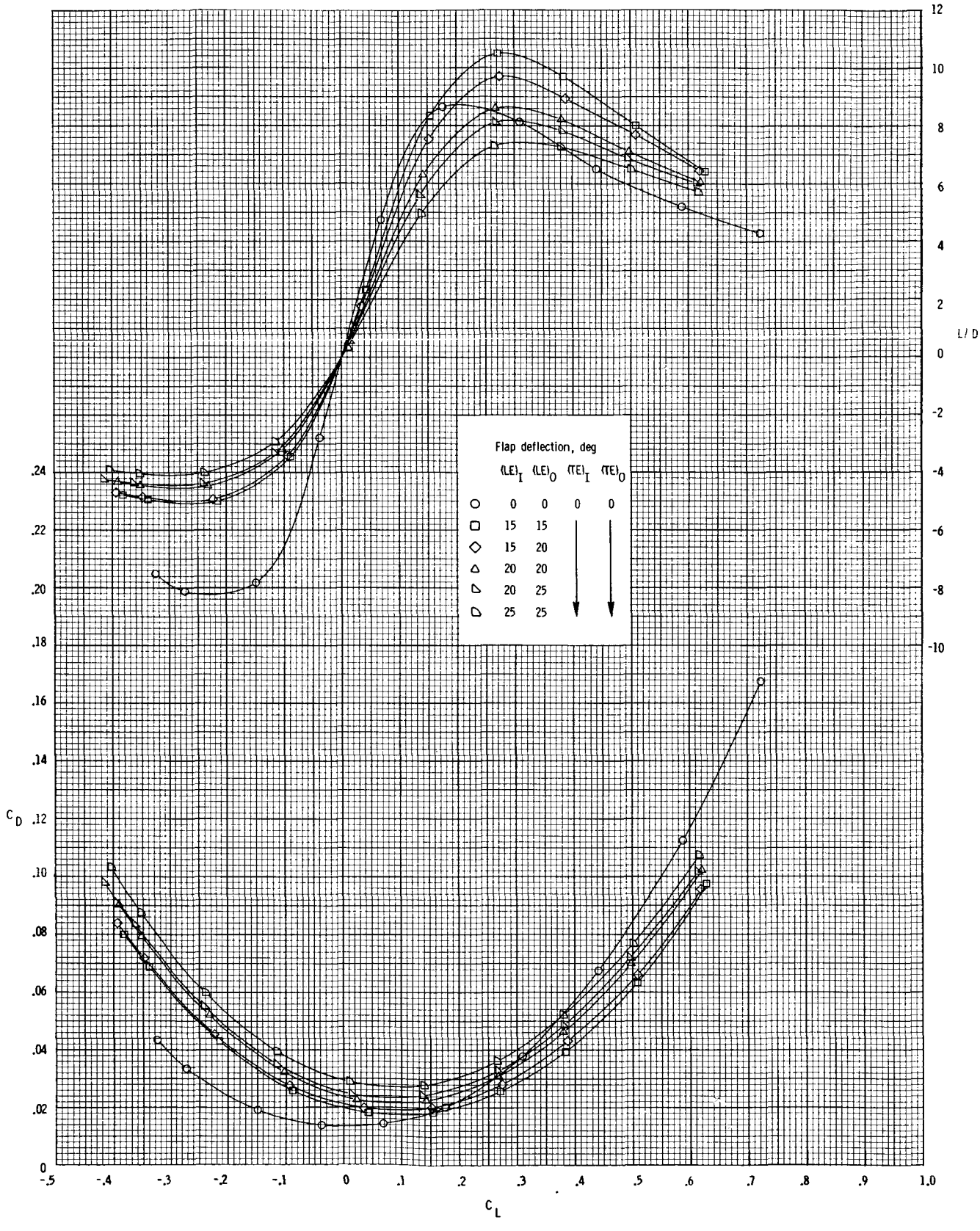

(c) M = 0.7.

Figure A1.- Continued.

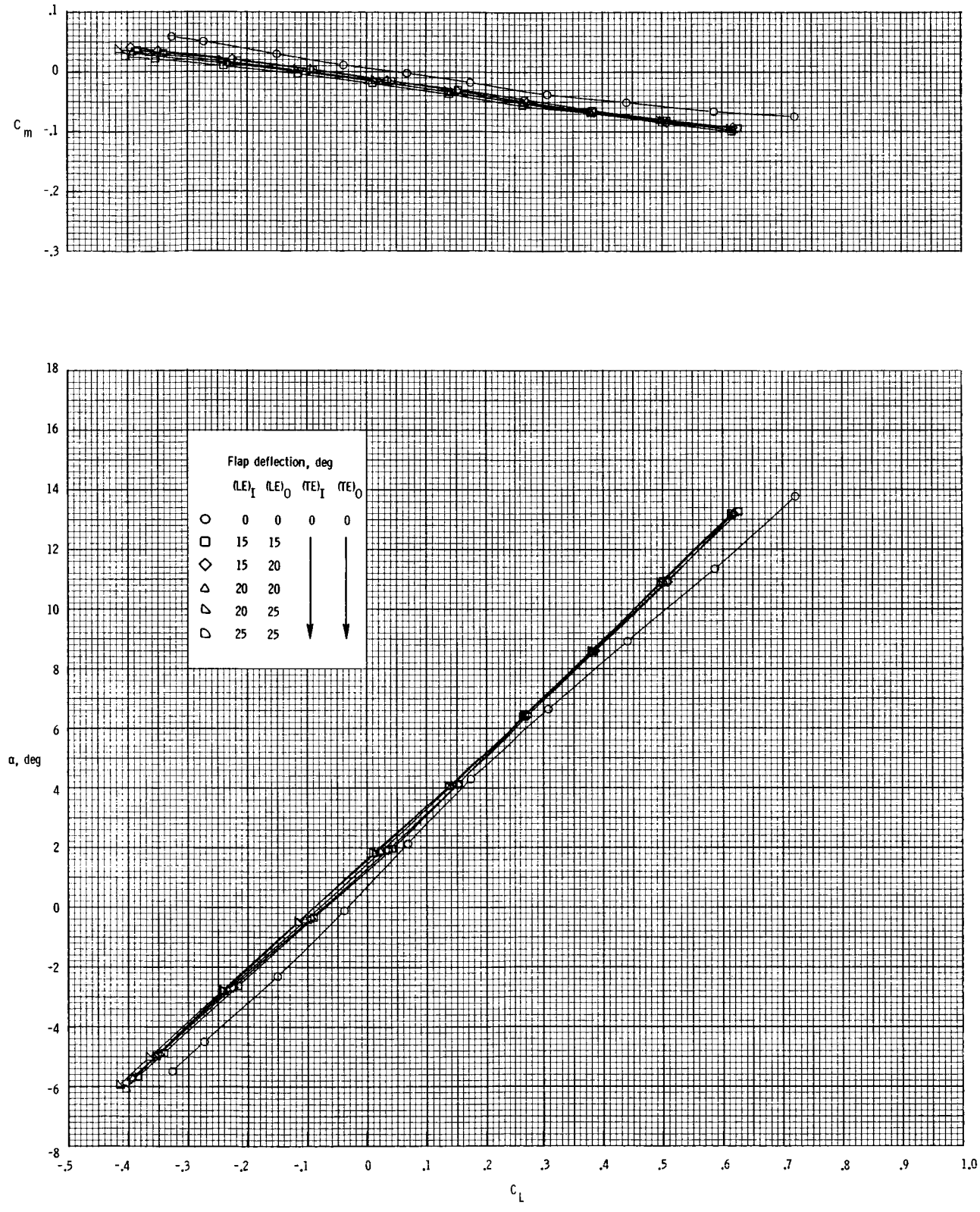

(c) Concluded.

Figure A1.- Concluded.

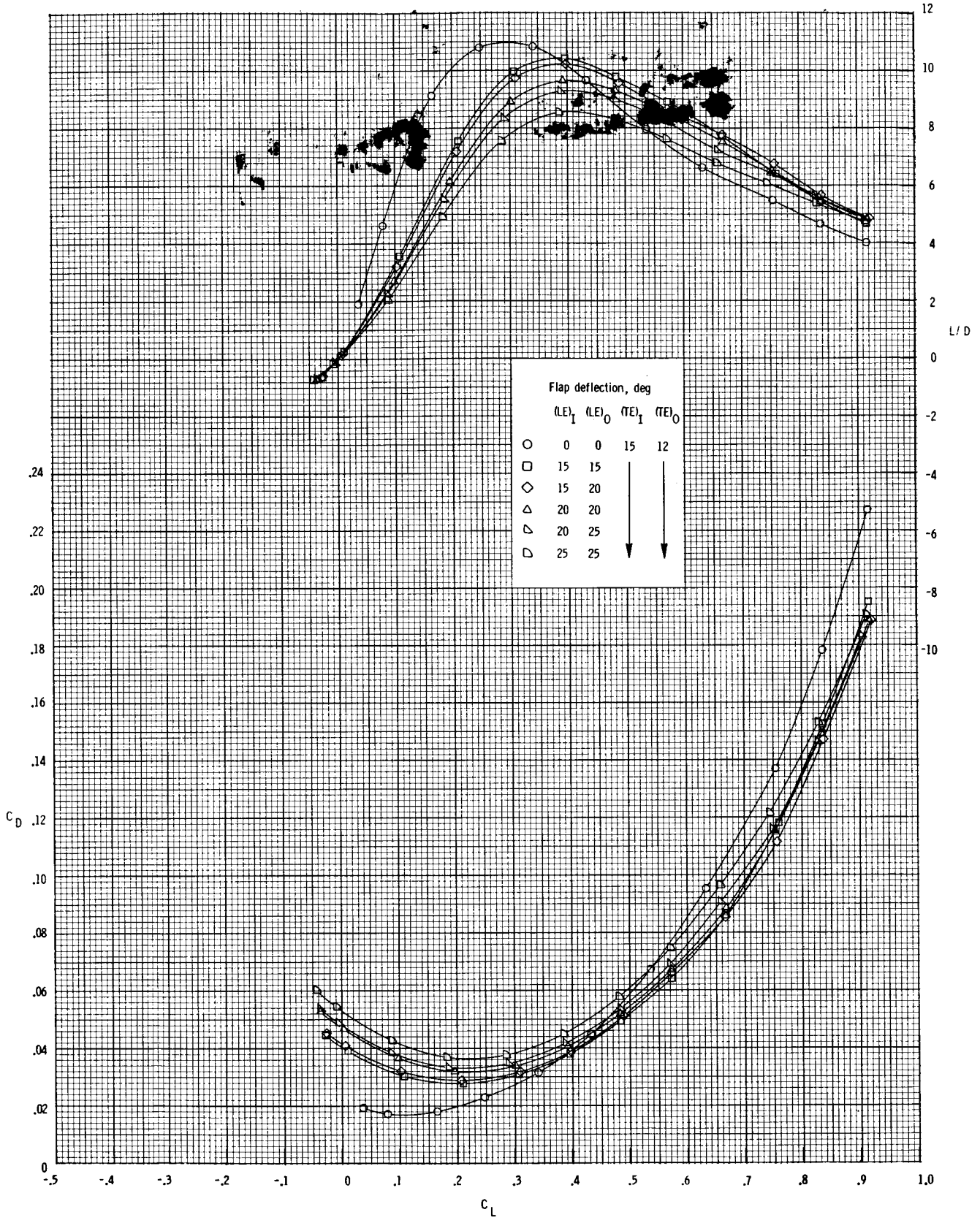

(a) M = 0.3.

Figure A2.- Effect of leading-edge deflection with trailing-edge deflection for flap A.

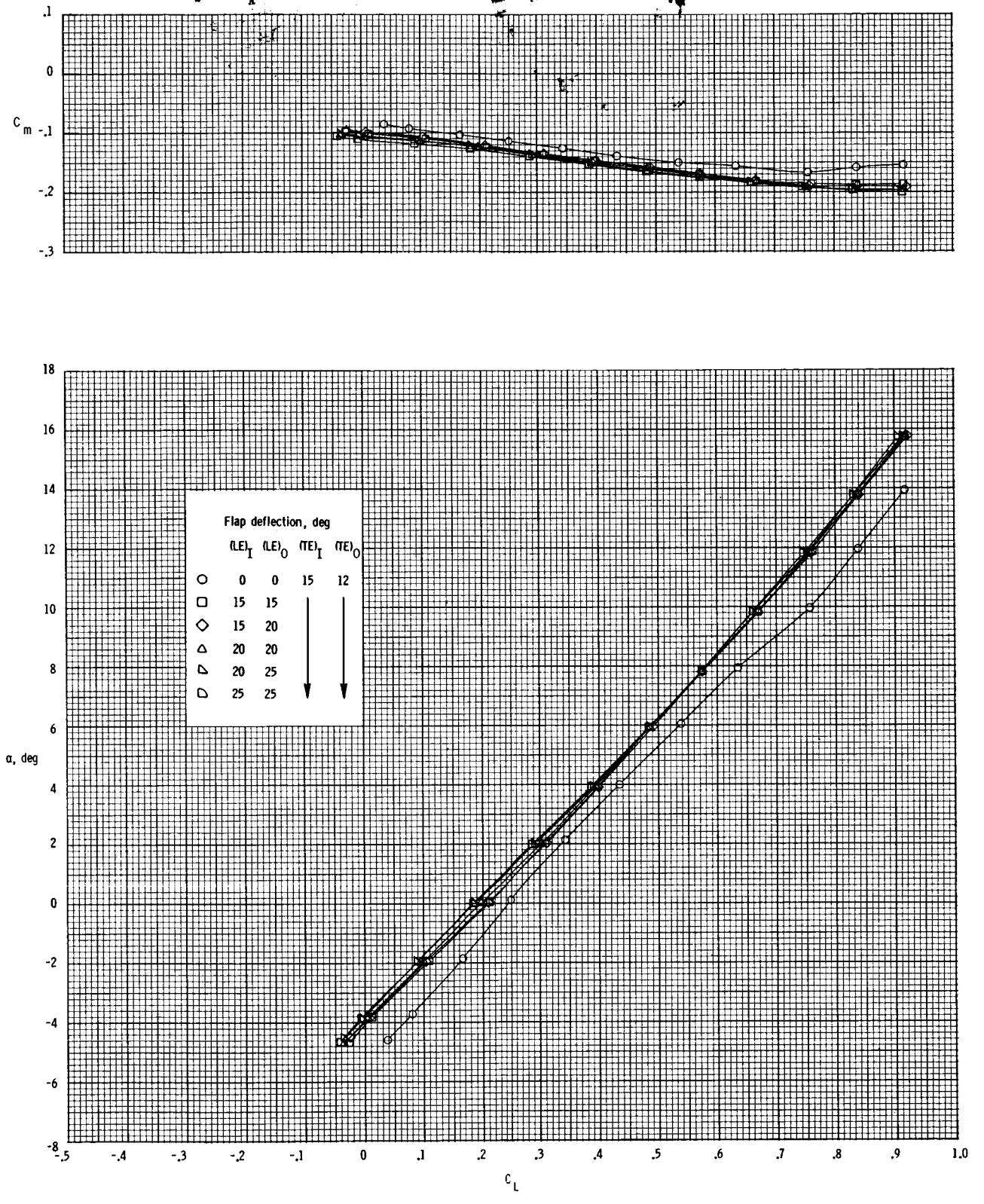

(a) Concluded.

Figure A2.- Continued.

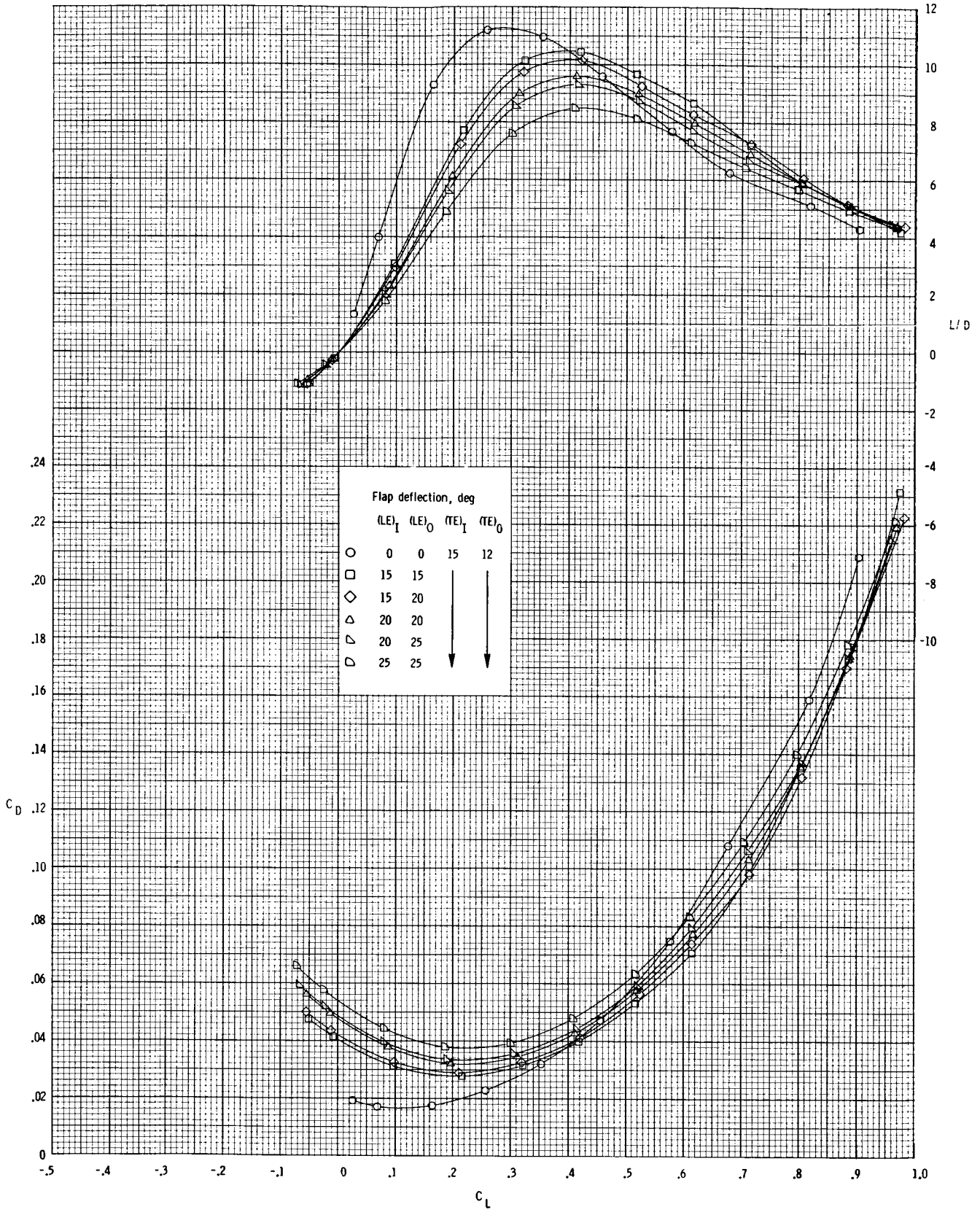

(b) M = 0.5.

Figure A2.- Continued.

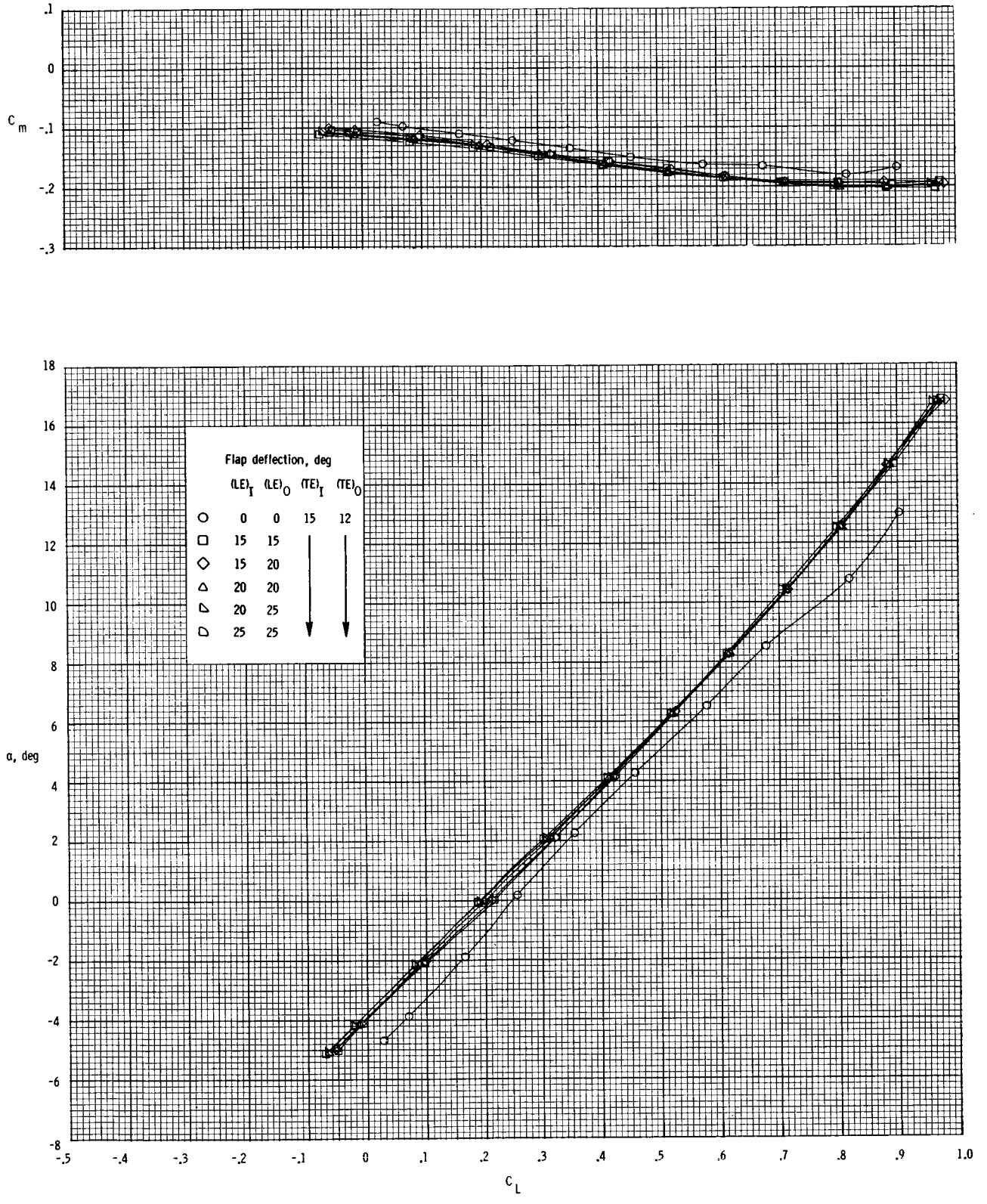

(b) Concluded.

Figure A2.- Continued.

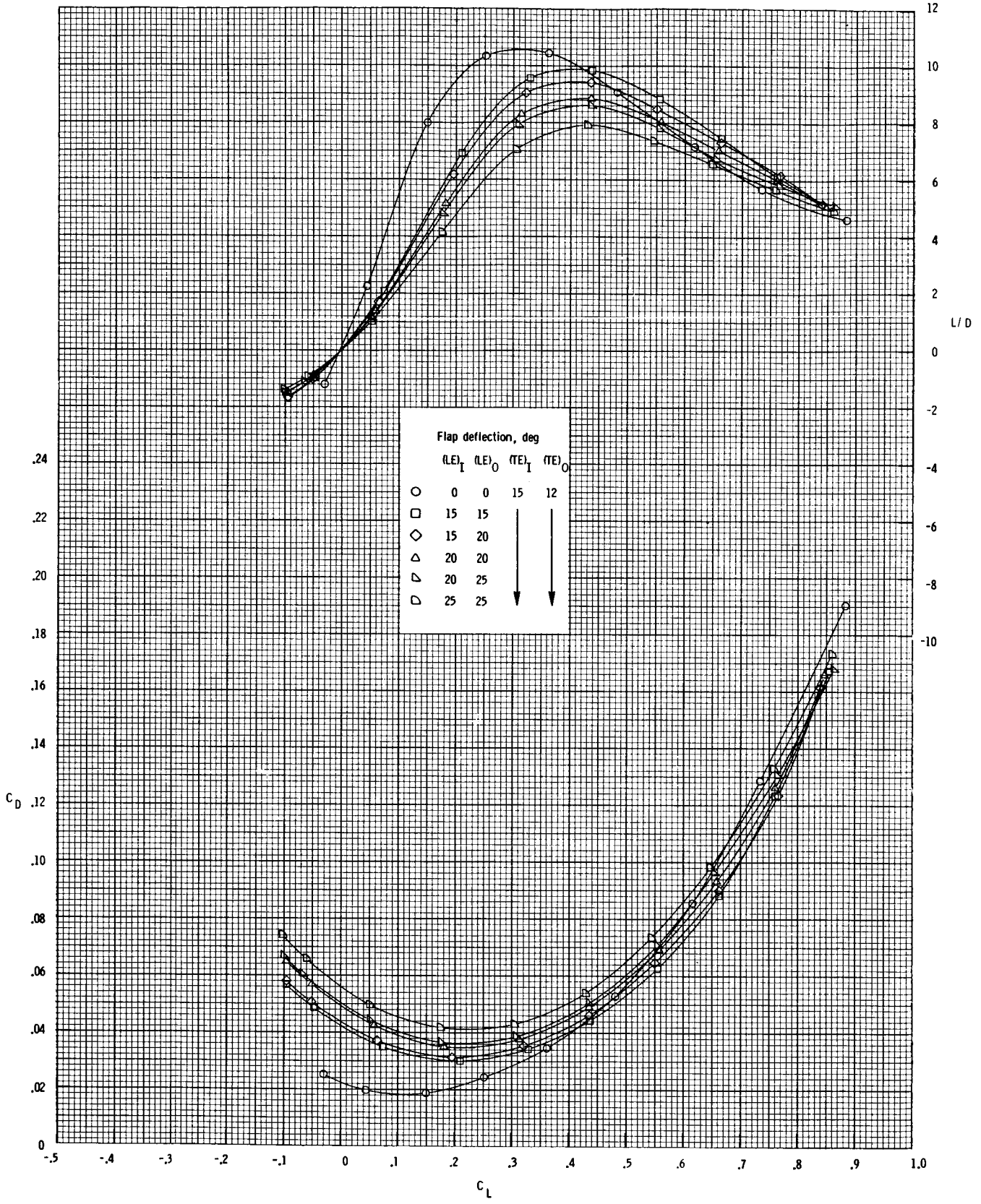

(c) M = 0.7.

Figure A2.- Continued.

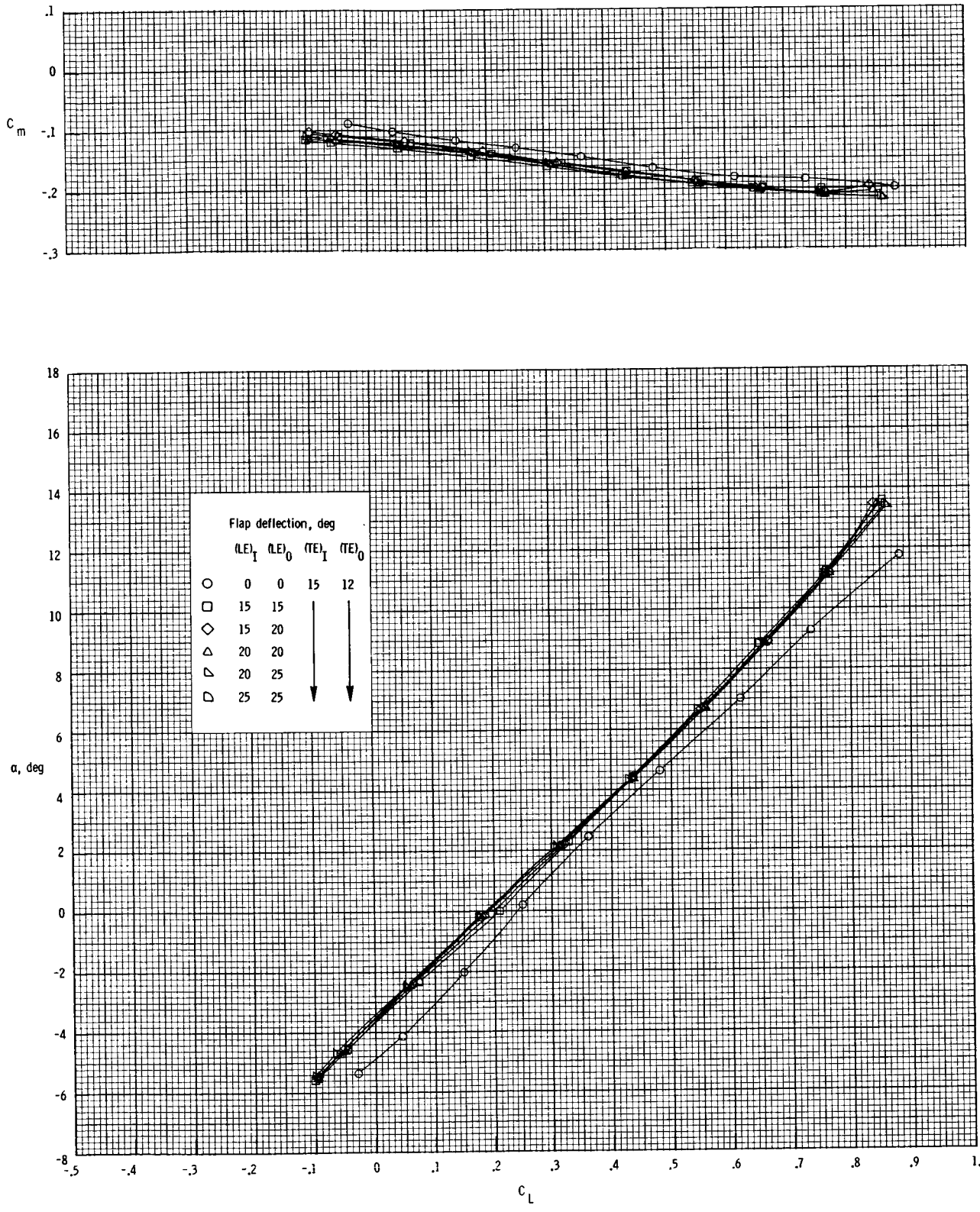

(c) Concluded.

Figure A2.- Concluded.

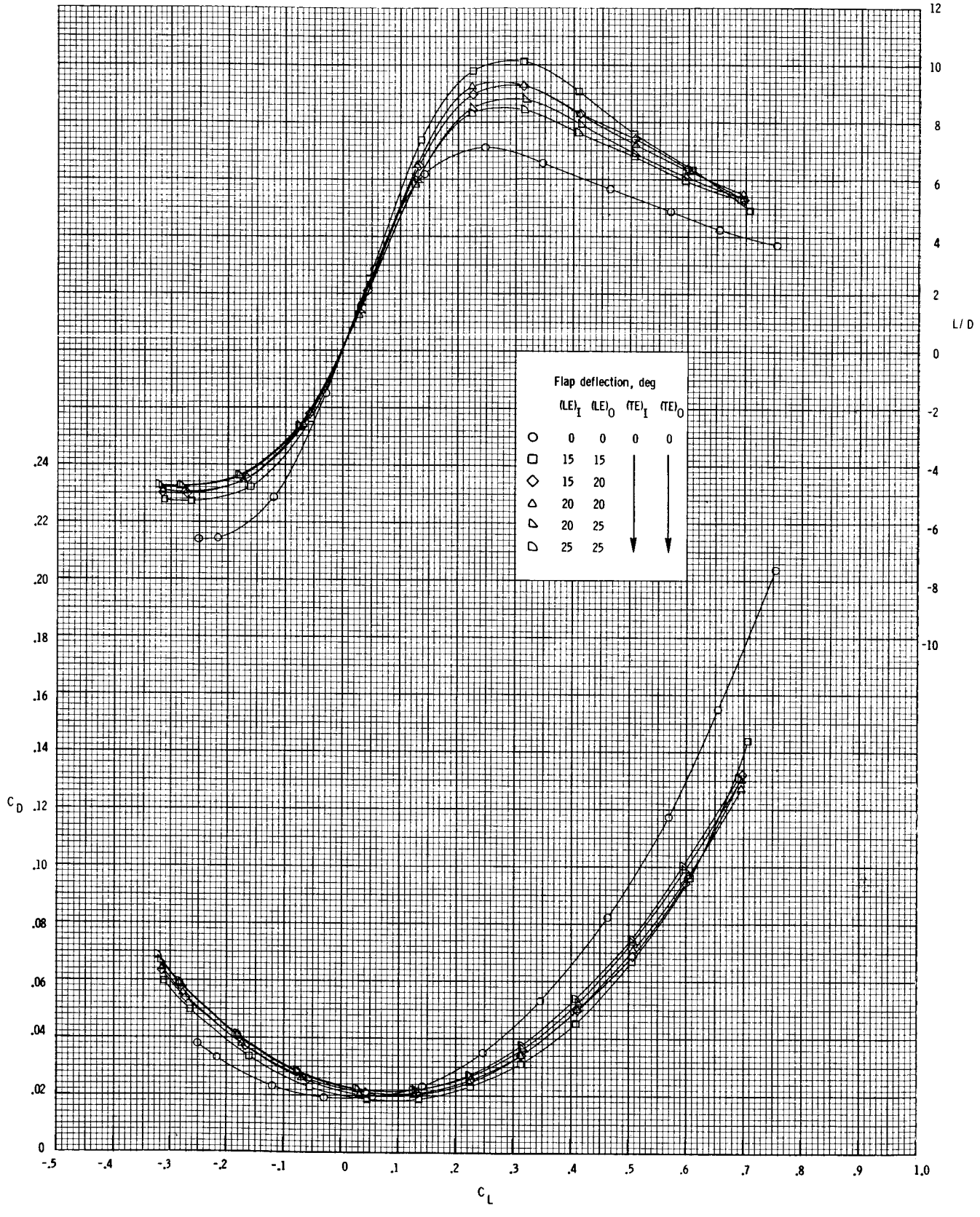

(a) M = 0.3.

Figure A3.- Effect of leading-edge deflection with no trailing-edge deflection for flap B.

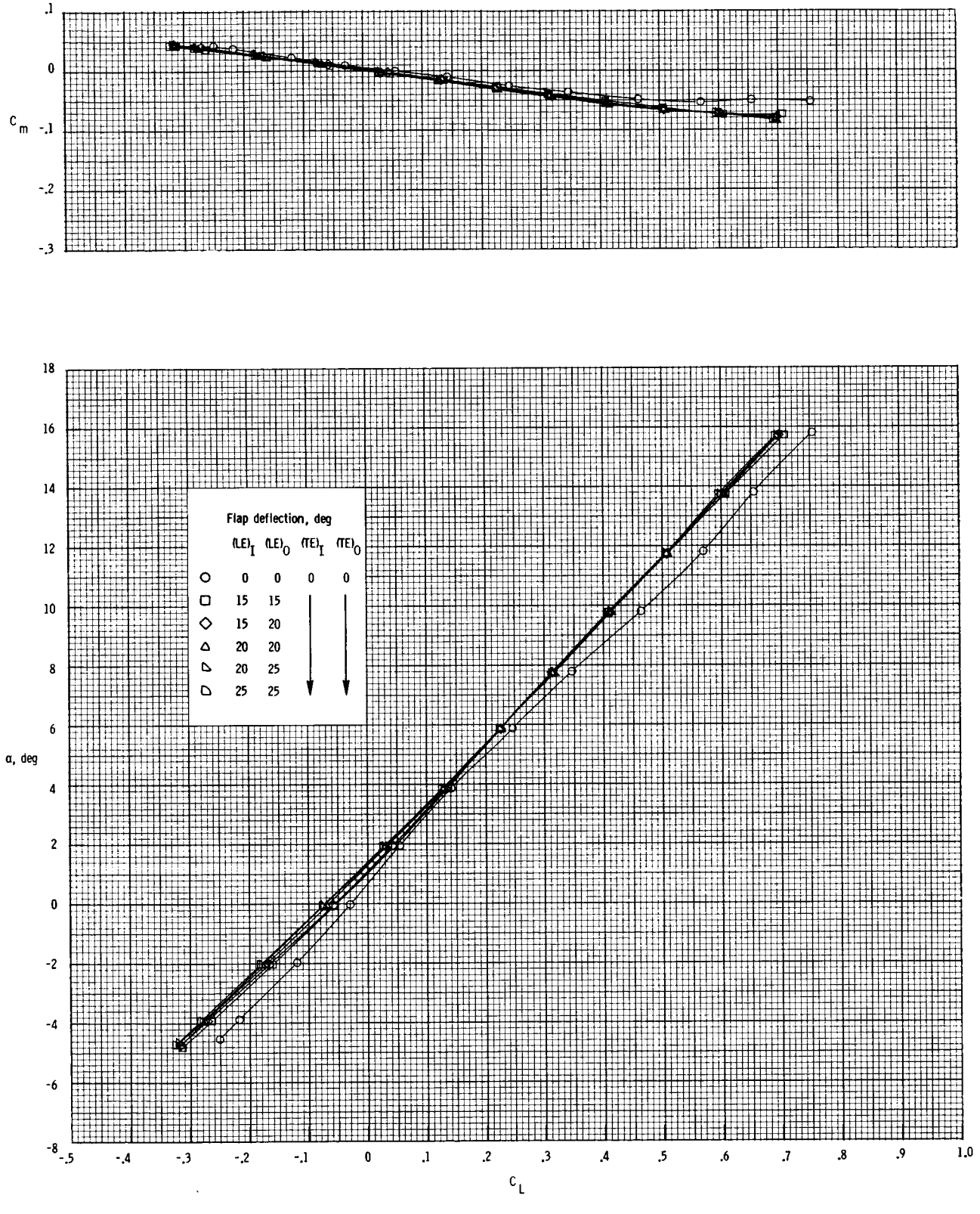

(a) Concluded.

Figure A3.- Continued.

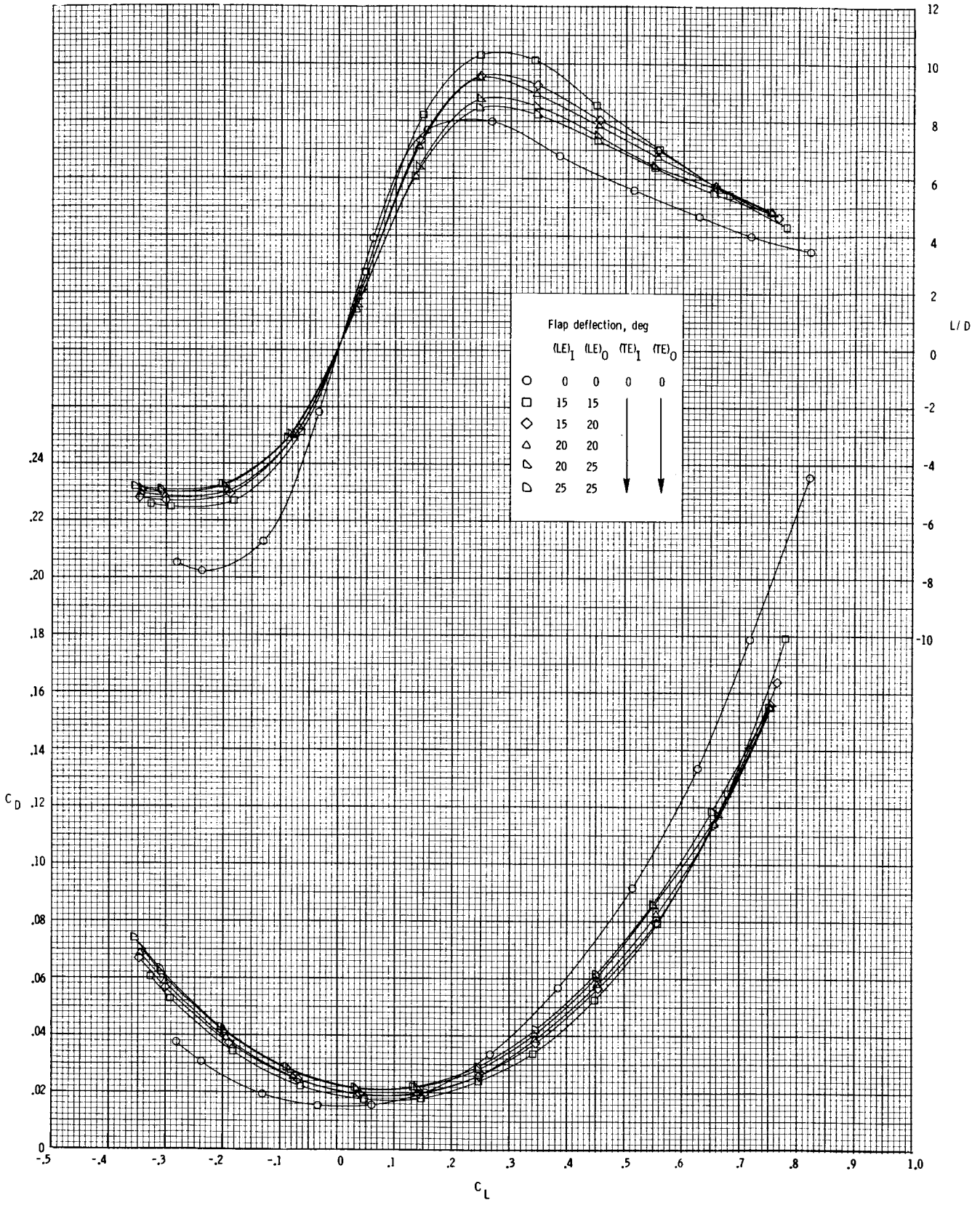

(b) M = 0.5.

Figure A3.- Continued.

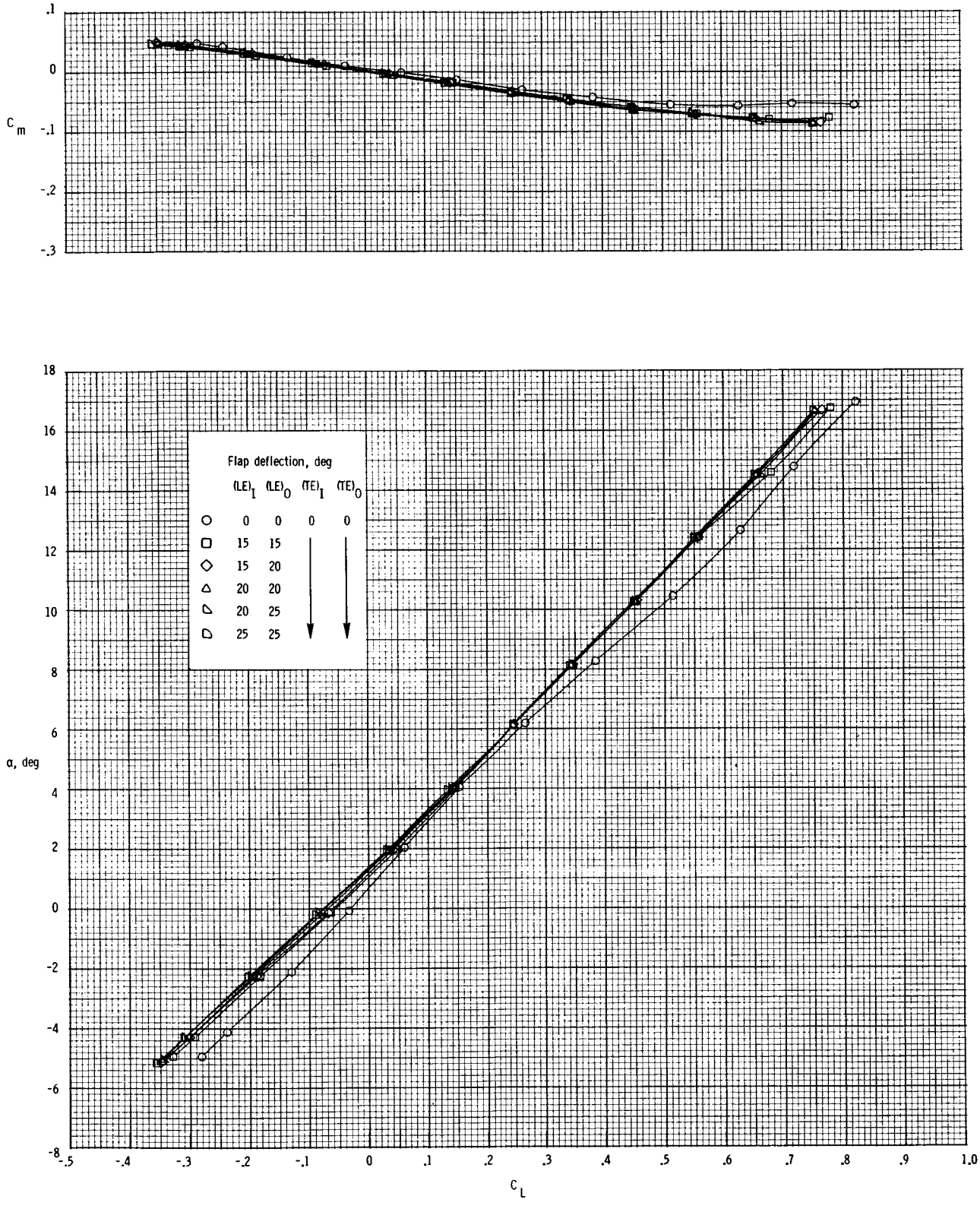

(b) Concluded.

Figure A3.- Continued.

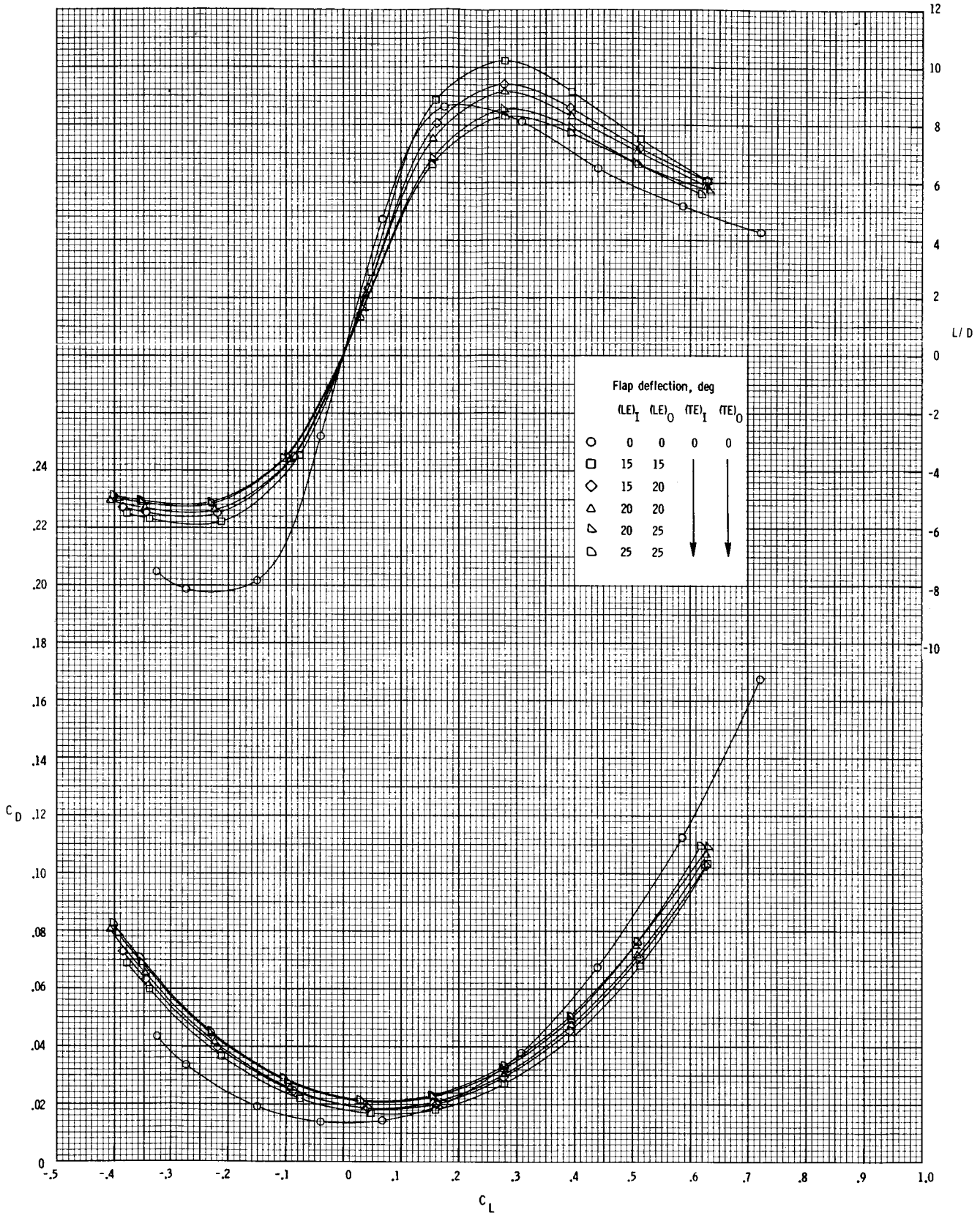

(c) M = 0.7.

Figure A3.- Continued.

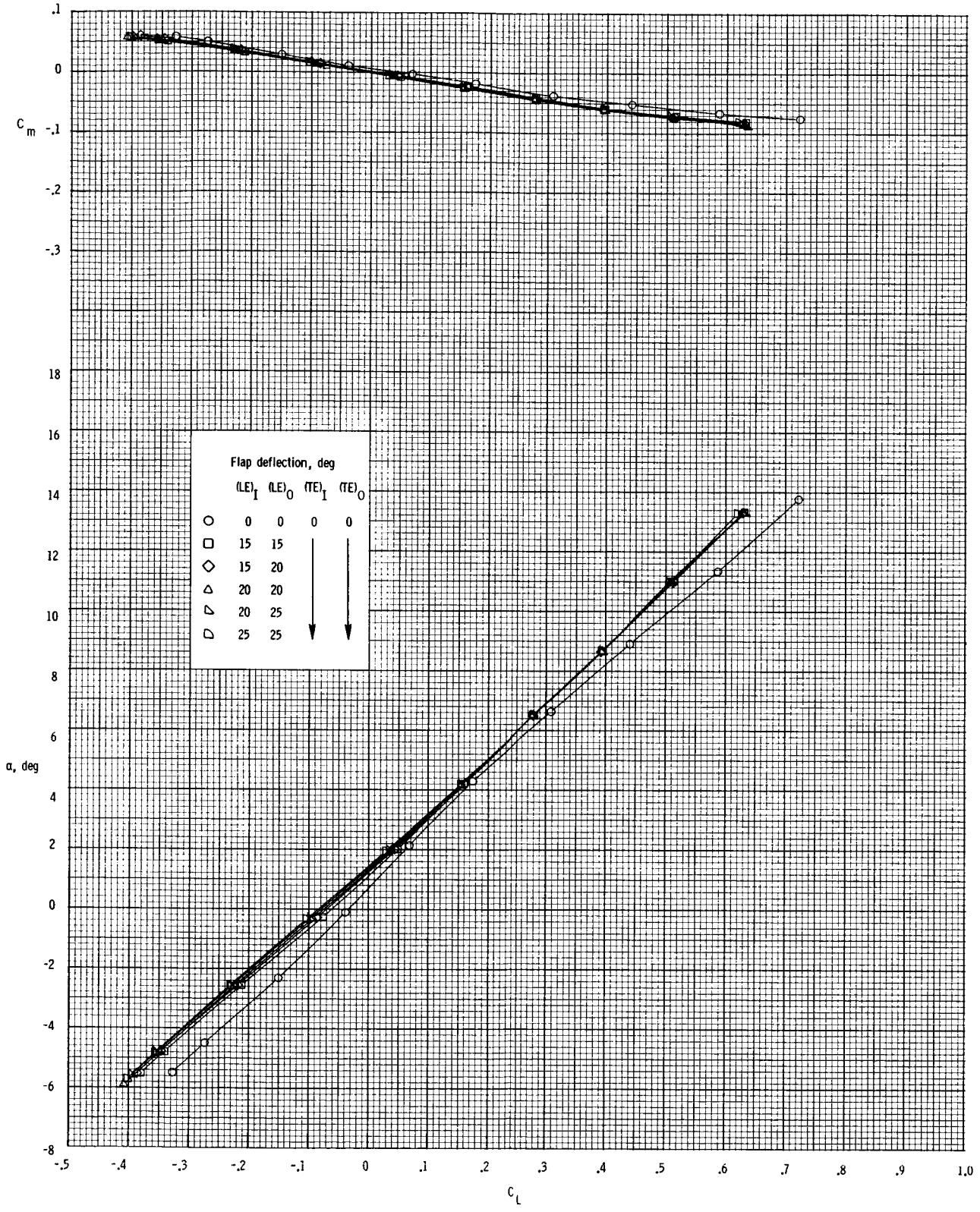

(c) Concluded.

Figure A3.- Concluded.

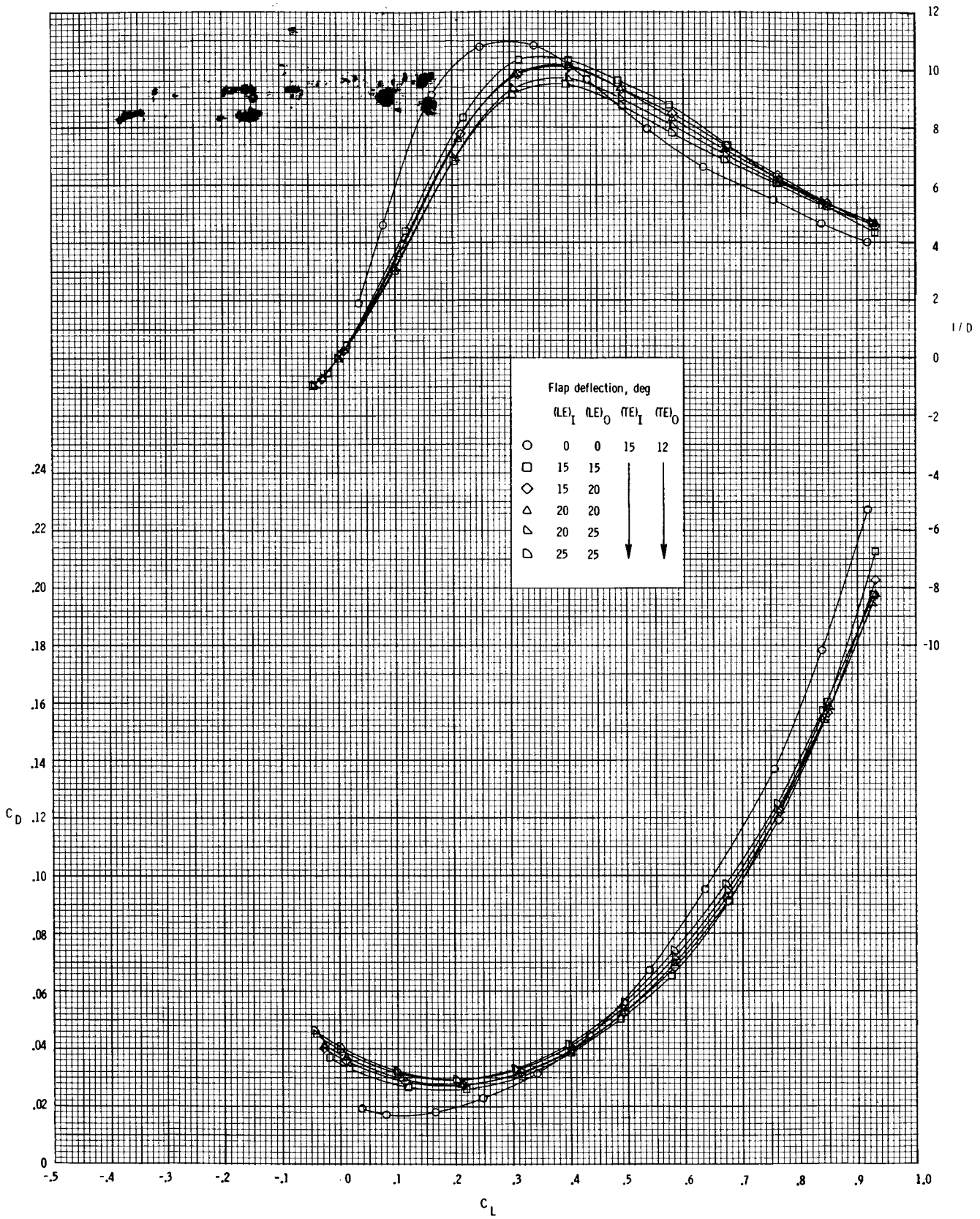

(a) M = 0.3.

Figure A4.- Effect of leading-edge deflection with trailing-edge deflection for flap B.

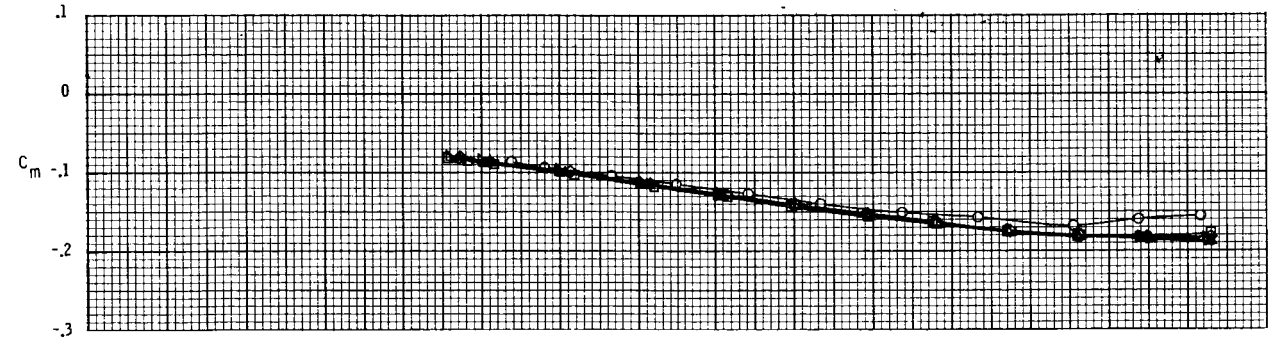

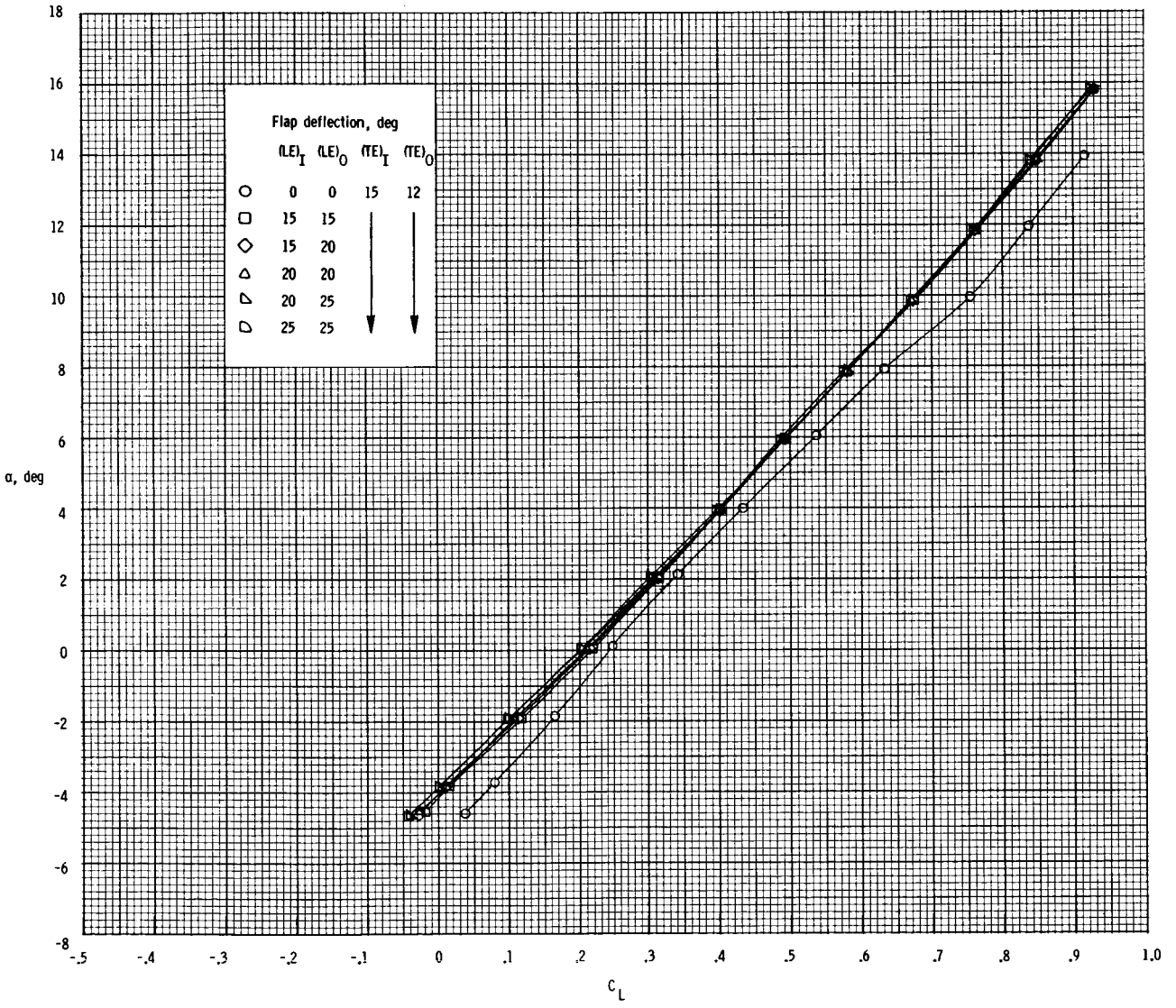

(a) Concluded.

Figure A4.- Continued.

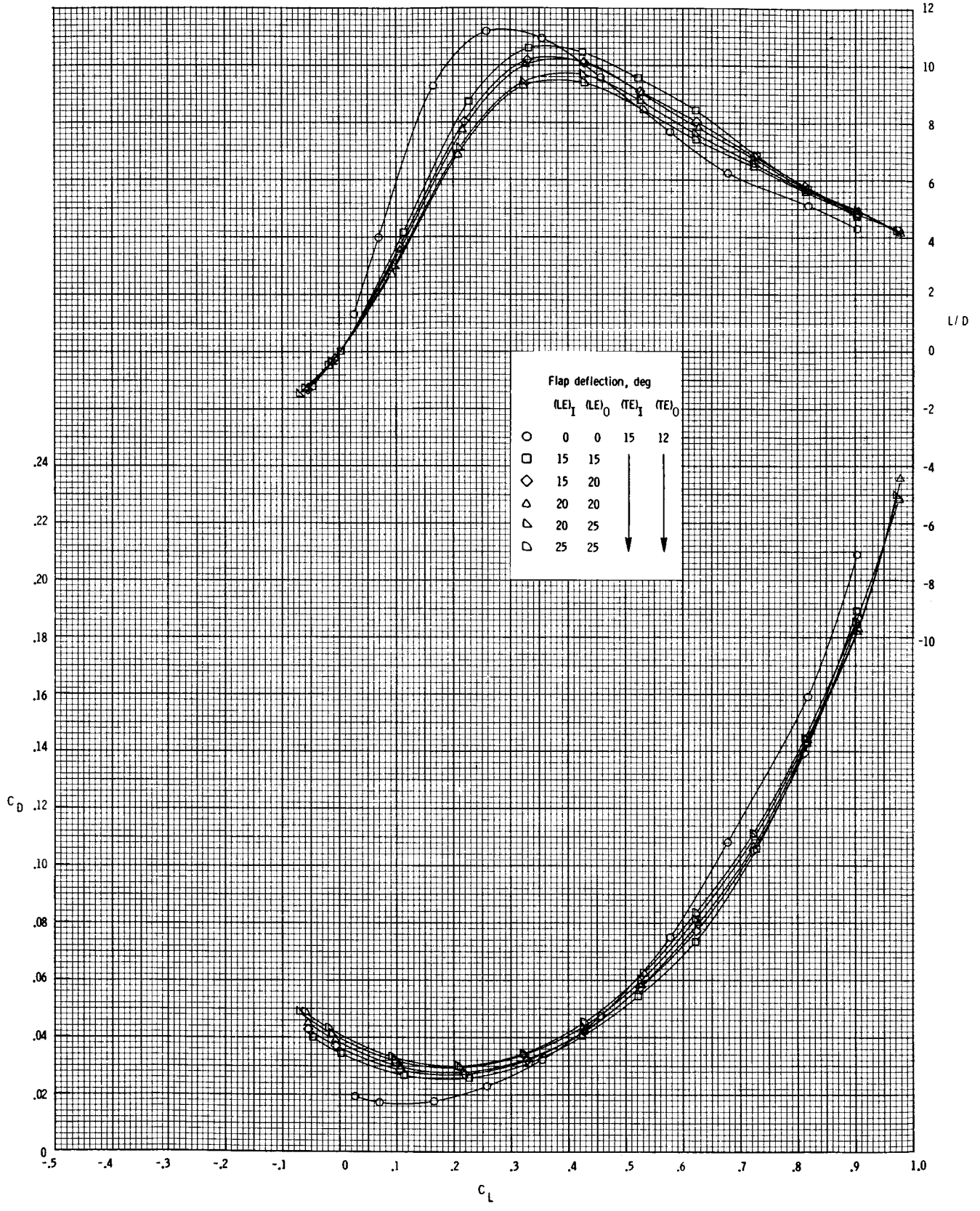

(b) M = 0.5.

Figure A4.- Continued.

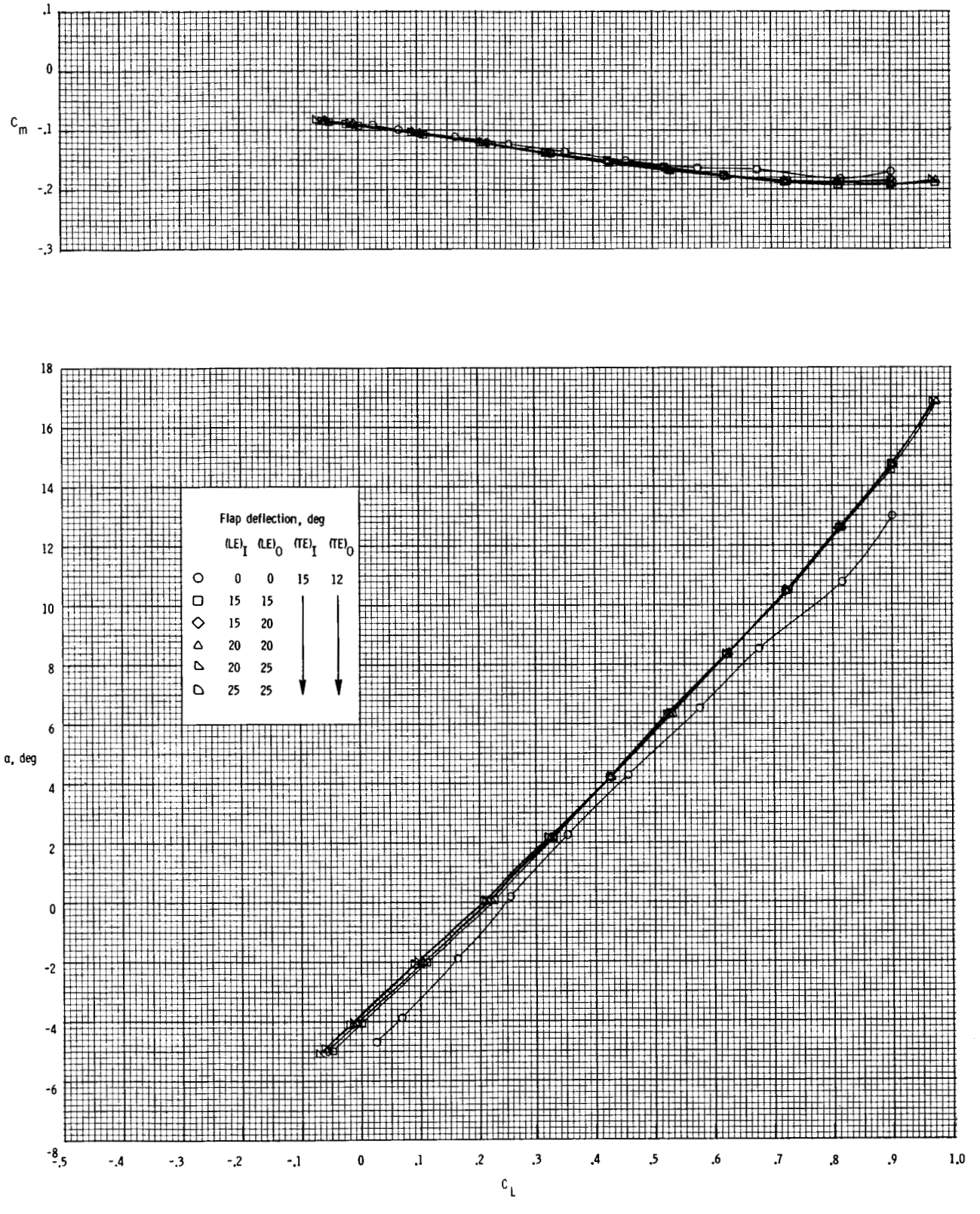

(b) Concluded.

Figure A4.- Continued.

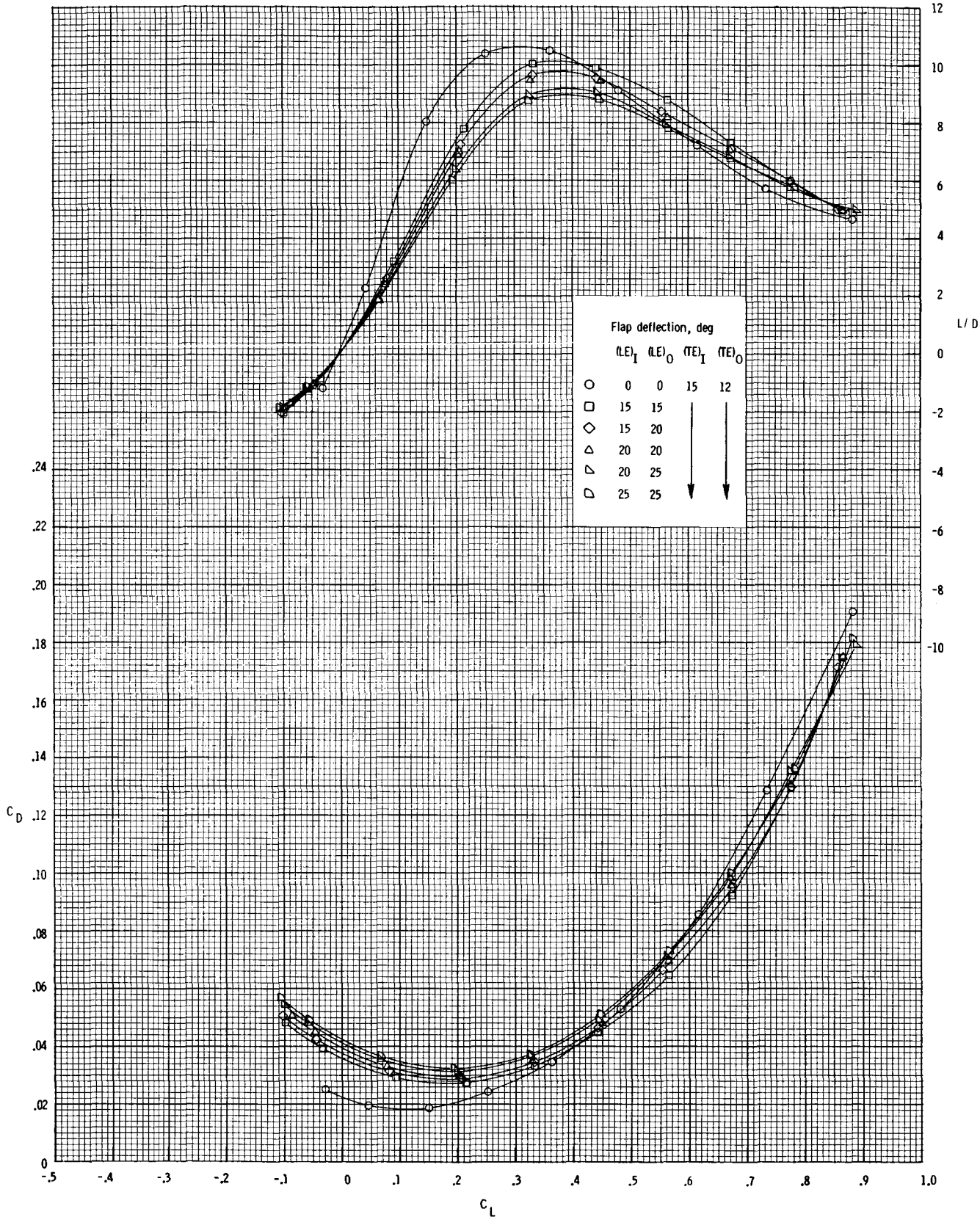

(c) M = 0.7.

Figure A4.- Continued.

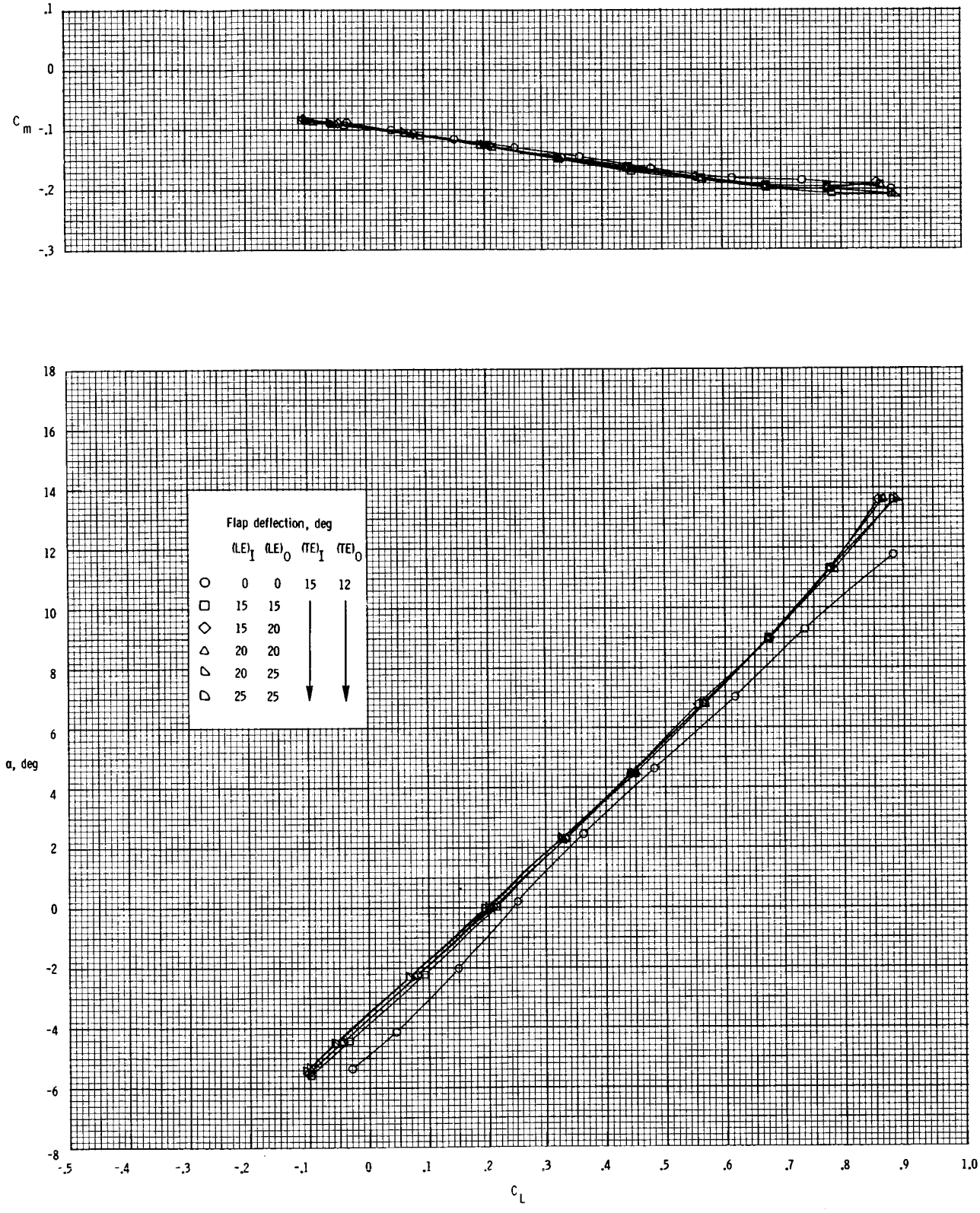

(c) Concluded.

Figure A4.- Concluded.

APPENDIX B

OIL-FLOW PHOTOGRAPHS

Oil-flow photographs for all configurations in which oil-flow test runs were made are presented in this appendix (figs. B1 to B7). Beside each photograph can be found the angle of attack and lift coefficient that correspond to that picture. Figure B1 shows model geometry features as they appear in a typical oil-flow photograph.

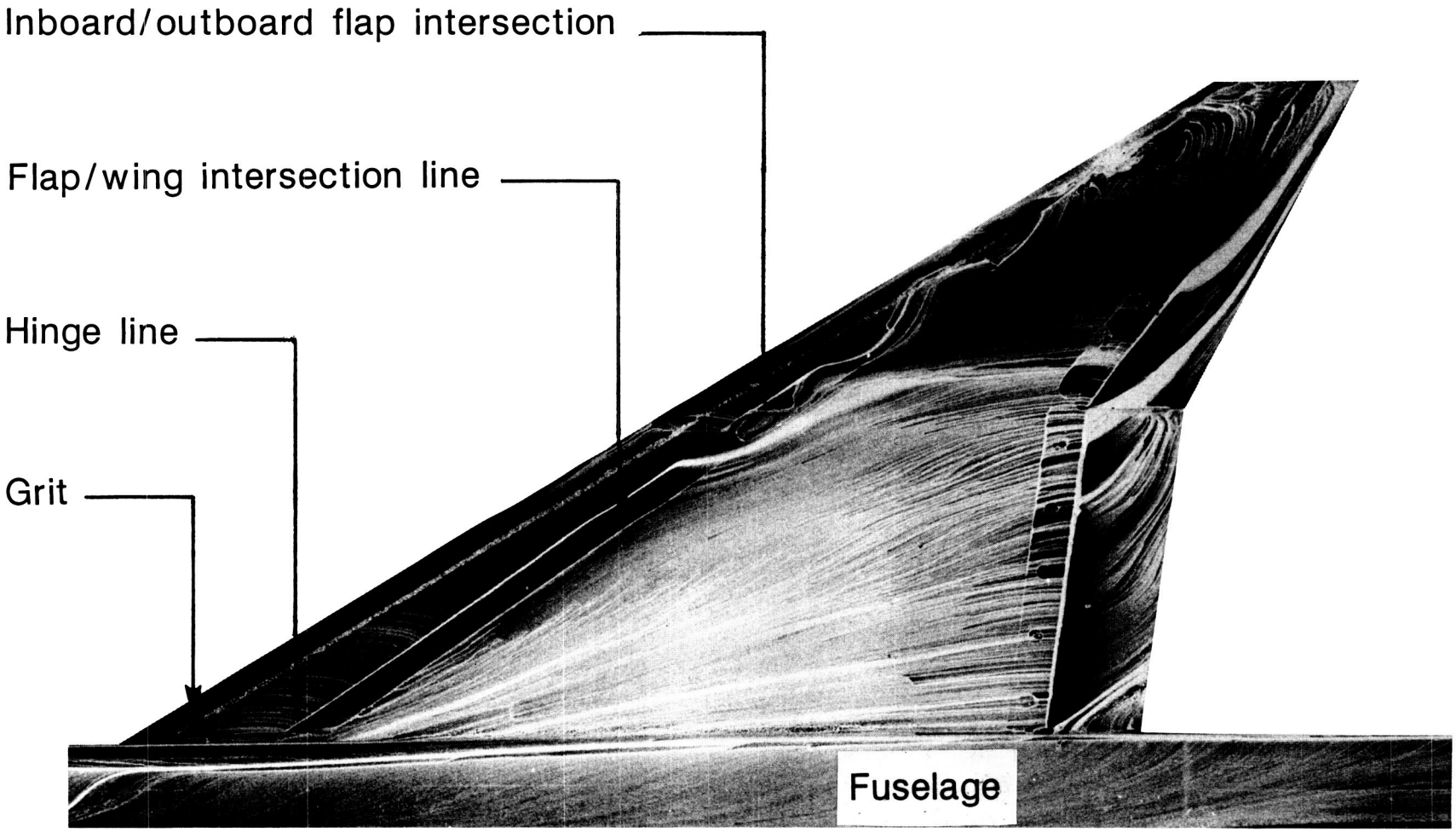

L-86-391

Figure B1.- Typical oil-flow photograph detailing wing geometric characteristics.

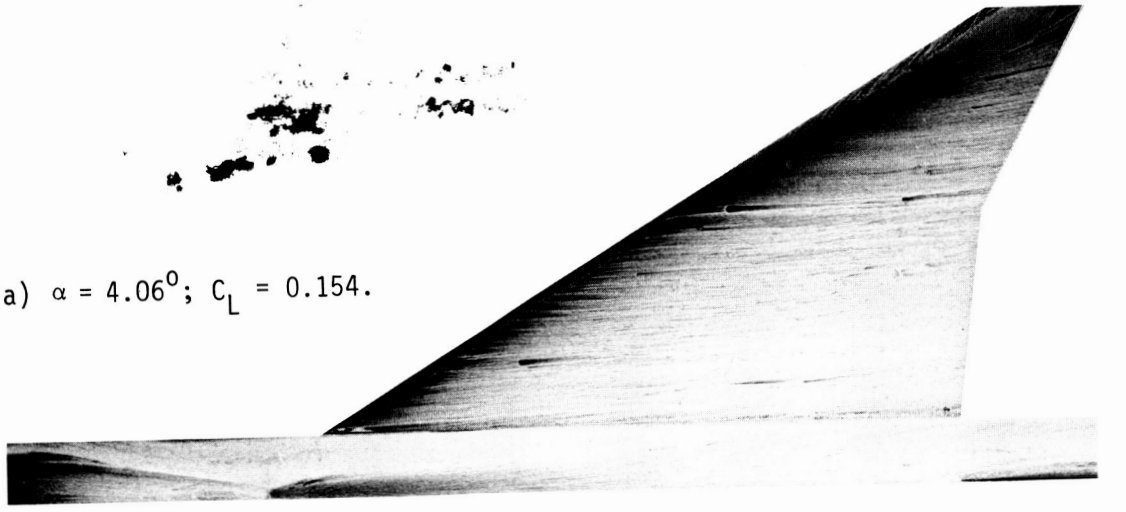

(a) $\alpha = 4.06^{o}$; $C_L = 0.154$.

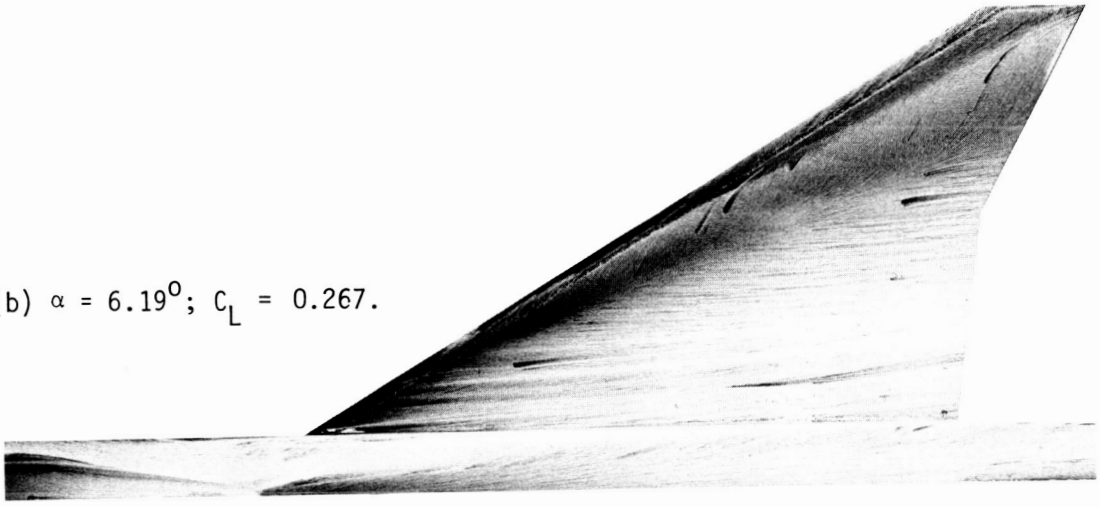

(b) $\alpha = 6.19^{o}$; $C_L = 0.267$.

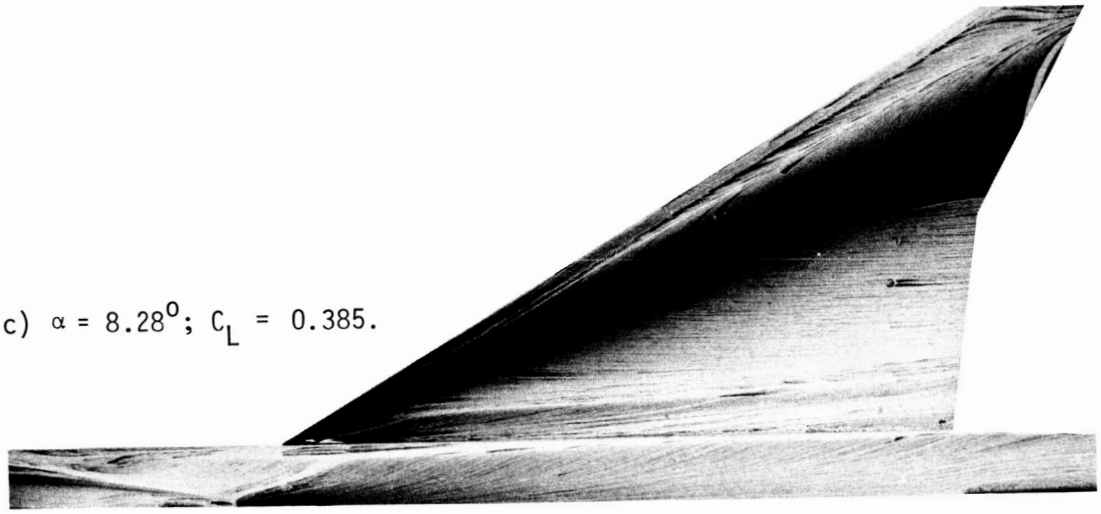

(c) $\alpha = 8.28^{o}$; $C_L = 0.385$.

L-86-392

Figure B2.- Oil-flow photographs of 0/0/0/0 configuration. M = 0.5.

(d) $\alpha = 12.64^{o}$; $C_L = 0.627$.

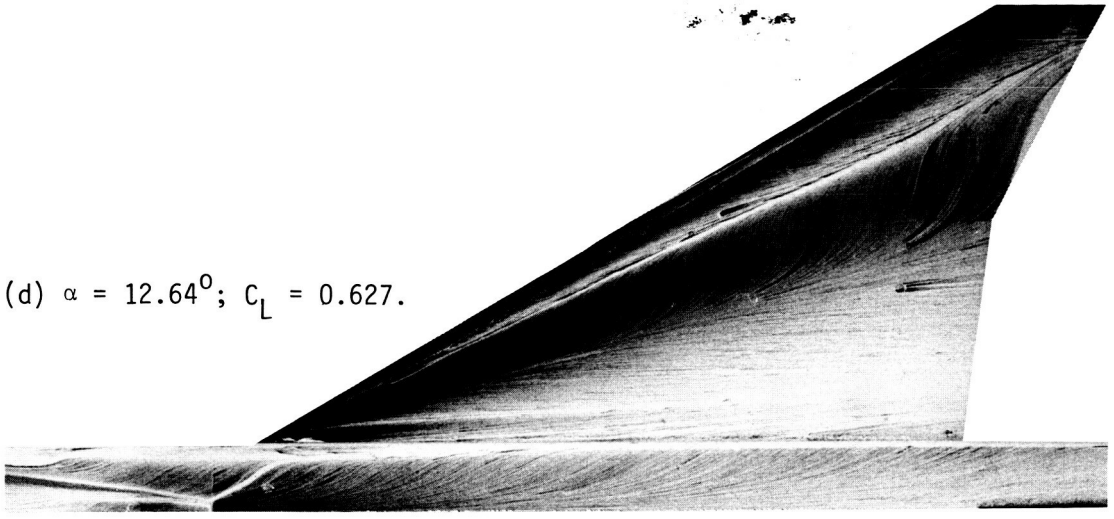

(e) $\alpha = 14.78$; $C_L = 0.717$.

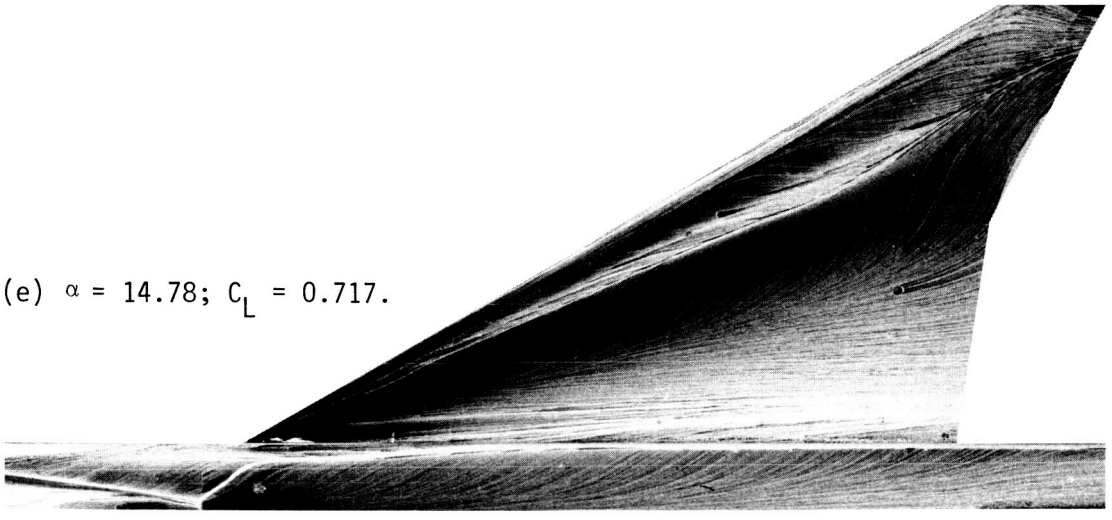

(f) $\alpha = 16.94^{o}$; $C_L = 0.821$.

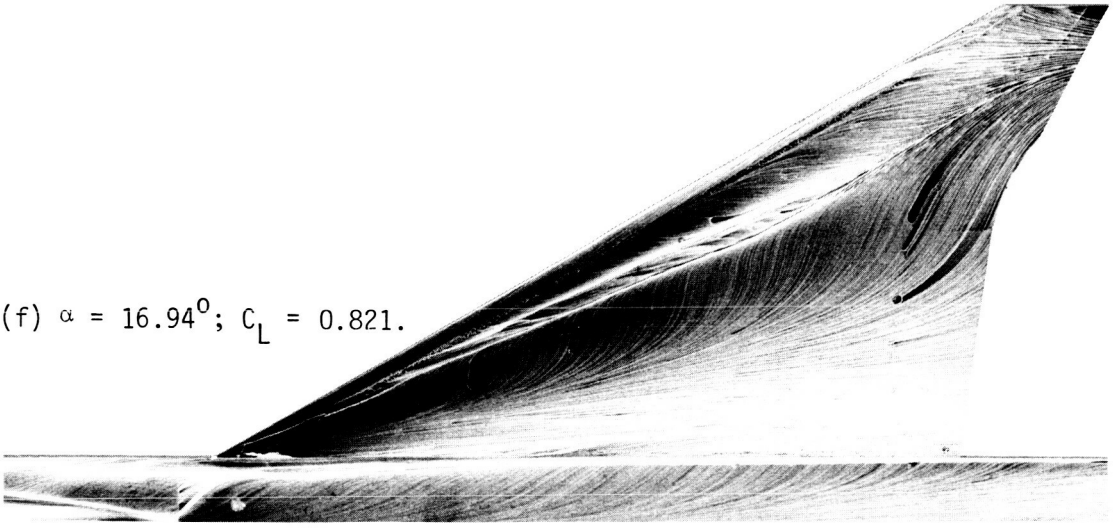

L-86-393

Figure B2.- Concluded.

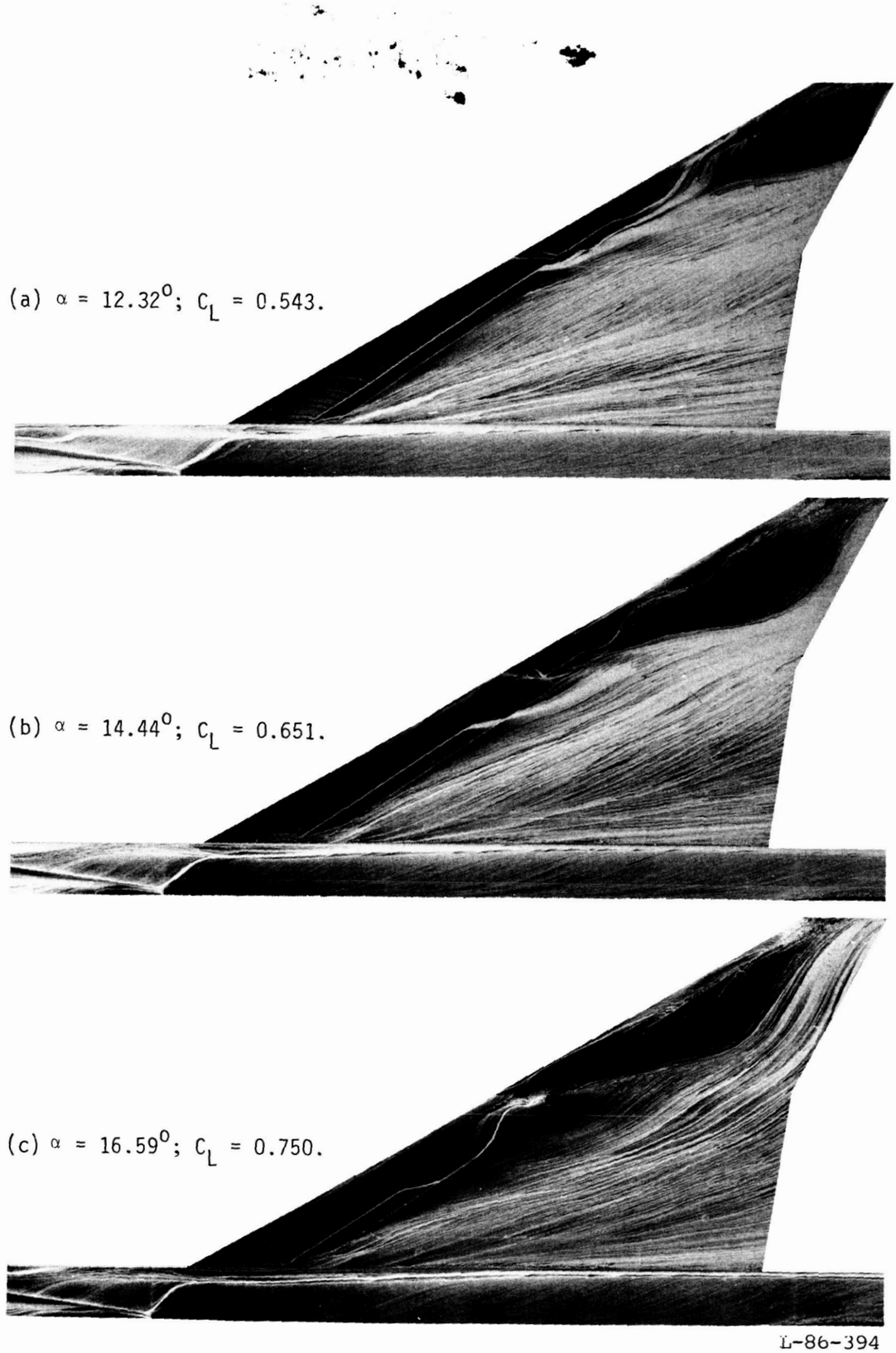

L-86-394

Figure B3.- Oil-flow photographs of 15/15/0/0 configuration. M = 0.5; flap A.

(a) $\alpha = 8.54^{o}$; $C_L = 0.677$.

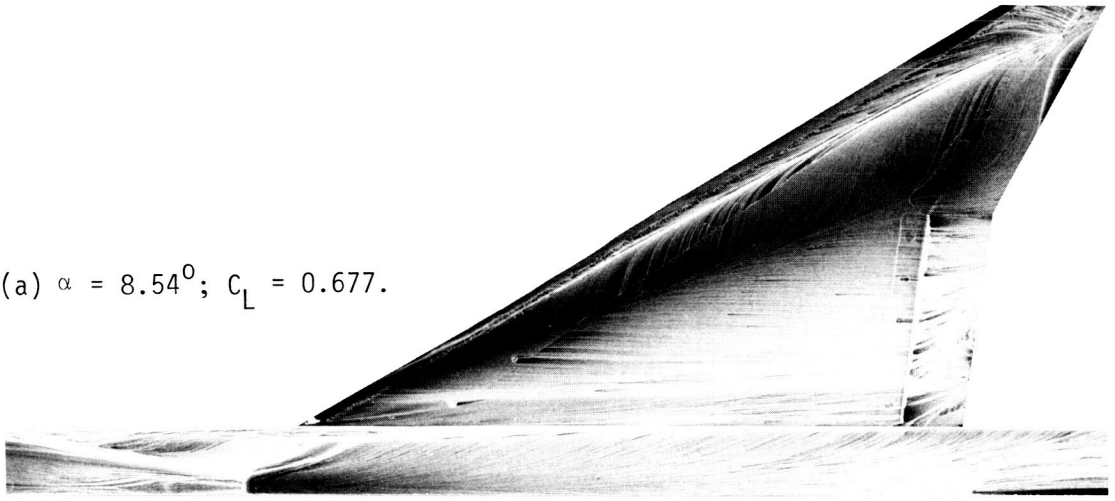

(b) $\alpha = 10.79^{o}$; $C_L = 0.817$.

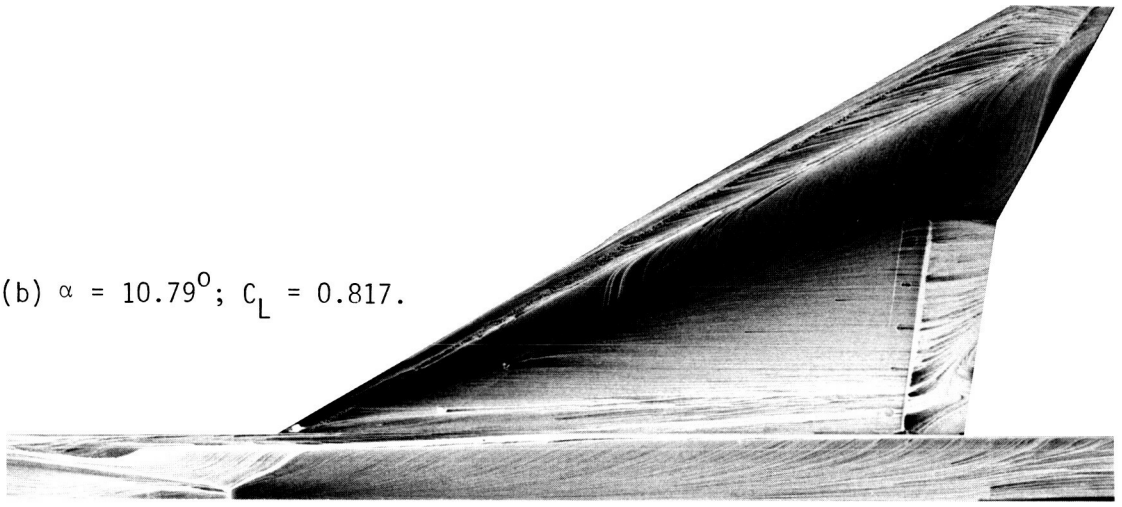

(c) $\alpha = 13.01^{o}$; $C_L = 0.902$.

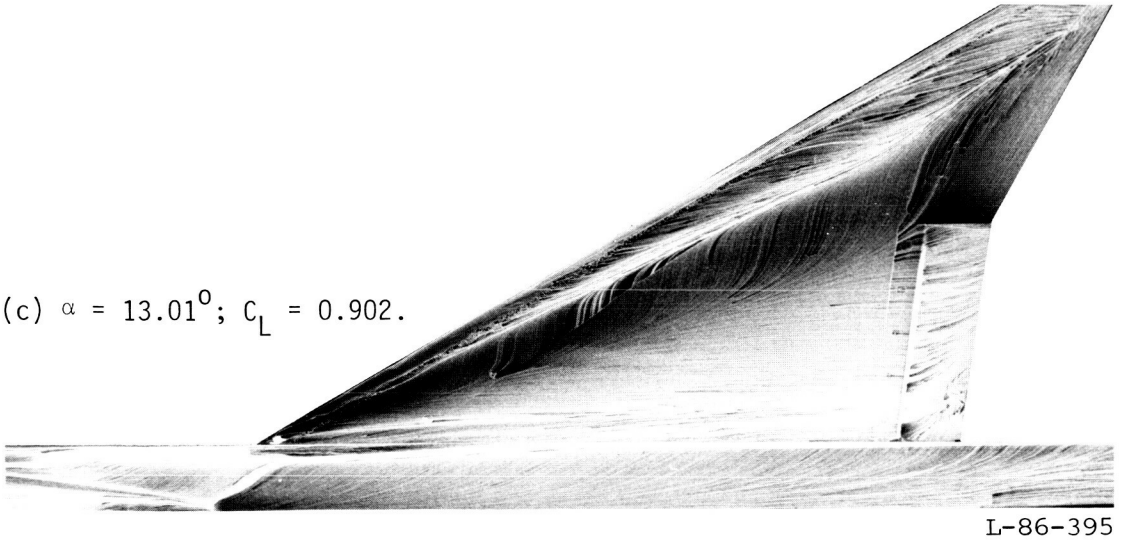

L-86-395

Figure B4.- Oil-flow photographs of 0/0/15/12 configuration. M = 0.5.

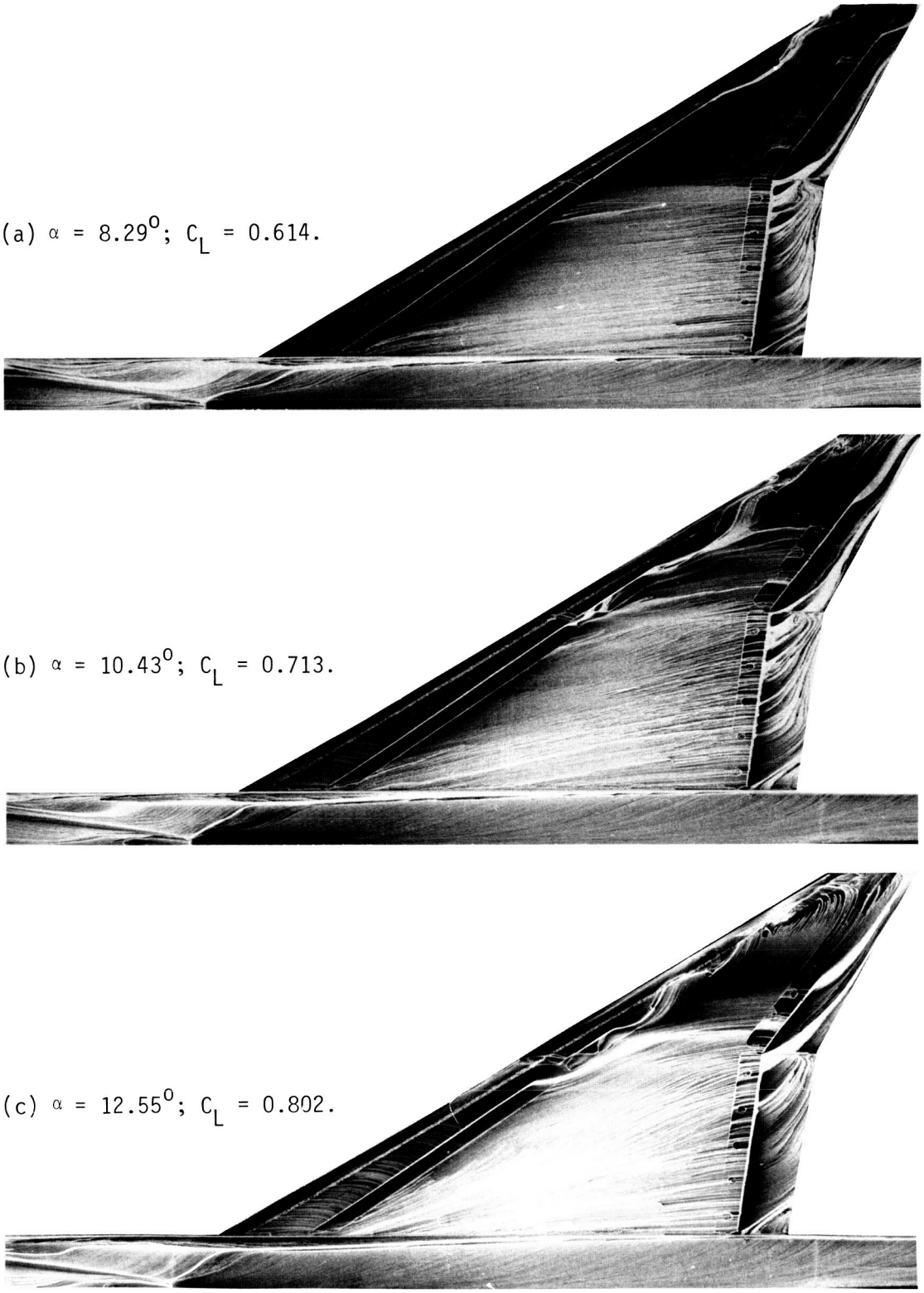

L-86-396

Figure B5.- Oil-flow photographs of 15/15/15/12 configuration. M = 0.5; flap A.

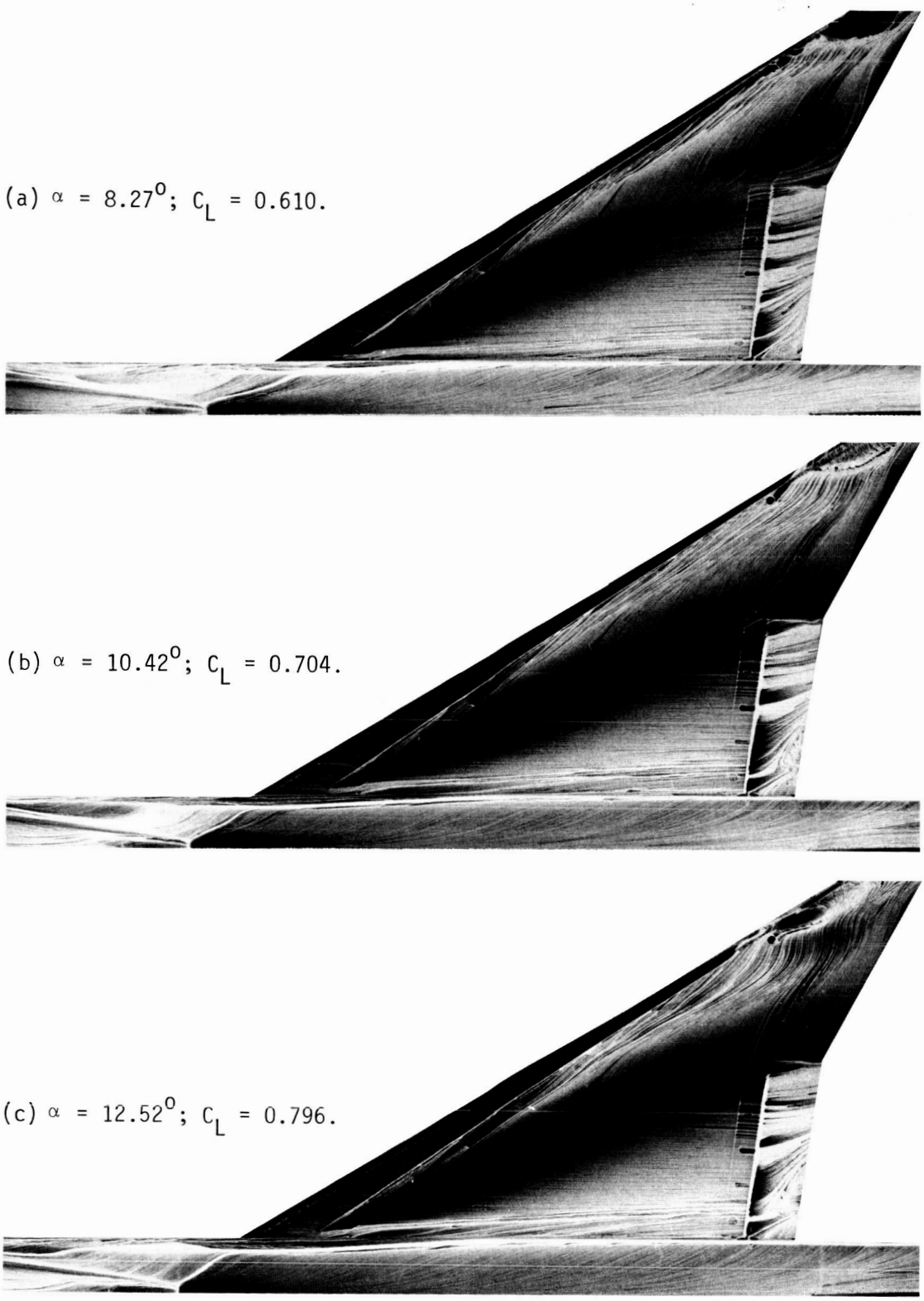

Figure B6.- Oil-Flow photographs of 25/25/15/12 configuration. M = 0.5; flap A.

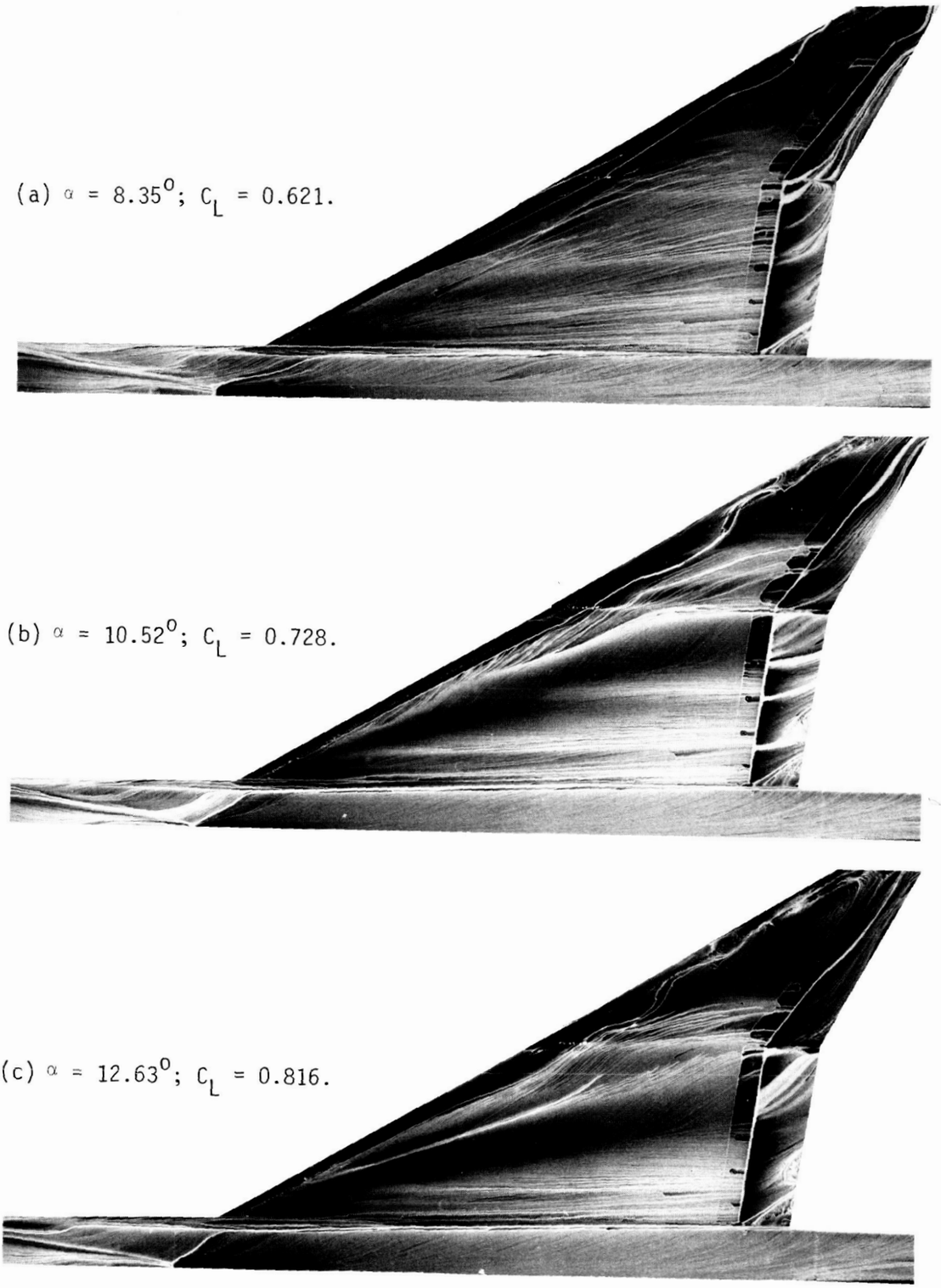

L-86-398

Figure B7.- Oil-flow photographs of 15/15/15/12 configuration. M = 0.5; flap B.

Standard Bibliographic Page

1. Report No.	2. Government Accession No.	3. Recipient's Catalog No.
NASA TP-2642		

4. Title and Subtitle	5. Report Date
Subsonic Maneuver Capability of a Supersonic Cruise Fighter Wing Concept	January 1987
	6. Performing Organization Code: 505-61-71-05
7. Author(s)	8. Performing Organization Report No.
Gregory D. Riebe and Charles H. Fox, Jr.	L-16097
9. Performing Organization Name and Address	10. Work Unit No.
NASA Langley Research Center Hampton, VA 23665-5225	11. Contract or Grant No.
12. Sponsoring Agency Name and Address	13. Type of Report and Period Covered: Technical Paper
National Aeronautics and Space Administration Washington, DC 20546-0001	14. Sponsoring Agency Code

15. Supplementary Notes

16. Abstract

A theoretical and experimental investigation was conducted of the subsonic maneuver capability of a fighter wing concept designed for supersonic cruise. To improve the subsonic maneuver capability, the wing utilized full-span leading- and trailing-edge flaps that were designed with the aid of a subsonic-analysis computer program. Wind-tunnel tests were made at Mach numbers of 0.3, 0.5, and 0.7. Force and moment data obtained were compared with theoretical predictions at Mach 0.5 from two subsonic-analysis computer programs. The two theoretical programs gave a good prediction of the lift and drag characteristics but only a fair prediction of the pitching moment. The experimental results of this study show that with the proper combination of leading- and trailing-edge flap deflections, a suction parameter of nearly 90 percent can be attained at a Mach number of 0.5 and a lift coefficient of 0.73; this is a three-fold improvement from 30 percent for the basic wing.

17. Key Words (Suggested by Authors(s))	18. Distribution Statement
Supersonic cruise fighter Flaps Transonic maneuver	Unclassified - Unlimited Subject Category 02

19. Security Classif.(of this report)	20. Security Classif.(of this page)	21. No. of Pages	22. Price
Unclassified	Unclassified	73	A04

For sale by the National Technical Information Service, Springfield, Virginia 22161